

**LIBRARY
Michigan State
University**

This is to certify that the
dissertation entitled

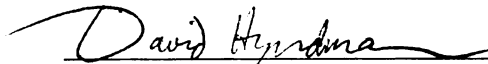
EXPLORING THE INFLUENCE OF LAND-USE AND CLIMATE ON
REGIONAL HYDROLOGY AND GROUNDWATER RECHARGE

presented by

DUSHMANTHA HELAPRIYA JAYAWICKREME

has been accepted towards fulfillment
of the requirements for the

Ph.D. degree in Geological Sciences



Major Professor's Signature

12-11-2008

Date

**EXPLORING THE INFLUENCE OF LAND-USE AND CLIMATE ON REGIONAL
HYDROLOGY AND GROUNDWATER RECHARGE**

By

Dushmantha Helapriya Jayawickreme

A DISSERTATION

**Submitted to
Michigan State University
in partial fulfillment of the requirements
for the degree of**

DOCTOR OF PHILOSOPHY

Geological Sciences

2008

ABSTRACT

EXPLORING THE INFLUENCE OF LAND-USE AND CLIMATE ON REGIONAL HYDROLOGY AND GROUNDWATER RECHARGE

By

Dushmantha Helapriya Jayawickreme

Global energy, water, and bio-geochemical cycles are strongly linked to land-use and land-cover characteristics. Land-use and land-cover is also a component of the environment extensively impacted and continuously altered by human activity. Population growth, food, energy and other needs coupled with human ingenuity has greatly altered and will continue to change the terrestrial biosphere across the globe. With additional concerns for significant and widespread land-use/land-cover transformations due to global climate change, a need to better understand the effects of these transformations on environmental systems from local, regional, to global scale has emerged in the recent decades.

In this dissertation I have investigated the impacts of land-use and land-cover (i.e. vegetation) on groundwater recharge, which is a critical component of the hydrologic cycle. The dependence of people and many sensitive ecosystems around the world on groundwater alone warranted a closer look at how changing land-use/cover and climate are affecting the quantity and quality of groundwater. By evaluating streamflow, climate, land-cover, and other attributes in Michigan's watersheds we showed that intense agriculture reduced summer time

streamflow, hence groundwater recharge in such watersheds. By quantifying baseflow discharges relative to precipitation in July-September peak growing season over multiple years we found that recharge in primarily agricultural (>70% agricultural uses by land area) watersheds was only one third of the recharge in watersheds that are mix use (<50% agricultural uses).

To better grasp how land-cover; specifically vegetation, vegetation differences, and vegetation dynamics affect recharge we adopted geophysical techniques, a step beyond the traditional uses of geophysical methods as well as an unorthodox approach to terrestrial ecosystem investigations. It was hypothesized that there would be observable differences in the way vegetation interacts with the shallow subsurface and such interactions could be quantified with geophysical methods. Based on multi-year geophysical monitoring of soil moisture at a forest-grassland ecotone we found large seasonal and long-term differences in the way vegetation affects groundwater recharge as well as shallow groundwater environments. Apart from water use differences, we show that soil temperature as well as salt dynamics even at very local scales are affected by vegetation differences. For example we observed that forests in shallow groundwater regions are likely to increase groundwater salinity compared to grasslands in similar settings. These findings contribute to developing greater insights into the functioning of the natural environment and how anthropogenic forcings through land-use change may imperil or help protect the health of hydrologic systems in a range of regions.

ACKNOWLEDGEMENTS

First and foremost I express my sincere gratitude to Dr. David Hyndman, my dissertation advisor, from whom I received knowledge, guidance, and unwavering support throughout my time as a graduate student at Michigan State University. Members of my committee, Dr. Phanikumar Mantha, Dr. Jiaguo Qi offered valuable advice and their time at many occasions. Their insights have vastly improved the quality of my work and shaped my scientific thinking. Dr. Remke van Dam, my fourth committee member generously poured his time and knowledge in to this work. It is with his effort and many time consuming trips to field sites especially when I couldn't keep up with it that I was able to complete my dissertation research.

During the five years of my graduate work many others contributed to the successful outcome I have experienced with this research. Dr. Jeff Andreasen, Dr. Dennis Gilliland, Dr. Alvin Smucker, and Dr. Jan Stephenson are thanked for their support with data and field equipment. Dr. Bryan Pijanowski, Dr. Jim Butler, and Dr. Jan Hendrix are acknowledged for their support with manuscripts and presentations. Michael Mores, Matt Malkowski, Samer Hariri, Cheryl Kendall, Matt Parsons, Dave Szymanski, Abby Norton, Randy Klevikas, and Paul Bloes provided many hours of arduous field and lab support. Without their help very little would have been accomplished.

Karen Tefend and Anthony Kendal became the most generous of hosts and best of friends at times that were the most difficult. Along with them Colleen McLean, Nick Welty, Amy Lansdale, and many others are greatly acknowledged for their years of friendship.

Udeni, my wife and our daughter Hiru made the most sacrifices and provided utmost support so that I could see the end and reach a goal I had set for myself some years ago. For them I dedicate this dissertation.

TABLE OF CONTENTS

List of Tables	viii
List of Figures	x
Chapter One: General Introduction.....	1
Objective.....	6
References	9
Chapter Two: Evaluating the influence of land cover on seasonal water budgets using Next Generation Radar (NEXRAD) rainfall and streamflow data	15
Abstract.....	16
Introduction	17
Approach	19
Study Sites.....	23
Evaluation of NEXRAD Rainfall Data.....	25
Results and Discussion.....	33
Summary and Conclusions	48
Acknowledgments.....	51
References	53
Chapter Three: Subsurface imaging of vegetation, climate, and root-zone moisture interactions	57
Abstract.....	58
Introduction	59
Methods	61
Results	65
Conclusions	70
Acknowledgements.....	71
References	72

Chapter Four: Integrating geophysics and hydrologic models to evaluate land-use impacts on groundwater resources.....	75
Introduction	75
Study sites	79
Field observations.....	83
Electrical Resistivity data acquisition and processing	86
Electrical resistivity and soil moisture.....	94
Soil Moisture Dynamics and Relevance to Recharge	95
Hydrologic simulations	99
Discussion and Conclusion.....	112
References	114
Chapter Five: Evaluating a range of approaches to derive hydrogeological information from electrical resistivity data.....	118
Introduction	118
Electrical Resistivity Imaging (ERI)	120
ERI and environmental variability	122
Electrical conductivity and volumetric soil moisture	122
Soil temperature and electrical conductivity.....	128
The effect of pore-water conductivity	132
ERI and time-lapse differencing.....	137
Soil moisture estimates with resistivity ratios	144
Conclusions	146
References	148

List of Tables

Table 2-1. Spearman's Ranked Correlation Statistics for Mean July to September (2002-2004) Volume Ratios and Other Watershed Variables for the 40 Selected Watersheds. Statistical significance ($p < 0.05$) is indicated by bold typeface.	35
Table 2-2. Spearman's Nonparametric Correlation Statistics for Land Cover and Other Watershed Variables for the 40 Selected Watersheds. Statistical significance is indicated by bold typeface.	39
Table 2-3. Multiple Regression Statistics for July September Mean (2002-2004) Streamflow:Rainfall and Base Flow:Rainfall Ratios and Watershed Attributes. The residuals from both fits were tested for normality with the Anderson-Darling test. Normality was not rejected; p values are 0.27 and 0.35, respectively.	40
Table 2-4. Estimated Annual Growing Season Recharge Amounts (July-September); in terms of annual rainfall and actual amounts in centimeters.	42
Table 4-1. Estimated soil hydraulic parameters for the three soil layers in the forest with standard errors of regression coefficients (S.E. Coeff) and confidence intervals.	106
Table 4-2. Estimated soil hydraulic parameters for the three soil layers in the grassland.	106
Table 4-3. Sensitivity of simulated cumulative transpiration $\sum T$ and bottom pressure head (h) in the forest to different root distributions. ERI Root is root distribution estimated with resistivity data, deRosany model used with a distribution coefficient of -0.9 (de Rosnay and Polcher 1998).	110

Table 4-4. Sensitivity of simulated evaporation (ΣE), transpiration (ΣT), and model bottom pressure head (h) in the forest to a $\pm 10\%$ adjustment in root water abstraction parameters (Feddes et al. 1974). ΣE , and ΣT are given as percent changes relative the base model. h_1 -minimum pressure head for active transpiration, h_2 -pressure- head for maximum transpiration efficiency, h_3 -limiting pressure head where transpiration ceases to occur at maximum efficiency, and h_4 -wilting point..... 110

Table 4-5. Sensitivity of cumulative infiltration (ΣI), transpiration (ΣT), evaporation (ΣE), and bottom pressure head (h) in the forest to a $\pm 10\%$ adjustment in soil parameters. ΣI , ΣT , and ΣE shown are percent changes compared to the base model with optimized soil hydraulic parameters..... 111

Table 5-1. Parameters for Archie's equation from laboratory measurements of soils at the study site. ρ_s is obtained from field resistivity data (for sand estimated with resistivity data from below the water table, and for clay estimated from datasets collected when the site was extremely wet). 124

List of Figures

- Figure 2-1. Locations of our study watersheds (shaded) with NEXRAD radar and rain gauge locations. Dashed lines show the effective range of the radar detectors. 23**
- Figure 2-2. RMS differences between NEXRAD and ground-based precipitation measurements at various sites with data spanning the 2002, 2003, and 2004 growing seasons. 27**
- Figure 2-3. Map of the percent absolute differences (calculated relative to observed gauged precipitation) between the 2004 (April-November) gauge and NEXRAD rainfall data. The Grand Rapids, Lansing, Flint, and Alpena gauges are known to be used by the WSR-88D system for real-time calibration of radar rainfall estimates (Ann Arbor and Grayling are missing 1 month of data, Harbor Beach is missing 2 months, and Montague is missing 3 months, and thus these months were not used in this analysis. 30**
- Figure 2-4. RMS differences for eight gauge locations using 2002, 2003, and 2004 monthly radar and ground-based gauge precipitation data. May RMSD calculation is based only on data from 2002 and 2004 due to missing NEXRAD grid data in MAY 2003. 31**
- Figure 2-5. Comparison of monthly (July-September) observed gauge and NEXRAD rainfall for 2002, 2003, and 2004. RMSE and bias (average NEXRAD rainfall-average observed gauge rainfall) are given in mm. 33**
- Figure 2-6. Percentage of agricultural land cover in watersheds compared to streamflow:rainfall ratios for July to September periods of 2002-2004. Each data point represents a watershed, and three watersheds with greater than 30% clay sediments are marked with a gray oval. 34**
- Figure 2-7. Average 2002-2004 quarter year base flow:drainage area ratios in high-intensity (>70%) and moderate-intensity (<50%) agricultural watersheds. The difference of the flow between the two types of watersheds are statistically significant (p value <0.05) in all quarters except January-March. 42**

Figure 2-8. Average of 2002-2004 January to May streamflow:drainage area ratios (cm). Higher values likely indicate greater snowmelt influence on the watershed hydrology. The contour map was generated by kriging the ratio calculated from data at the 113 USGS streamflow gauges shown on the map. Images in this dissertation are presented in color..... 43

Figure 2-9. The 2002-2004 monthly base flow:drainage area ratios and average monthly rainfall for 40 selected watersheds in Michigan. The peak growing season is clearly marked by higher leaf area indexes (LAI), which corresponds well with the decline in stream base flow during the same period. 45

Figure 2-10. Measured water table depths in two shallow wells in the northern portion of Michigan’s Lower Peninsula (see Figure 2-1for locations). A steady decline in water level is evident during the growing season (land use percentages in the watershed containing B12 are forests ~65%, shrubs/open land ~35%; G13, forests ~66%, agriculture ~28%). Note that the minimum water level is delayed significantly from the peak LAI and minimum base flow levels shown in Figure 2-9. 46

Figure 2-11. Recharge estimates for the July to September period, as a percent of NEXRAD bias adjusted rainfall in high-intensity agricultural (>70%) and moderate-intensity agricultural (<50%) watersheds. The difference in baseflow:rainfall ratios between the two types of watersheds are statistically significant (p value <0.05) in all years..... 48

Figure 2-12. Total monthly streamflow, and overland flow volumes normalized by watershed area along with rainfall averaged across the 40 study watersheds. ... 49

Figure 3-1. Soil moisture from probes at the site and the average of the 20 and 86.5 cm depth ERI moisture estimates for all datasets corrected with site temperatures. Precipitation data is shown for a nearby gage. The color bar shows the state of the forest canopy, vertical lines mark data collection dates, and shaded areas above the bar are differential inversion periods for Figure 3-2. Images in this dissertation are presented in color..... 63

Figure 3-2. Differential resistivity panels for approximately one-month periods. a) Early fall (10/18 – 11/15), b) late fall (11/22 – 12/20), c) winter (1/5 – 2/9), d) spring (3/16 – 4/20), and e) summer (6/10 – 7/2). Trees are not to scale; 80 cm of relief along the array is included in the inversion. Red triangles locate moisture probes and temperature arrays. A decrease in resolution with depth and associated smoothing artifacts can cause resistivity differences below the water table. Images in this dissertation are presented in color..... 66

Figure 3-3. Spatial and temporal distribution of soil moisture estimated across the ecotone. Images in this dissertation are presented in color. 69

Figure 3-4. Laterally averaged changes in soil moisture below the forest (36-51 m) and the grassland (92-107 m) between early-growing (April to early May) and peak-growing periods (July to August). Images in this dissertation are presented in color. 71

Figure 4-1. Locations of East Lansing and Traverse City, Michigan field sites where soil moisture dynamics were imaged with ERI. 79

Figure 4-2. East Lansing field site. A-B: electrode array with 84 electrodes at 1.5m separation. E3, E26, E70 are groundwater observation wells. Temperature/soil moisture sensor locations have moisture probes at 20 & 80 cm depth. Temperature probes are at 5, 10, 20, 40, 80,117, and 147cm depth at each location. 81

Figure 4-3. Traverse City study site. A-B: electrode array with 84 electrodes at 1.5m separation. B3 is the groundwater observation well. Moisture sensor locations shown have probes at 20 and 80 cm depths, and temperature sensors are at 5, 10, 20, 40, 80, 117, and 147 cm depths. 82

Figure 4-4. Groundwater observations since October 2007 at the East Lansing study site. Depth to water from the surface is shown for each well. Since the surface elevation at the forest well (E3, Figure 4-2) is 99 cm lower than the surface elevation at the grassland well the two vertical axis are offset by a similar amount. The wells are approximately 90 meters apart. 84

Figure 4-5. Groundwater observations at the Traverse City study site. Annual recharge-discharge cycles related to the growing season and spring snowmelt are evident in this well record. 85

Figure 4-6. Soil moisture measurements below forest and the grassland at the East Lansing site. 86

Figure 4-7. Cross-sectional view of the East Lansing study site with a representative late-summer subsurface resistivity distribution. Images in this dissertation are presented in color. 88

Figure 4-8. Cross-sectional view of the Traverse City study site with a representative late-summer subsurface resistivity distribution. Images in this dissertation are presented in color..... 89

Figure 4-9. The temporal variability of subsurface (0-6m, surface to below seasonal water table) resistivity distribution below the forest and the grassland at the East Lansing site on selected dates. Mean, 25th & 75th percentiles, and the range for each date are shown. 91

Figure 4-10. Mean resistivity values in the 0-2m and 2-4m depths through time. Similar resistivities in the 2-4m range during the latter part of the study period shown coincide with higher observed groundwater elevations at the research site..... 93

Figure 4-11. ERI estimated soil moisture and the observed moisture in the East Lansing study site (Forest). The arithmetic average of the 20 and 80cm cm moisture observations are shown. 95

Figure 4-12. ERI calculated transient soil moisture (20-80cm cm arithmetic average) in the grassland and the forest. Higher moisture levels in the grassland are observed on each of the ERI data collection dates. 96

Figure 4-13. Temporal soil moisture changes in ~15 wide zones below the grassland and the forest. Cooler colors indicate moisture increases and warmer colors are moisture decreases. C is the main fall recharge period, followed by spring snowmelt (D). A, B, and E are growing season moisture deficits due to plant water use. Images in this dissertation are presented in color. 98

Figure 4-14. A simplified illustration of the soil texture and stratigraphy (from soil cores) in the forest and the grassland. Different soil texture units identified in field soil cores were combined to three representative layers in the vadose zone flow model (right). Images in this dissertation are presented in color..... 100

Figure 4-15. Conceptual framework for integrating geophysical soil moisture estimates with hydrologic modeling to estimate groundwater recharge. Soil parameters θ_s , α , n , K_s are optimized in stage 2, and plant water stress function parameters h_1 , h_2 , h_3 , h_4 , are calibrated in stage 3. 101

Figure 4-16. Laterally averaged changes in soil moisture below the forest and the grassland between early-growing (April to early May) and peak-growing periods (July to August) (from Jayawickreme et al., 2008)..... 103

Figure 4-17. Cumulative precipitation throughfall (a), representative leaf area indexes (b) from MODIS, calculated cumulative potential transpiration (c) and soil evaporation (d) inputs for hydrologic simulations from ILHM. 104

Figure 4-18. Simulated vs. ERI estimated soil moisture in the forest. Data is from 10 depths within the first 3m of the subsurface..... 105

Figure 4-19. Simulated vs. ERI estimated soil moisture in the grassland with data from nine depths in the first 3m of the subsurface. 105

Figure 4-20. Measured and simulated groundwater table in the forest with optimized soil hydraulic parameter sets in the 1D-Hydrus model. These observation data were not used in the optimization for hydraulic parameters in the forest. 107

Figure 4-21. Measured and simulated groundwater table in the grassland with optimized soil hydraulic parameter. 107

Figure 4-22. Observed (ERI calculated) vs. simulated moisture in the forest during summer (June-October, 2007)..... 109

Figure 4-23. Observed vs. simulated soil moisture in the grassland from June to October, 2007..... 109

Figure 5-1 Electrode positions for Wenner (top) and Dipole-dipole (bottom) electrode configurations. A, B are current electrodes and M, N are potential electrodes. 'a' is the distance between electrodes used for measurements, and n is an integer. 121

Figure 5-2. Data coverage for Wenner and dipole-dipole electrode configurations for an 84 electrode array with 1.5m electrode separations. Higher data density near the electrode positions is obtained with the dipole-dipole configuration compared to Wenner, where data coverage is evenly distributed. 1453 and 1134 measurements are obtained with these dipole-dipole and Wenner arrays respectively..... 121

Figure 5-3. Soil moisture estimates from ERI (dipole-dipole) data compared to other independent measurements of soil moisture at the study site. 125

Figure 5-4. The sensitivity of ERI derived saturation to m , and ρ_s estimates. The high (grassland-98 Ohm-m) and low (forest-65 Ohm-m) values for saturated resistivity were derived from field resistivity data. Some of the differences in saturated resistivity between the grassland and forest are due to observed groundwater conductivity differences. 126

Figure 5-5. Water table elevation observations and resistivity measurements in the forest (a), grassland (b) from November 2007 to June 2008. The correlation between water table elevation and contours of the resistivity estimates is much clearer in the forest relative to the grassland. Images in this dissertation are presented in color. 127

Figure 5-6. Seasonal grassland soil temperature fluctuations at the study site. Inset shows diurnal soil temperature differences between the grassland and the forest stand over a span of three days in June. 129

Figure 5-7. The influence of temperature on resistivity and the resulting difference in calculated soil moisture with Archie's equation. 130

Figure 5-8. The influence of m on soil resistivity-temperature dependence at two different soil temperatures (28°C and 12°C). The sensitivity to m is important at higher temperature ranges. 131

Figure 5-9. Percent change in resistivity from August 10, 2007 to January 11, 2008 without (a) and with (b) temperature correction. Prominent changes in the grassland (a) do not appear once the temperature correction is added (b). Images in this dissertation are presented in color. 131

Figure 5-10. Groundwater conductivity measured at the research site in the grassland and forest observation wells (a). Pore-water and bulk electrical resistivity relationship calculations based on Archie's equation for various degrees of saturation (b). A soil with 30% porosity, fitting constant, $m=1.16$ and an n value of 2, characteristic of sandy soils, was used in the calculation. 133

Figure 5-11. Potential influence of groundwater conductivity differences below the grassland and forest. Higher resistivity values below water table (~4 m from surface) in the grassland is likely due to the lower measured groundwater conductivities in the grassland. Data shown is temperature corrected and the soils are similar on either side of the ecotone (the forest-grassland boundary). Images in this dissertation are presented in color. 135

Figure 5-12. Measured bulk electrical resistivity difference between the grassland and the forest ($\rho_{grassland}-\rho_{forest}$). Higher resistivities below the water table in the grassland are consistent with the lower measured groundwater conductivities there. The shaded area indicates the approximate range of water table change in the grassland between March and June 2008. 136

Figure 5-13. Data characteristics of three resistivity data sets from the study site, which were used for difference inversion method analysis. Images in this dissertation are presented in color..... 139

Figure 5-14. Comparisons of base dataset effects. B1, B2, and B3 are three separate inverted field datasets. The notation B1>>B3 refers B3 calculation with B1 as the base dataset in the difference inversion. Only the data from the top 5m were selected for the analysis. 141

Figure 5-15. Comparison of computed B1, B2, B3 with different with respect to others in the difference inversion..... 142

Figure 5-16. Spatial distribution of differences from difference inversions with B1, B2, and B3 datasets. Correlations between each dataset are shown in Figure 5-15. The choice of base dataset has a larger impact on the resistivity based interpretations in the forest. Images in this dissertation are presented in color. 143

Figure 5-17. Laboratory measure resistivity and soil water contents for soil samples collected from multiple locations at the study site. Images in this dissertation are presented in color..... 144

Figure 5-18. Soil moisture ratios observed with point gauges and soil moisture ratios calculated with ERI near the location where point gauges are located... 145

Chapter One

General Introduction

Land-use and land cover (LULC) changes have important consequences on the functioning of regional to global environmental systems. Significant land use changes may seriously impact a region's water resources by altering surface water, groundwater, and soil moisture patterns, and perturb groundwater recharge processes (Zhang et al. 2001; Walker et al. 2002; Jayawickreme and Hyndman 2007; Pijanowski et al. 2007) and water quality (Lenat and Crawford 1994; Paul and Meyer 2001; Tong and Chen 2002; Wayland et al. 2003). LULC also has a strong influence on land-atmosphere interactions and energy exchange characteristics at the surface-atmosphere boundary layer with global climate consequences. Land-use characteristics affect the partitioning of surface incident energy into latent and sensible heat components. Alterations to these surface fluxes of water vapor and heat can affect regional atmospheric temperatures, precipitation, and other climate variables (Pitman et al. 2004; Pielke 2005). Local- to regional-scale land-use changes and global climate teleconnections are also well documented (Marland et al. 2003; Koster et al. 2004; Werth and Avissar 2005).

Continued global population growth and demand for food and energy security are likely to locally accelerate the rate of LULC change in many parts of the world. Additionally, regional scale changes will be brought about by an increasingly warming global climate with elevated atmospheric CO₂

concentrations and other environmental changes (Houghton 1994). Beyond the impacts on ecosystems and bio-diversity, LULC change may have significant world-wide socioeconomic and geopolitical consequences. Understanding, managing and mitigating the implications of LULC change is therefore imperative for environmental and societal sustainability.

Throughout human history, people have been affecting the terrestrial biosphere through land-use changes for agriculture, energy, natural resources and other purposes. However, an interest in understanding the consequences of these land-use changes on the hydrologic cycle, particularly the subsurface components has emerged only recently. As a result substantial knowledge gaps exist in our understanding of both short and long-term impacts of LULC and LULC change on water resources. The potential impacts of these changes on subsurface hydrology and hydrologic processes are significant (Scanlon et al. 2005). Alterations to groundwater recharge processes due to LULC change can damage the viability of groundwater resources that are a critical source of fresh water around the world. At current consumption and population growth rates (United Nations, 1999), significant conversions of natural ecosystems to agriculture will occur in the next half century (Tilman et al. 2001). Population growth will also result in conversion of substantial natural lands to urban land-uses. In the US alone the proportion of developed land base is projected to approximately double by 2025 (Alig et al. 2004). While similar global projections are not readily available, current trends in economic and social development in Asia, South America, and other regions is likely to increase the

current urban/suburban land base substantially (Lambin et al. 2001).

Compounding the impacts of these issues are population migrations that will result from climate change driven sea level rises and increased aridity in some regions of the world (Byravan and Rajan 2006).

Changes in LULC can alter soil characteristics, thereby affecting runoff and infiltration properties of soils. Soil tillage with agricultural land-uses for example affect groundwater recharge by changing the soil structure (Oleary 1996; Leduc et al. 2001). Increased percentages of impervious surfaces with urbanization are known to generally increase runoff, evaporation, and decrease groundwater recharge (Grove et al. 2001; Rose and Peters 2001; Burns et al. 2005; Jayawickreme and Hyndman 2007). Significant and dynamic changes in recharge are also accompanied by changes in vegetation where one or more species is supplanted by another in a landscape (Engel et al. 2005; Noretto et al. 2007; Scanlon et al. 2007). Such changes can lead to modifications of fractional vegetation cover and hence precipitation interception, solar insolation, and wind turbulence characteristics. Perennial, deciduous, or transient traits of vegetation species can introduce important seasonal forcings on the environment.

Replacing perennial vegetation with annual crops and crop rotations for example have lead to increased recharge during fallow periods (Oconnell et al. 1995; Zhang et al. 1999). Changes in rooting depths with crop rotations can affect both the quantity and quality of groundwater. Increased recharge and solute mobilization have caused soil salinization and water quality degradation in large areas of southwestern Australia after land clearing (Schofield and Ruprecht

1989; Schofield 1992; Pierce et al. 1993; Petheram et al. 2002). In regions where deep rooted trees and other woody plants are gradually replacing shallow rooted grasslands, decreased recharge and increased discharge of groundwater by trees reaching deeper into the subsurface have been observed (Jobbagy and Jackson 2004). Woody plant encroachment of native grasslands has also increased in North America during the last century with fire suppression and other land management practices (Van Auken 2000; Coppedge et al. 2001; Heisler et al. 2003; Pielke et al. 2007). In northern latitudes, vegetation changes can alter frozen soil dynamics by affecting snow accumulation and snowpack stability during the winter months (van der Kamp et al. 1999; van der Kamp et al. 2003). With deeper frozen soil columns, recharge potential is likely to be reduced during the spring snowmelt, which is an important period of groundwater recharge in these regions (Hayashi et al. 2003).

The vadose zone is the critical link between groundwater and the land surface. The partitioning of precipitation into runoff and infiltration is largely governed by the physical characteristics of the near surface soils or other geologic materials. The fraction of infiltrated precipitation volume that eventually reach the water table depends on the properties and processes of the vadose zone. Principal among properties are the soil water retention and hydraulic conductivities of the constituent materials. Where these physical conditions are favorable, a significant portion of the infiltrated water can reach the water table. In natural settings however, vegetation has evolved to effectively utilize the reservoir of water in the vadose zone, and hence these dynamics play an

important role in groundwater recharge. It is often recognized that vegetation density and diversity across landscapes is a reflection of soil moisture and nutrient dynamics (Baillie et al. 1987; Swaine 1996). Central to understanding the influence of vegetation on subsurface water fluxes is plant root distribution and dynamics. This is also a topic of substantial importance for understanding ecosystem carbon and water fluxes (Rodriguez-Iturbe 2000; Koster and Suarez 2001; Katul et al. 2007).

Root distributions and water abstraction characteristics (i.e. wilting point) of vegetation vary significantly between species and regions (Canadell et al. 1996; Jackson et al. 1996). Despite being studied for over two centuries (Jackson et al. 1996), there are significant knowledge gaps about the spatiotemporal functions of plant roots. Existing insights are primarily from studies that have employed techniques from excavations to radio-isotopes (Dambrine et al. 1997; Boutton et al. 1999). While these have been immensely helpful for conceptualizing root zone geometries and some aspects of root zone dynamics, the static and localized nature of these observations limit their use in large scale models. Newer approaches that can link subsurface processes with above-ground remotely-sensed large scale observations from space and air borne platforms can contribute significantly to improving and incorporating vegetation dynamics in regional hydrologic, climate, and other models.

Objective

The broad objective of this research is to identify and quantify the potential impacts of land-use (the manner in which the land is used), land-cover (the physical and biological cover over land surface), and vegetation on groundwater recharge. The research presented focuses on the temperate American mid-west where land use is dominated by agriculture and vegetation being the primary land cover. Groundwater recharge in the region primarily occurs through diffuse recharge processes and is strongly influenced by vegetation and seasonal climate dynamics. The vadose zone, through which recharge primarily occurs, is an important focus of this research. This zone is also the region where plants obtain most or all of their nutrients and water required for growth and maintenance. Gaining insights into the vadose zone and its processes is therefore necessary to understand land-use impacts on groundwater recharge. In this research, a novel approach is used to explore and quantify dynamic vadose zone interactions between vegetation, climate, and soil moisture.

The research in this dissertation is presented in five chapters. Chapter two examines the implications of LULC on groundwater recharge at watershed scales by analyzing streamflow across a range of watersheds. Baseflow (groundwater contribution to streamflow), overland flow, (surface flow due to infiltration excess precipitation), and total flow (sum of baseflow and overland flow) components of streamflow in watersheds ranging from 20 to >1000 km² are linked with land-uses (forests, agriculture, urban etc.), soil, and morphological attributes using statistical measures. Various spatial and non-spatial data sources, both

customary and non-traditional, were evaluated and utilized to quantify the watershed hydrologic budgets and identify how LULC affect various flux components of the water budget.

In chapter three, the vadose zone interactions between climate, soil moisture, and vegetation is explored. A novel approach combining geophysics and petrophysical models is utilized to image subsurface soil moisture dynamics across a forest-grassland ecotone. Electrical resistivity data collected at the ecotone over multiple seasons is first converted to soil moisture using petrophysical relationships based on laboratory analysis of soils from the study site. The two dimensional soil moisture distributions obtained are then correlated with the vegetation across the ecotone. Seasonal soil moisture differences identified and correlated with vegetation at the study site highlight potentially significant implications of large scale biological land cover changes on hydrology and groundwater recharge.

Chapter four integrates geophysical measurements with hydrologic modeling to quantify groundwater recharge differences that result from above ground vegetation differences. The geophysical estimates of soil moisture are used to derive soil hydraulic parameters for a one dimensional flow model to represent the field site. Evidence of root zone geometries and distributions from geophysical data is used to define the influence of vegetation on subsurface soil moisture dynamics. However, coupling subsurface geophysical observations with process-based hydrologic models remains a difficult task and as such the integration made in this research is only presented as a first approximation.

The potential of electrical resistivity method for investigating and acquiring subsurface hydrologic characteristics and quantities is explored in Chapter five of this dissertation. The strong dependence of electrical conductivity on soil moisture provides the basis for its use in hydrologic investigations. However, deriving soil moisture from resistivity data involves several other considerations. Data acquisition and processing, as well as the effects of other environmental variables all influence the ability to derive accurate estimates of soil moisture from resistivity data. The potential implications of these are discussed and possible improvements are suggested in chapter five with field examples from our research site.

References

- Alig, R.J., J.D. Kline, et al. 2004. Urbanization on the us landscape: Looking ahead in the 21st century. *Landscape and Urban Planning* 69:219-234.
- Baillie, I.C., P.S. Ashton, et al. 1987. Site characteristics and the distribution of tree species in mixed dipterocarp forest on tertiary sediments in central sarawak, malaysia. *Journal of Tropical Ecology* 3:201-220.
- Boutton, T.W., S.R. Archer, et al. 1999. Stable isotopes in ecosystem science: Structure, function and dynamics of a subtropical savanna. *Rapid Communications in Mass Spectrometry* 13:1263-1277.
- Burns, D., T. Vitvar, et al. 2005. Effects of suburban development on runoff generation in the croton river basin, new york, usa. *Journal of Hydrology* 311:266-281.
- Byravan, S., and S.C. Rajan. 2006. Providing new homes for climate change exiles. *Climate Policy* 6:247-252.
- Canadell, J., R.B. Jackson, et al. 1996. Maximum rooting depth of vegetation types at the global scale. *Oecologia* 108:583-595.
- Coppedge, B.R., D.M. Engle, et al. 2001. Landscape cover type and pattern dynamics in fragmented southern great plains grasslands, usa. *Landscape Ecology* 16:677-690.
- Dambrine, E., M. Loubet, et al. 1997. Localisation of mineral uptake by roots using sr isotopes. *Plant and Soil* 192:129-132.
- Engel, V., E.G. Jobbagy, et al. 2005. Hydrological consequences of eucalyptus afforestation in the argentine pampas. *Water Resources Research* 41.

- Grove, M., J. Harbor, et al. 2001. Impacts of urbanization on surface hydrology, little eagle creek, indiana, and analysis of lthia model sensitivity to data resolution. *Physical Geography* 22:135-153.
- Hayashi, M., G. van der Kamp, et al. 2003. Focused infiltration of snowmelt water in partially frozen soil under small depressions. *Journal of Hydrology* 270:214-229.
- Heisler, J.L., J.M. Briggs, et al. 2003. Long-term patterns of shrub expansion in a c-4-dominated grassland: Fire frequency and the dynamics of shrub cover and abundance. *American Journal of Botany* 90:423-428.
- Houghton, R.A. 1994. The worldwide extent of land-use change. *Bioscience* 44:305-313.
- Jackson, R.B., J. Canadell, et al. 1996. A global analysis of root distributions for terrestrial biomes. *Oecologia* 108:389-411.
- Jayawickreme, D.H., and D.W. Hyndman. 2007. Evaluating the influence of land cover on seasonal water budgets using next generation radar (nexrad) rainfall and streamflow data. *Water Resources Research* 43:W02408.
- Jobbagy, E.G., and R.B. Jackson. 2004. Groundwater use and salinization with grassland afforestation. *Global Change Biology* 10:1299-1312.
- Katul, G., A. Porporato, et al. 2007. Stochastic dynamics of plant-water interactions. *Annual Review of Ecology Evolution and Systematics* 38:767-791.
- Kearey, P., and M. Brooks. 1991. An introduction to geophysical exploration. Second edition ed. Blackwell Science.
- Koster, R.D., P.A. Dirmeyer, et al. 2004. Regions of strong coupling between soil moisture and precipitation. *Science* 305:1138-1140.

- Koster, R.D., and M.J. Suarez. 2001. Soil moisture memory in climate models. *Journal of Hydrometeorology* 2:558-570.
- Lambin, E.F., B.L. Turner, et al. 2001. The causes of land-use and land-cover change: Moving beyond the myths. *Global Environmental Change-Human and Policy Dimensions* 11:261-269.
- Leduc, C., G. Favreau, et al. 2001. Long-term rise in a sahelian water-table: The continental terminal in south-west niger. *Journal of Hydrology* 243:43-54.
- Lenat, D.R., and J.K. Crawford. 1994. Effects of land-use on water-quality and aquatic biota of 3 north-carolina piedmont streams. *Hydrobiologia* 294:185-199.
- Marland, G., R.A. Pielke, et al. 2003. The climatic impacts of land surface change and carbon management, and the implications for climate-change mitigation policy. *Climate Policy* 3:149-157.
- Nosetto, M.D., E.G. Jobbagy, et al. 2007. The effects of tree establishment on water and salt dynamics in naturally salt-affected grasslands. *Oecologia* 152:695-705.
- Oconnell, M.G., G.J. Oleary, et al. 1995. Potential groundwater recharge from fallowing in north-west victoria, australia. *Agricultural Water Management* 29:37-52.
- Oleary, G.J. 1996. The effects of conservation tillage on potential groundwater recharge. *Agricultural Water Management* 31:65-73.
- Paul, M.J., and J.L. Meyer. 2001. Streams in the urban landscape. *Annual Review of Ecology and Systematics* 32:333-365.
- Petheram, C., G. Walker, et al. 2002. Towards a framework for predicting impacts of land-use on recharge: 1. A review of recharge studies in australia. *Australian Journal of Soil Research* 40:397-417.

- Pielke, R.A. 2005. Land use and climate change. *Science* 310:1625-1626.
- Pielke, R.A., J. Adegoke, et al. 2007. An overview of regional land-use and land-cover impacts on rainfall. *Tellus Series B-Chemical and Physical Meteorology* 59:587-601.
- Pierce, L.L., J. Walker, et al. 1993. Ecohydrological changes in the murray-darling basin .3. A simulation of regional hydrological changes. *Journal of Applied Ecology* 30:283-294.
- Pijanowski, B., D.K. Ray, et al. 2007. Using backcast land-use change and groundwater travel-time models to generate land-use legacy maps for watershed management. *Ecology and Society* 12.
- Pitman, A.J., G.T. Narisma, et al. 2004. Impact of land cover change on the climate of southwest western australia. *Journal of Geophysical Research-Atmospheres* 109.
- Rodriguez-Iturbe, I. 2000. Ecohydrology: A hydrologic perspective of climate-soil-vegetation dynamics. *Water Resources Research* 36:3-9.
- Rose, S., and N.E. Peters. 2001. Effects of urbanization on streamflow in the atlanta area (georgia, usa): A comparative hydrological approach. *Hydrological Processes* 15:1441-1457.
- Scanlon, B.R., R.W. Healy, et al. 2002. Choosing appropriate techniques for quantifying groundwater recharge. *Hydrogeology Journal* 10:18-39.
- Scanlon, B.R., I. Jolly, et al. 2007. Global impacts of conversions from natural to agricultural ecosystems on water resources: Quantity versus quality. *Water Resources Research* 43:W03437.
- Scanlon, B.R., R.C. Reedy, et al. 2005. Impact of land use and land cover change on groundwater recharge and quality in the southwestern us. *Global Change Biology* 11:1577-1593.

- Schofield, N.J. 1992. Tree planting for dryland salinity control in australia. *Agroforestry Systems* 20:1-23.
- Schofield, N.J., and J.K. Ruprecht. 1989. Regional-analysis of stream salinization in southwest western-australia. *Journal of Hydrology* 112:19-&.
- Swaine, M.D. 1996. Rainfall and soil fertility as factors limiting forest species distributions in ghana. *Journal of Ecology* 84:419-428.
- Tilman, D., J. Fargione, et al. 2001. Forecasting agriculturally driven global environmental change. *Science* 292:281-284.
- Tong, S.T.Y., and W.L. Chen. 2002. Modeling the relationship between land use and surface water quality. *Journal of Environmental Management* 66:377-393.
- Van Auken, O.W. 2000. Shrub invasions of north american semiarid grasslands. *Annual Review of Ecology and Systematics* 31:197-215.
- van der Kamp, G., M. Hayashi, et al. 2003. Comparing the hydrology of grassed and cultivated catchments in the semi-arid canadian prairies. *Hydrological Processes* 17:559-575.
- van der Kamp, G., W.J. Stolte, et al. 1999. Drying out of small prairie wetlands after conversion of their catchments from cultivation to permanent brome grass. *Hydrological Sciences Journal-Journal Des Sciences Hydrologiques* 44:387-397.
- Walker, G.R., L. Zhang, et al. 2002. Estimating impacts of changed land use on recharge: Review of modelling and other approaches appropriate for management of dryland salinity. *Hydrogeology Journal* 10:68-90.
- Wayland, K.G., D.T. Long, et al. 2003. Identifying relationships between baseflow geochemistry and land use with synoptic sampling and r-mode factor analysis. *Journal of Environmental Quality* 32:180-190.

Werth, D., and R. Avissar. 2005. The local and global effects of african deforestation. Geophysical Research Letters 32.

Zhang, L., W.R. Dawes, et al. 1999. Estimating episodic recharge under different crop/pasture rotations in the mallee region. Part 2. Recharge control by agronomic practices. Agricultural Water Management 42:237-249.

Zhang, L., W.R. Dawes, et al. 2001. Response of mean annual evapotranspiration to vegetation changes at catchment scale. Water Resources Research 37:701-708.

Chapter Two

Jayawickreme, D. H., and D. W. Hyndman (2007), Evaluating the influence of land cover on seasonal water budgets using Next Generation Radar (NEXRAD) rainfall and streamflow data, *Water Resour. Res.*, 43, W02408, doi:10.1029/2005WR004460.

Abstract

Accurate estimates of fluxes between different components of the hydrosphere are needed for water resources management at the watershed scale. Runoff and evapotranspiration are critical fluxes that are heavily influenced by land cover characteristics; however, our understanding of the interactions between land cover attributes and these fluid fluxes is generally limited by inadequate regional data to capture variations in both climatic conditions and landscape characteristics. This limitation is largely avoided by integrating data from Next Generation Radar (NEXRAD) precipitation systems with widely available streamflow, land cover, and other Geographic Information System data sets. Such data integration facilitates development of rapid and reliable methods for estimating hydrologic fluxes at desirable temporal and spatial scales. In this study, we calculate ratios of streamflow to NEXRAD rainfall over the peak growing season for 40 watersheds across Michigan and use these to evaluate the landscape factors that influence groundwater recharge rates. Results indicate that ratios of streamflow and baseflow to rainfall are strongly influenced by land cover attributes. Stream baseflow analyses indicate that approximately 5% of the July to September rainfall becomes recharge in high-intensity agriculture (>70%) watersheds compared to 15% in moderate intensity agriculture (<50%) watersheds across our study region during the same period. A strong negative correlation was also found between intensive agriculture and the streamflow:rainfall ratio during summer and early fall periods.

Introduction

Understanding and evaluating water budgets in small to regional watersheds is critical for a range of resource management decisions. Water fluxes between different components of the hydrosphere change over a range of temporal and spatial scales due to variations in climatic conditions and landscape characteristics. Surface hydrological properties and processes such as soil moisture, runoff, and evapotranspiration are heavily influenced by land use and land cover characteristics, which we will refer to as land cover for simplicity. In addition, human activities and the accompanied land cover changes have the potential to significantly alter the local hydrology and cause long-term environmental changes (Dow and DeWalle, 2000; Walker et al., 2002; Costa and Foley, 2000; Pielke et al., 1998). Despite this potential, our understanding of the interactions between land cover and hydrology has been limited by inadequate data collection and integration at regional scales.

Runoff, evapotranspiration (ET), groundwater recharge, and changes in aquifer storage due to groundwater outflows and pumping are the main processes that redistribute precipitation in hydrologic systems in addition to snowmelt in colder regions. While runoff and aquifer storage can often be evaluated with a reasonable degree of accuracy, the most important components for watershed management, ET and groundwater recharge, are difficult to quantify. Commonly used methods including hydrograph separation, groundwater budget analysis, and tracer analysis coupled with groundwater models can be used to estimate recharge rates at various spatial scales (Scanlon

et al., 2002). However, large data requirements and other limitations have made it difficult for watershed managers and other decision makers to develop accurate estimates using such methods. Partly in response to these limitations, relatively simpler techniques using water balance models and Geographic Information Systems (GIS) have recently been introduced (e.g., Cherkauer and Ansari, 2005; Szilagyi et al., 2004). Nevertheless, most such approaches do not describe the impact of land cover on watershed hydrology and groundwater recharge at short timescales. In regions such as Michigan, with distinct seasonal changes in land cover (vegetation) and spatially diverse land use practices, vegetation dynamics are a key component of any hydrologic analysis. This paper examines the influence of land cover attributes on hydrologic fluxes at watershed scales on a seasonal basis. We use commonly available data sources to obtain watershed attributes and flux budgets for 40 watersheds, and we statistically link the flux budget characteristics with the watershed attributes. Since evapotranspiration (ET) is a key component of the water budget during the growing season and it is directly related to land cover characteristics (Mo et al., 2004; Finch, 1998), we also compare the streamflow and groundwater recharge differences of high-intensity and moderate-intensity agricultural systems. This analysis provides insight into the potential impacts of land use decisions on watershed hydrology.

Approach

Seasonal analysis of the ratio between total water input (precipitation) and outflows (streamflow and its components; overland flow and base flow) to a watershed during specified time intervals can provide insight into the mechanisms that redistribute moisture (e.g., runoff, recharge, ET). We evaluated correlations between streamflow: rainfall ratios and watershed characteristics (e.g., land cover, geologic materials, and soils) to help understand how these attributes influence hydrologic processes at watershed scales. We calculated the streamflow:rainfall ratios over the approximate peak growing season for 40 different watersheds using hourly Next Generation Radar (NEXRAD) precipitation data from the National Weather Service (NWS) and streamflow from U.S. Geological Survey (USGS) daily records. Prior to this analysis, the accuracy of NEXRAD data was evaluated by comparing it to observations from ground-based gauges, as described in more detail below in section 4.

The July-September period was chosen for the water budget calculations both to minimize the effects of snowmelt recharge on the analysis and to capture the influence of vegetation on watershed hydrology. This period corresponds to both the low streamflow period based on USGS records and the peak growing season of the region based on mean leaf area index (LAI, one-sided green leaf area or projected needle leaf area per unit ground area). The LAI values for the region were obtained from the 1-km Moderate Resolution Imaging Spectroradiometer (MODIS) 8 day composite data product (version 4) from the National Aeronautic and Space Administration (NASA). We used the MODIS

Reprojection Tool (USGS, 2004) to convert MODIS data in hierarchical data format (HDF) into Georeferenced Tag Image File Format (GEOTIFF) and ESRI grids. The spatial analyst extension and zonal statistics tools in ESRI ArcGIS software were used to extract mean LAI values for watersheds by overlaying a watershed boundary coverage on the LAI grids in ESRI ArcMap (version 9.1).

The spatially averaged NEXRAD precipitation values for each study watershed were calculated using the ArcMap zonal statistics tool on 100 m resampled NEXRAD grid cells within each watershed boundary. Daily, monthly, and longer-period precipitation estimates were subsequently derived from the hourly precipitation estimates. We automated the hourly precipitation extraction process using custom scripts (included in the auxiliary material) written in Visual Basic for Applications (VBA) integrated with ESRI ArcGIS, which load and unload data from ArcMap, and calculate mean watershed precipitation amounts with zonal statistics tools. This significantly improved the efficiency of processing 2000 individual NEXRAD grids for each of the 40 watersheds. Correction coefficients obtained from the regressions between July–September monthly NEXRAD and monthly gauged precipitation were used to adjust for the bias from NEXRAD data before utilizing it in mass balance analyses.

Total monthly base flow and overland flow volumes were estimated from the daily mean streamflow records using the PART computer program (Rutledge, 1998), which estimates base flow from daily streamflow records based on antecedent streamflow recession. This approach assumes spatially diffused recharge to the water table, uniform aquifer thicknesses, uniform hydraulic

conductivities and storage characteristics as well as minimal regulation and diversion of streamflow within the gauged watershed. Although these assumptions are essentially never met in real aquifer systems, this provides an objective tool to evaluate base flow. In addition, heterogeneities in soil properties tend to be at a much smaller scale than that of the watersheds we analyzed in this study, thus the localized impacts likely average out. Base flow estimates obtained with PART have been shown to be comparable to that obtained with various other manual methods (Rutledge, 1998). Linear interpolation of base flows during times that do not fit the antecedent criteria used in PART would lead to base flow estimation errors. However, errors resulting from the linear interpolation have been shown to be minimal for monthly or longer timescales (Rutledge, 1998).

Land cover percentages (croplands, forests, urban areas, wetlands, etc.) for watersheds were calculated based on the National Land Cover Dataset (NLCD) (USGS, 1999) and Anderson level I classes (Anderson et al., 1976). The forest cover percentage for each watershed was obtained by aggregating the deciduous, evergreen and mixed forest classes in NLCD. Pasture/hay, row crops, and small grain classes were combined to obtain the total percentage of agricultural uses. Total urban land cover percentages were obtained by combining low-intensity residential, high-intensity residential, and commercial/industrial/transportation classes.

The distribution of Quaternary geologic materials was obtained from a digital coverage of Farrand and Bell (1982) (data available at

<http://www.mcqi.state.mi.us/mgdl/>), and were aggregated into five broad classes (glacial tills, end moraine tills, outwash sand and gravel, lacustrine clay and silt, and lacustrine sand and gravel) for each watershed. On the basis of State Soil Geographic (STATSGO) database for Michigan (available at http://www.nrcs.usda.gov/products/data_sets/statsgo/data/index.html), we also categorized the watershed soils into three different drainage classes that were expected to influence streamflow characteristics in the study region (extremely to somewhat extremely well drained, well to moderately well drained, and poorly to very poorly drained). Statistical correlations between watershed attributes (land cover, Quaternary geology, soil drainability, and watershed morphology) and the average 2002–2004 volume ratios (streamflow:rainfall, overland flow:rainfall, and base flow:rainfall) were evaluated using nonparametric Spearman's correlations. The Kruskal-Wallis (nonparametric) test along with the chi-square approximation for its two-sided p value was used to compare base flow and recharge differences in high intensity (>70%) and moderate-intensity (<50%) agricultural watersheds. Two-sided p values at level 0.05 were used to test statistical significance. Nonparametric statistical methods were used in this study to minimize the effects of assumptions associated with parametric correlation methods. We also used stepwise multiple regressions and standard least squares fits as exploratory methods to evaluate variability of streamflow:rainfall and base flow:rainfall ratios between watersheds, and to explain the variability of the ratios in terms of land cover and other watershed attributes.

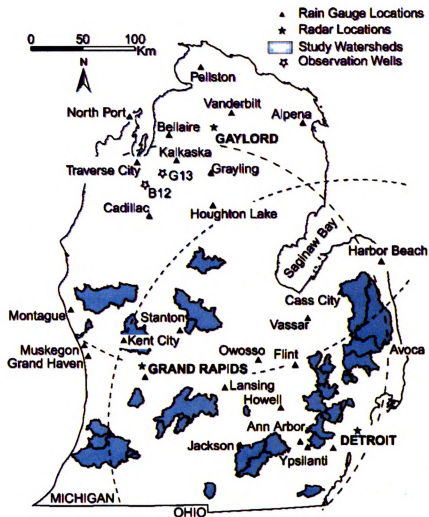


Figure 2-1. Locations of our study watersheds (shaded) with NEXRAD radar and rain gauge locations. Dashed lines show the effective range of the radar detectors.

Study Sites

Forty Michigan watersheds with drainage areas ranging from 20 km² to 1000 km² with an average of 312 km² (USGS station IDs and names are provided in the auxiliary material) were chosen that span a range of land cover characteristics and have sufficient data for our analysis (Figure 2-1). The primary

land cover types in the selected watersheds are agriculture, forests, and urban, followed by the minor proportions of wetlands, grasslands, and open water. The percentage of agricultural land in the study watersheds ranges from about 6 to 85%, with a mean of 51%. Corn, beans, and alfalfa are the main crops cultivated in the state, which have growing seasons ranging from late April/early May to about mid-November. The percentage of forest cover in the study watersheds ranges from about 8 to 55, with a mean of 26%; and nearly all of the forests in our study watersheds are deciduous. The amount of urban area in the study watersheds ranges from nearly 0 to 70%, with a mean of 11%. Urban and suburban land covers are more common in the southeastern part of the state with most of the forest land in the northwestern regions of Michigan's Lower (or southern) Peninsula.

Quaternary glacial advances and retreats shaped the regional geology of Michigan. The surficial deposits of the state are mostly glacial outwash and till deposited during the Pleistocene continental glaciation. Glacial outwash deposits are more abundant in the north/northwestern and southwestern portions of Michigan's Lower Peninsula, while till deposits are prominent in the central and eastern half of the Lower Peninsula, extending from the Saginaw Bay area to the Ohio border. Lacustrine clays are common in the Saginaw Bay area and along the eastern fringe of the southern half of the state where artificial irrigation management practices, such as tile drains, are common. 78% of our study watersheds had less than 10% clay and only 17% had more than 20% clay.

Evaluation of NEXRAD Rainfall Data

Starting in 1980, the National Weather Service (NWS) established the nationwide NEXRAD network of Doppler radar stations (Weather Surveillance Radar (WSR) –1988 Doppler (88D)). There are approximately 158 operational WSR-88D stations throughout the US, with some overseas locations. Information from these radar stations is commonly used to issue warnings of severe weather and flash floods to the public, and provide information for air traffic safety, water management, and outdoor activities.

The detailed spatial and temporal coverage of NEXRAD data makes it a useful input to hydrologic models and provides an invaluable resource where ground-based rain gauges are scarce. The Army Corps of Engineers, U.S. Department of Agriculture, and National Weather Service all use radar data in hydrologic models. Within the research community, radar rainfall data have mainly been used to simulate streamflow response to storm events. Some examples include Neary et al. (2004), who used radar rainfall data to derive basin averaged hourly precipitation to simulate streamflow using a HEC-HMS model. Di Luzio and Arnold (2004) used the NEXRAD hourly grids in Soil and Water Assessment Tool (SWAT) model to predict hourly streamflow in response to storm events. In a similar manner, Carpenter et al. (2001) used NEXRAD precipitation data in a spatially distributed hydrologic model to simulate runoff and streamflow to evaluate the use of distributed hydrologic models in an operational environment. In this study, we are mainly interested in quantifying the influence of watershed characteristics on water balances, which could not be

accurately evaluated based on ground-based gauges alone due to the general sparse nature of the rain gauge networks. We overcame this obstacle by calculating basin-averaged hourly precipitation rates from NEXRAD grids, which were then summed into monthly and growing season volumes for each study watershed. The primary radar rainfall product from the WSR-88D, called the Digital Precipitation Array (DPA), is generated by processing the radar information using a Precipitation Processing System (PPS). The PPS is a set of algorithms that use information from two external functions for precipitation detection (effective within a 230 km radius from the radar station) and rain gauge data acquisition, and five internal functions for data preprocessing, radar to rainfall rate conversions, rainfall accumulation calculations, gauge-radar adjustments, and product generation (Fulton et al., 1998). The hourly precipitation products used in this study have a 4 km x 4 km spatial resolution and are generated from base Doppler radar data (reflectivity, mean radial doppler velocity and spectrum width) using the PPS.

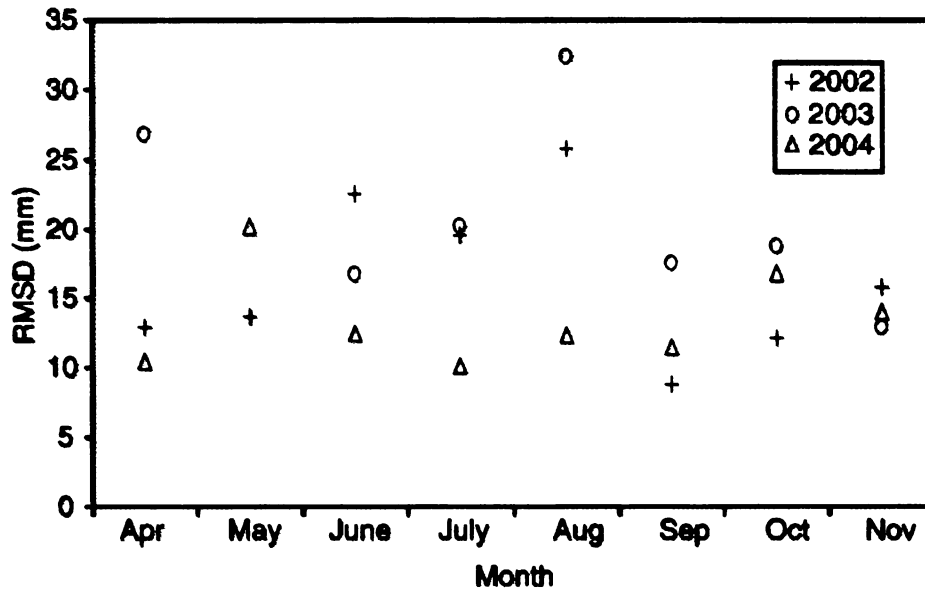


Figure 2-2. RMS differences between NEXRAD and ground-based precipitation measurements at various sites with data spanning the 2002, 2003, and 2004 growing seasons.

There are several sources of systematic and random error associated with radar rainfall estimates (Seo et al., 1999). The uncertainties in reflectivity (the quantity measured by the radar) to rainfall conversion, which is highly nonlinear, is recognized as one of the main sources of error (Neary et al., 2004).

Differences in radar instrument calibration from station to station, distance from radar stations or the range effect (Sharif et al. 2002), radar scan angles, local topography (Young et al., 1999), and climate conditions (Smith et al., 1996) can all cause significant error in radar rainfall estimates. We evaluated the accuracy of NEXRAD data calculated on the basis of the three WSR- 88D weather radar stations in Michigan (Figure 2-1) relative to point observations of precipitation at NWS and other independent stations at daily and monthly timescales. This

involved comparing 4 km x 4 km spatial rainfall grids provided by the Michigan State University Geography Department to point rainfall data for 28 locations in Michigan's Lower Peninsula with sufficient data from April to November of 2002–2004 (Figure 2-1). Root-mean-square differences (RMSD) between radar and direct measurements were computed for the radar and gauge pairs. We also assessed temporal variations in NEXRAD errors over monthly and growing season timescales.

Comparison of NEXRAD and ground-based precipitation data from May–November indicate that August has the largest monthly RMSD in the 2002 and 2003 data sets (Figure 2-2). This is mainly due to relatively large differences between NEXRAD and ground-based precipitation at a few gauge locations: Detroit, Bellaire, Grayling, and Ypsilanti in 2003; and Detroit, Bellaire, Grand Haven, Muskegon, and Howell in 2002. Nearly all of the monthly RMS differences remained below 25 mm throughout each of these growing seasons.

The largest percent absolute difference (calculated relative to gauged precipitation) between the radar estimated and gauged rainfall within the study region for the 2004 growing season (May–November) was 13% at the Grand Haven gauge location (Figure 2-3). This amounts to a 50 mm difference between the radar and gauge systems for the entire growing season. The largest absolute differences were concentrated in the northwestern corner of Michigan's Lower Peninsula, where the highest errors ranged from about 25% to 38% in 2002 at five locations (North Port, Traverse City, Cadillac, Kalkaska, and Houghton). All watersheds from the northwestern region were thus excluded from this study.

The lower absolute differences in the southern half of the state are partially due to the use of at least some of Grand Rapids, Lansing and Flint station data by the WSR-88D system for real-time corrections of the precipitation predictions. At most locations, NEXRAD estimates tend to be smaller than the precipitation recorded by the ground-based gauges.

Although most of the discrepancy between observed and NEXRAD precipitation is likely due to errors in radar estimates, some of the differences can also be attributed to inaccuracies in the ground-based precipitation observations. Mechanical failures associated with tipping bucket gauges often give rise to random errors, and the aerodynamic design of the gauges frequently result in systematic error in rainfall measurements (Sevruk, 1996; Heinemann et al., 2002). Habib et al. (2001) have shown that sampling frequency, bucket size and precipitation characteristics also contribute to errors in tipping bucket rainfall data. Errors in ground-based observations discussed here would generally result in an under estimation of actual rainfall, particularly during heavy precipitation events. These errors contribute to a larger RMSD and would count the same as radar overestimates.

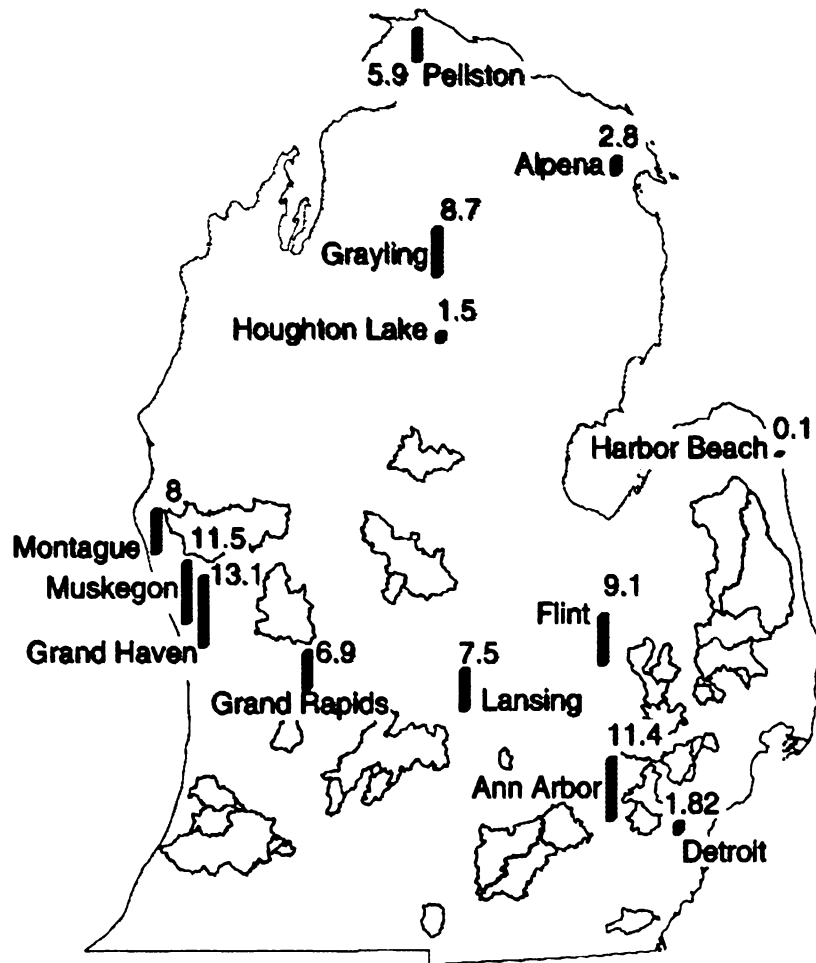


Figure 2-3. Map of the percent absolute differences (calculated relative to observed gauged precipitation) between the 2004 (April-November) gauge and NEXRAD rainfall data. The Grand Rapids, Lansing, Flint, and Alpena gauges are known to be used by the WSR-88D system for real-time calibration of radar rainfall estimates (Ann Arbor and Grayling are missing 1 month of data, Harbor Beach is missing 2 moths, and Montague is missing 3 months, and thus these months were not used in this analysis).

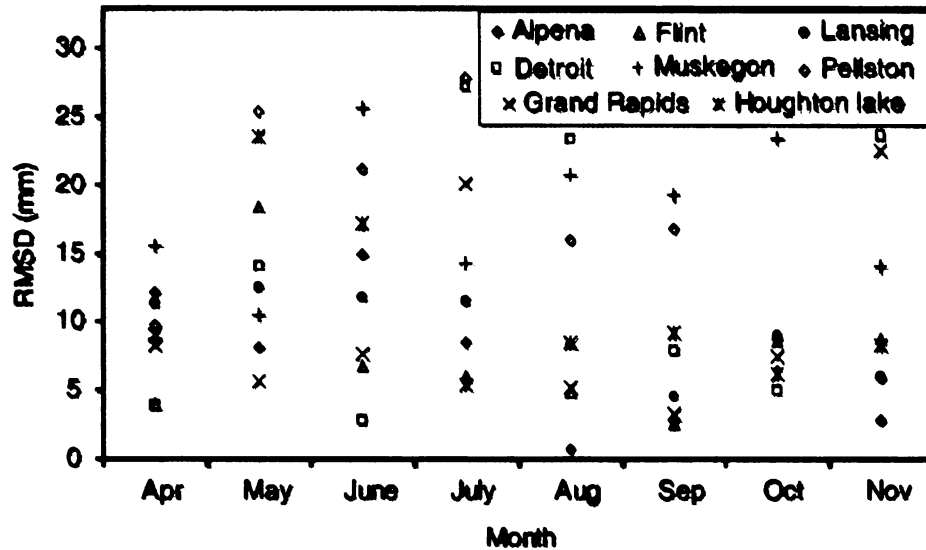


Figure 2-4. RMS differences for eight gauge locations using 2002, 2003, and 2004 monthly radar and ground-based gauge precipitation data. May RMSD calculation is based only on data from 2002 and 2004 due to missing NEXRAD grid data in MAY 2003.

The accuracy of the NEXRAD estimates relative to ground-based observations for the eight gauges across the region with continuous precipitation records from 2002 to 2004 is shown in Figure 2-4 (see Figure 2-1 for locations). On the basis of this analysis, there does not appear to be any significant spatial trend in NEXRAD precipitation estimates except for the already mentioned larger error to the northwest corner of the Lower Peninsula. The Muskegon gauge was the only location that showed consistently higher RMSD values throughout the analysis period. In general there seems to be relatively higher variability at all gauge locations beginning in May and continuing through August. This may be due to intense precipitation events associated with convective weather systems that are relatively common during this period. Under such conditions, both

ground based gauges (Heinemann et al., 2002) and radar systems (Krajewski and Smith, 2002) are known to be less accurate, which contributes to the relatively large RMSD during such periods.

As is commonly the case, the total radar rainfall estimates for the evaluation period are generally lower than the ground-based precipitation recorded during the same period at the gauge stations. A limited evaluation of event scale data (hourly NEXRAD versus observed precipitation) showed that radar system performed poorly during very small precipitation events. However, only a small percentage of the differences in monthly precipitation totals between radar and gauge data in Michigan can be attributed to such small events.

Another source of error is the comparison of precipitation derived from relatively large NEXRAD grid cells (4 km x 4 km) with point gauges. Event-scale NEXRAD data were not directly compared with ground based gauge data in this study because of difficulty in obtaining hourly precipitation data for a sufficient number of ground-based gauges. The 2004 data show the highest degree of correlation between monthly gauge and NEXRAD rainfall from July to September, our main study period for water budget evaluations (Figure 2-5), while 2002 and 2003 also had reasonable correlations to gauged data. Data from the 2002 to 2004 period were used for water budget calculations in this study after adjusting for the bias in NEXRAD precipitation using correction coefficients shown in Figure 2-5.

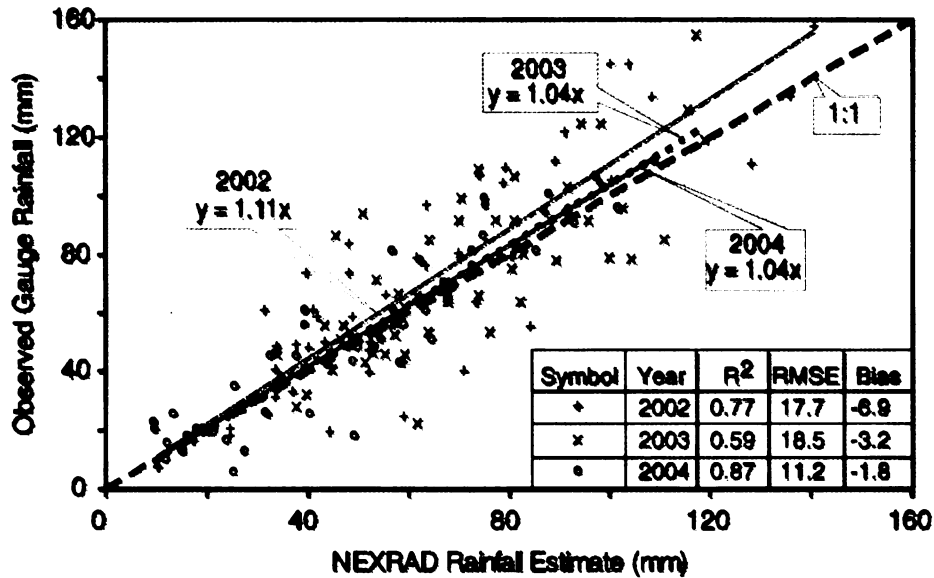


Figure 2-5. Comparison of monthly (July-September) observed gauge and NEXRAD rainfall for 2002, 2003, and 2004. RMSE and bias (average NEXRAD rainfall-average observed gauge rainfall) are given in mm.

Results and Discussion

A significant decrease in the July-September streamflow:rainfall ratio was observed with increasing agricultural land cover above about 60% in all years (Figure 2-6). This relationship has a smaller correlation in watersheds with lower-intensity agricultural land uses, likely due to the heterogeneity in land cover and morphological attributes that are characteristic of the lower-intensity agricultural systems, but it is still statistically significant across our 40 watershed sample according to the nonparametric correlation coefficients with a p value of 2.0×10^{-4} (Table 2-1). Comparatively, high-intensity agricultural systems tend to be relatively homogeneous with respect to vegetation and morphology. An additional factor that could contribute to the low streamflow:rainfall ratio in intensely

agricultural systems in some environments is the presence of tiled drains. However, such engineered drainage systems mainly exist in areas with significant proportion of clay rich soils. Only three watersheds with >30% clay rich soils were included in this analysis (circled on Figure 2-6), and two of these three have lower streamflow:rainfall ratios than other watersheds with similar agriculture percentages (Figure 2-6). agriculture percentages (Figure 2-6).

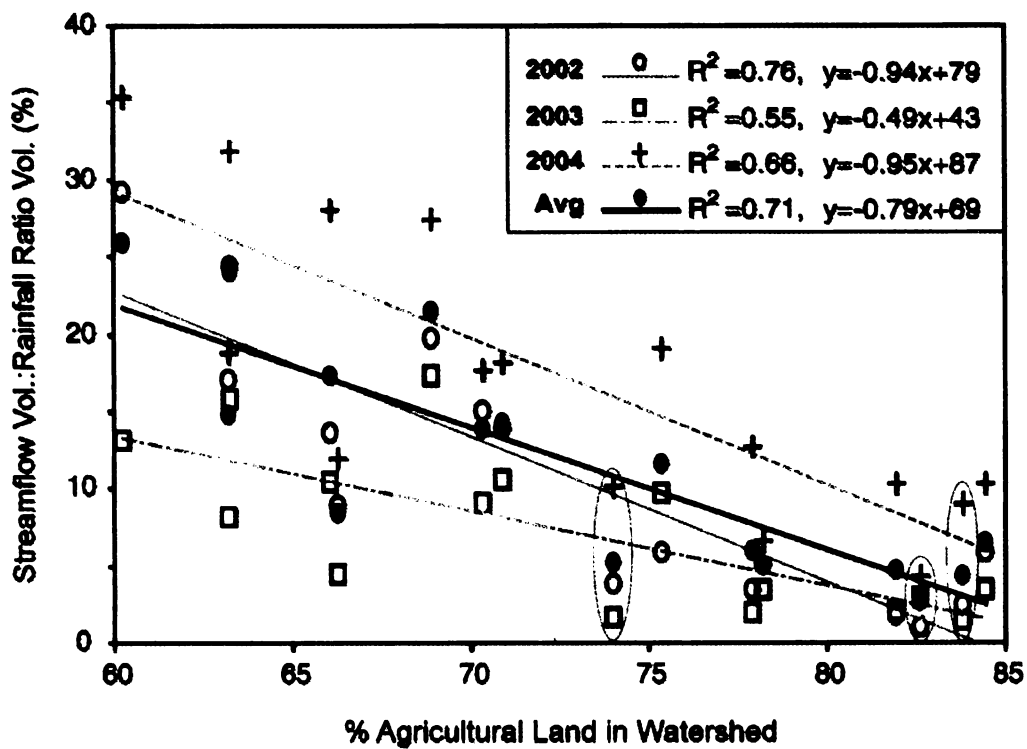


Figure 2-6. Percentage of agricultural land cover in watersheds compared to streamflow:rainfall ratios for July to September periods of 2002-2004. Each data point represents a watershed, and three watersheds with greater than 30% clay sediments are marked with a gray oval.

	Streamflow Volume/ Rainfall Volume		Overland Flow Volume/ Rainfall Volume		Stream Base Flow Volume/ Rainfall Volume	
	Spearman Rho	p Value	Spearman Rho	p Value	Spearman Rho	p Value
Urban	0.28	7.7E-02 ^b	0.37	1.8E-02	0.04	8.0E-01
Forest	0.27	9.3E-02	-0.04	8.3E-01	0.44	4.5E-03
All agriculture	-0.56	2.0E-04	-0.46	2.9E-03	-0.38	1.6E-02
Agriculture>60%	-0.86	1.8E-06	-0.29	2.8E-01	-0.83	6.3E-06
Extreme/somewhat extremely well drained soils	0.29	7.1E-02	-0.06	6.9E-01	0.44	4.7E-03
Outwash sand/gravel	0.22	1.6E-01	-0.07	6.5E-01	0.43	5.5E-03
Mean slope	0.18	2.5E-01	0.03	8.7E-01	0.31	5.4E-02

Table 2-1. Spearman's Ranked Correlation Statistics for Mean July to September (2002-2004) Volume Ratios and Other Watershed Variables for the 40 Selected Watersheds. Statistical significance ($p < 0.05$) is indicated by bold typeface.

An expected significant increase of overland flow in watersheds with urban land cover percentage is also evident from the correlation statistics (Table 2-1), even in this case where only 20% of the watersheds in this study had more than 10% urban land cover. A positive correlation was also observed between base flow:rainfall ratios in forested watersheds. The small p values (<0.05) in Table 2-2 indicate that the correlations between these land cover attributes and volume ratios in the analyzed watersheds are unlikely to be random. Other factors that show significant relationships with the volume ratios are the distribution of certain surficial glacial geologic materials and soil drainability classes. The amount of base flow is positively correlated with both the percent glacial outwash sand and gravel deposits and the extremely to somewhat extremely well drained soils, yet there was no statistically significant correlation between soil drainability and outwash deposits. Glacial outwash deposits were present in 90% of the investigated watersheds with varying degrees of abundances. Positive correlations also exist between glacial outwash deposits and forest cover percentages in the study watersheds, and between agricultural land uses and both poorly drained and low slope areas (Table 2-2). Seventy-three percent of the variability in the streamflow: rainfall ratio was explained by three watershed attributes (percentages of agriculture, open water, and glacial outwash sand and gravel) using a multiple linear regression analysis (Table 2-3). The proportion of agricultural land cover is the most significant attribute among the pool of watershed variables used for the exploratory multiple regression analysis. Poorly drained soils failed to explain a significant portion of the variability observed with

streamflow: rainfall ratio, indicating that low streamflow conditions in watersheds with high-intensity agriculture is more likely related to the land use and cover attributes, rather than simply the soils. A negative coefficient for open water (lakes, ponds, wetlands etc.) indicates that these areas are associated with reductions in streamflow, which is likely associated with direct evaporation from open water surfaces. In a similar manner as the streamflow:rainfall ratio, 75% of the variability associated with base flow:rainfall ratio in the study watersheds was explained by four watershed attributes (Table 2-3). Agriculture, open water, and glacial outwash sand and gravel explained most of the variability in base flow:rainfall ratio, followed by extremely to somewhat extremely well drained soils. One of the 40 watersheds was removed from the multiple regression analysis as an outlier due to unusually high streamflow conditions, likely related to urbanization effects since it was in the Detroit suburban area. Watersheds with high-intensity agriculture (>70%) tend to have lower base flows during the growing season than those with moderate-intensity (<50%) agriculture. Kruskal-Wallis tests had p values that indicate that April– June, July–September, and October–December base flow differences between high-intensity and moderate-intensity agricultural watersheds are statistically significant (Figure 2-7). A considerable drop in base flow is evident during the peak growing season (July to September) in both classes of watersheds. However, the decline is relatively larger in watersheds with intense agriculture. Watersheds with over 10% high-intensity urban land uses (NLCD classifications “high-intensity residential” and “commercial/industrial/ transportation”) were removed from the data set prior to

the base flow:rainfall comparison in Figure 2-7, to minimize the urban effects that tend to be hydrologically different from forest and agricultural systems. High ET demands by active crops and anthropogenic abstraction of water for irrigation are two factors that could contribute to low base flow in high-intensity agricultural watersheds. However, the persistence of low base flow across the range of studied watersheds suggests that ET demand is a major component of the water budget during the growing season. According to U.S. Department of Agriculture (USDA) statistics, only a small percentage (~5%) of Michigan's croplands are irrigated (Economic Research Service, 2004). Countywide surface and shallow water withdrawals in 2000 were nearly uniform across the study watersheds, thus it is unlikely that anthropogenic abstraction of water for irrigation is the main cause of the observed lower streamflows associated with high-intensity agricultural watersheds.

	Forest Percentage		Agriculture Percentage		Urban Percentage	
	Spearman Rho	p Value	Spearman Rho	p Value	Spearman Rho	p Value
Mean slope	0.67	1.90E-06	-0.36	2.20E-02	-0.01	9.30E-01
Poorly drained soils	-0.34	3.20E-02	0.37	1.70E-02	-0.27	9.20E-02
Extreme/somewhat extremely well drained soils	0.43	6.20E-03	0.03	8.70E-01	-0.25	1.20E-01
Well/moderately well drained soils	0.24	1.40E-01	-0.34	3.10E-02	0.30	5.90E-02
Glacial tills	-0.03	8.60E-01	0.29	6.80E-02	-0.31	4.90E-02
Outwash sand/gravel	0.47	2.30E-03	-0.22	1.80E-01	0.03	8.60E-01
Lacustrine clay/silt	-0.44	5.00E-03	0.03	8.30E-01	0.30	6.20E-02

Table 2-2. Spearman's Nonparametric Correlation Statistics for Land Cover and Other Watershed Variables for the 40 Selected Watersheds. Statistical significance is indicated by bold typeface.

Parameter Estimates					
Term	Estimate	SE	Probability> t	Summary of Fit	
<i>Streamflow:Rainfall Response Variable</i>					
Intercept	30.5	2.68	2.60E-13	R2=0.73	RMSE=5.61
Agriculture%	-0.3	0.04	8.50E-09		
Open Water%	-2.63	0.41	2.80E-07		
Outwash sand/gravel%	0.26	0.05	1.50E-06		
<i>Base Flow:Rainfall Response Variable</i>					
Intercept	13.3	2.23	8.80E-07	R2=0.75	RMSE=4.55
Extremely and somewhat extremely well drained soils	0.43	0.11	5.40E-04		
Agriculture percentate	-0.13	0.03	4.30E-04		
Open water percentage	-1.88	0.34	3.10E-06		
Outwash sand/gravel percentage	0.31	0.04	8.60E-10		

Table 2-3. Multiple Regression Statistics for July September Mean (2002-2004) Streamflow:Rainfall and Base Flow:Rainfall Ratios and Watershed Attributes. The residuals from both fits were tested for normality with the Anderson-Darling test. Normality was not rejected; p values are 0.27 and 0.35, respectively.

The differences in annual base flow between high intensity and moderate-intensity agricultural watersheds can also be attributed to early spring frozen soil conditions. High-intensity agricultural areas are more susceptible to frozen soils during the winter and early spring months, which would tend to lower the recharge rates during the important snowmelt period. In the absence of a persistent snowpack, soils in the region have been shown to freeze to about 5 cm depth even in warm winters (Isard and Schaetzl, 1998). Intermittent snowpack conditions in winter months are more likely in bare and exposed farmlands resulting in a thicker frozen soil layer. An increasing trend in groundwater recharge toward the northwestern and western parts of the state reported by Holtschlag (1997) is consistent with the larger snowpack and denser forest cover along the northwestern and western fringes of the state as observed with mean January through May streamflow:drainage area ratio (Figure 2-8). Spatial patterns in volume ratios for watersheds in this study, however, did not show any specific east–west trend during the July to September period.

Culmination of the growing season, as depicted by a sharp decrease in mean monthly LAI in Figure 2-9, initiates a period of steady increase in base flow. Correspondence between the LAI and the base flow:watershed area ratio is consistent with the expectation that transpiration significantly reduces the recharge rates in this region during the summer period.

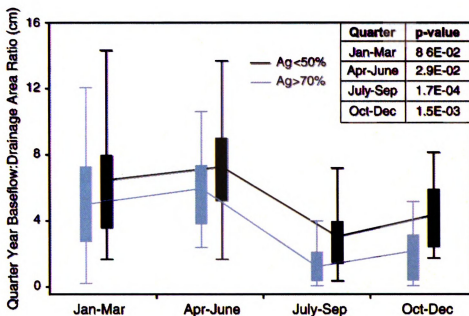


Figure 2-7. Average 2002-2004 quarter year base flow:drainage area ratios in high-intensity (>70%) and moderate-intensity (<50%) agricultural watersheds. The difference of the flow between the two types of watersheds are statistically significant (p value <0.05) in all quarters except January-March.

Parameter	2002	2003	2004	Average
<i>Agriculture <50%</i>				
Percent of rainfall	14.1	9.9	21.7	15.2
Actual amount, cm	2.6	2.4	3.9	3
<i>Agriculture >70%</i>				
Percent of rainfall	4.6	3.3	7.8	5.3
Actual amount, cm	0.7	0.8	1.5	1

Table 2-4. Estimated Annual Growing Season Recharge Amounts (July-September); in terms of annual rainfall and actual amounts in centimeters.

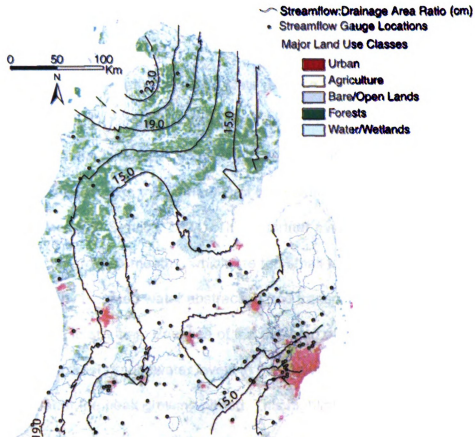


Figure 2-8. Average of 2002-2004 January to May streamflow:drainage area ratios (cm). Higher values likely indicate greater snowmelt influence on the watershed hydrology. The contour map was generated by kriging the ratio calculated from data at the 113 USGS streamflow gauges shown on the map. Images in this dissertation are presented in color.

The vegetation density associated with agricultural uses, calculated based on LAI, is significantly lower than that of forests, which is the most frequent land cover type in moderate-intensity agricultural watersheds. However, Figure 2-7 suggests that the high-intensity agriculture has a much more significant effect on hydrology than moderate-intensity agriculture during the peak growing season. The observed temporal changes in streamflow and volume ratios are also

evident in the region's groundwater system. Data from continuous water level transducers installed in a shallow aquifer in the Grand Traverse Bay Watershed located to the northwestern part of the state reveal a steady decline in water levels through late October followed by an increase thereafter (Figure 2-10). There is only minimal irrigation according to county statistics for the area where the wells are located, and the primary land cover within their watersheds is forest (Economic Research Service, 2004). This is further evidence of low recharge rates during the growing months, which are too small to compensate for the deficit created by elevated water abstraction and transpiration by plants and base flow discharges to streams. Because of the damping effects of the subsurface materials, the lowest groundwater levels in the region are generally observed a few months after the peak growing period. This highlights the difficulty in using alternative approaches that analyze only groundwater levels and budgets to estimate transient groundwater recharge rates.

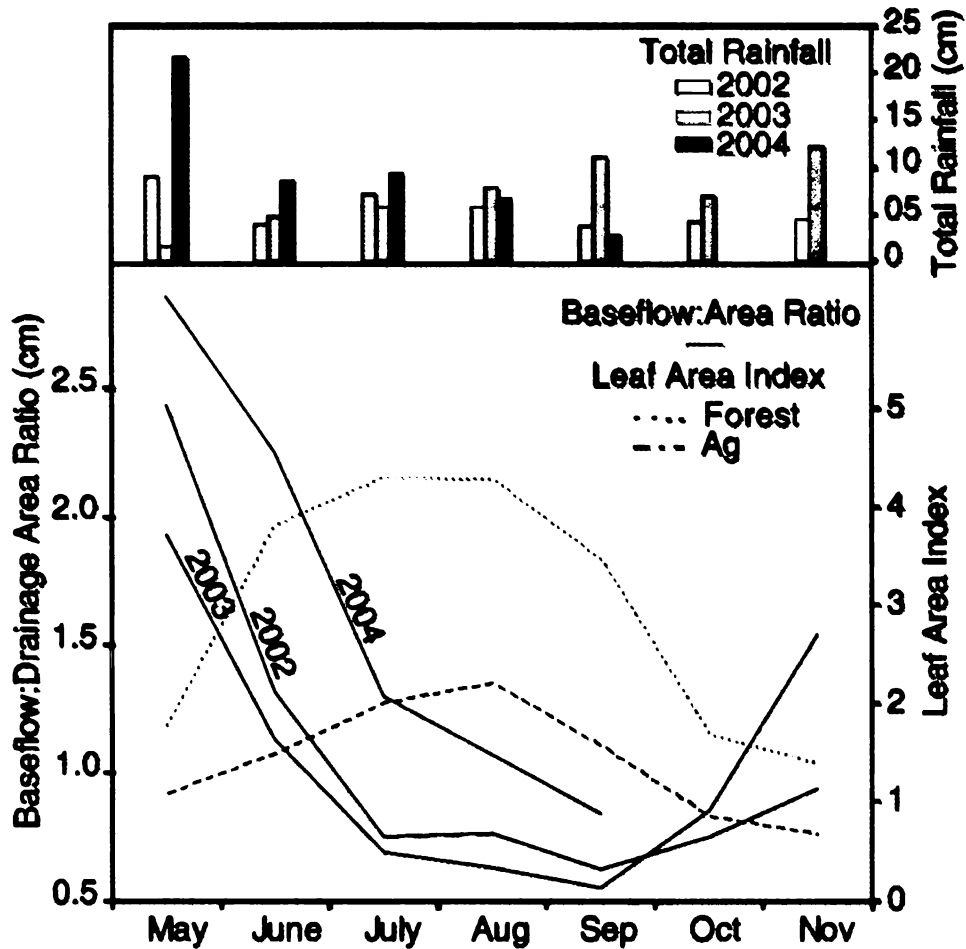


Figure 2-9. The 2002-2004 monthly base flow:drainage area ratios and average monthly rainfall for 40 selected watersheds in Michigan. The peak growing season is clearly marked by higher leaf area indexes (LAI), which corresponds well with the decline in stream base flow during the same period.

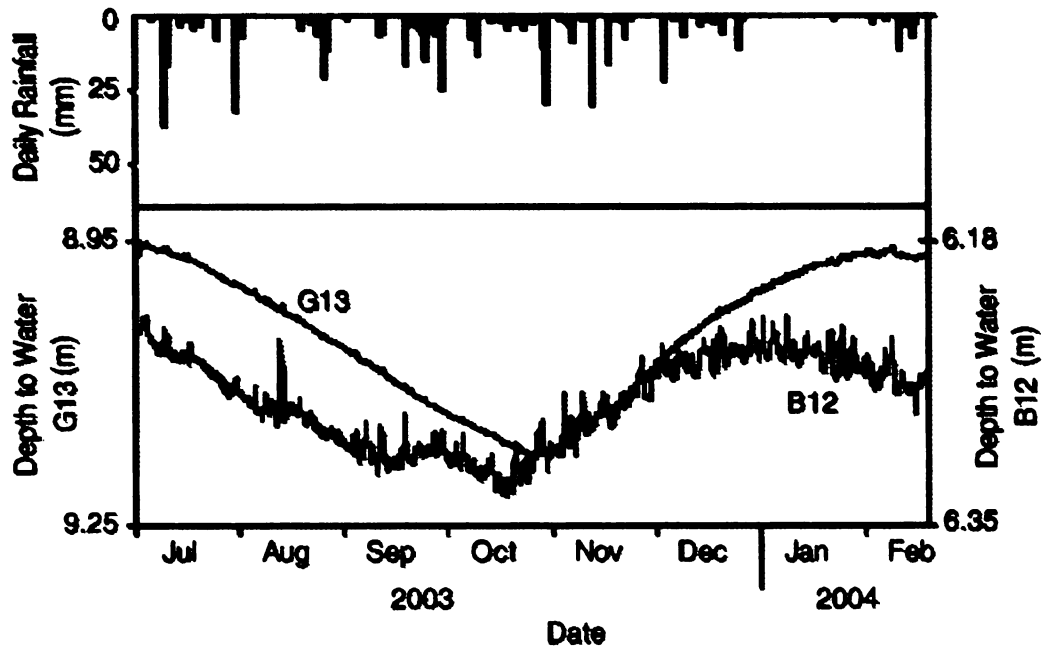


Figure 2-10. Measured water table depths in two shallow wells in the northern portion of Michigan's Lower Peninsula (see Figure 2-1 for locations). A steady decline in water level is evident during the growing season (land use percentages in the watershed containing B12 are forests ~65%, shrubs/open land ~35%; G13, forests ~66%, agriculture ~28%). Note that the minimum water level is delayed significantly from the peak LAI and minimum base flow levels shown in Figure 2-9.

The base flow:rainfall ratio for July September period of each year was analyzed to evaluate differences in recharge between high-intensity and moderate-intensity agricultural watersheds in each of the years from 2002 to 2004. Base flow:rainfall ratio is a good measure of groundwater recharge given the base flow estimates are reasonably accurate. According to our analysis, the average growing season recharge from 2002–2004 in high-intensity agricultural watersheds was ~5% of the total rainfall compared to 15% in moderate-intensity agricultural watersheds (Figure 2-11). According to the Kruskal-Wallis test, the difference of the mean base flow:rainfall ratio between the two types of

watersheds in each of the years is statistically significant (Figure 2-11). The above percentages amount to ~1.0 cm of growing season recharge in our high-intensity agricultural watersheds, compared to ~3.0 cm in moderate intensity agricultural watersheds (Table 2-4). The variability of recharge percent across the studied watersheds within a given year is likely related to both differences in land cover percentages and precipitation characteristics. The relatively higher ratios in 2004 are likely related to late spring snowmelt discharge effects and precipitation which contribute to higher streamflow conditions that sometimes extend to late June (Figure 2-12). In areas where times between recharge events and resulting discharge are relatively small (days to a few weeks), the ratio method presented in this paper could perhaps be applied at shorter temporal scales. Both the starting point and ending point for the analysis should include no significant rainfall events or recent increases in streamflow for several days to weeks, depending on the response time of the watershed of interest. However, larger uncertainties associated with both radar rainfall and base flow estimates at small time intervals would tend to increase the uncertainty in short time period recharge estimates with this approach.

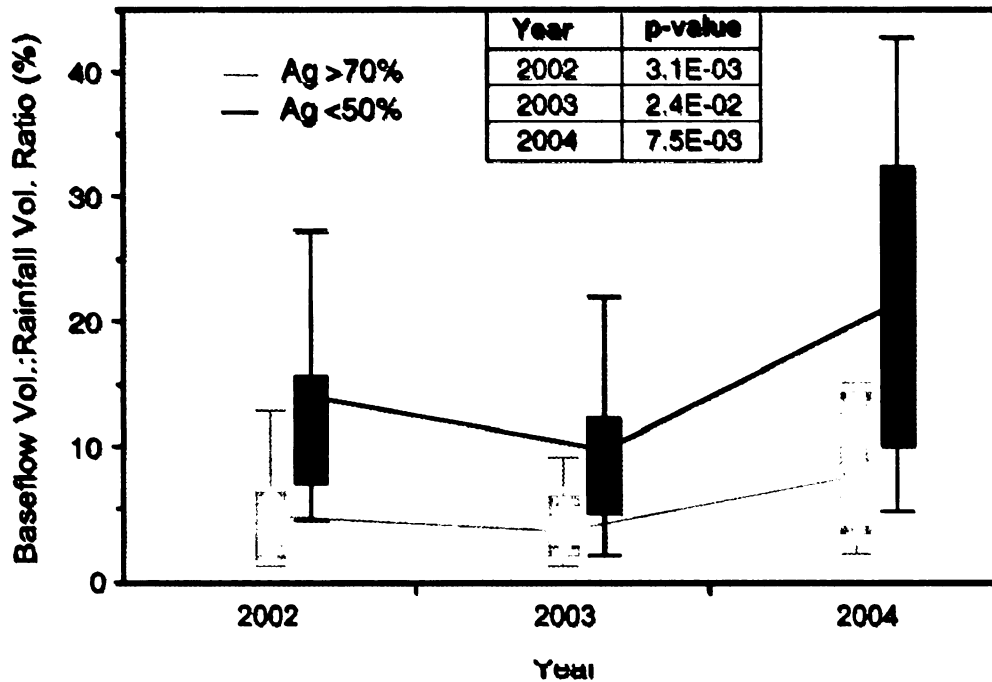


Figure 2-11. Recharge estimates for the July to September period, as a percent of NEXRAD bias adjusted rainfall in high-intensity agricultural (>70%) and moderate-intensity agricultural (<50%) watersheds. The difference in baseflow:rainfall ratios between the two types of watersheds are statistically significant (p value <0.05) in all years.

Summary and Conclusions

Despite recent advances that have been made to quantify groundwater recharge rates, existing methods are generally limited by insufficient data. Increasing concerns over the likelihood of unsustainable water resources in many regions of the world emphasize the need for simple approaches that use readily available data for water budget assessment. Many of the existing approaches for groundwater recharge assessment require long-term monitoring, cumbersome and complex watershed models, accurate subsurface parameter estimates that are difficult to acquire, and significant time commitments. As a

result these approaches often fail to deliver rapid water budget estimates for watersheds over critical time periods. To address these difficulties, we introduce a method that can be used to rapidly estimate water budgets and recharge rates over various temporal and spatial scales. We believe this approach can be adopted for rapid preliminary assessment of seasonal and longer term recharge conditions in most humid regions with relatively small unsaturated zones and no large artificial diversions of water. Data extraction and processing for this approach can be easily performed using GIS systems and simple database schemes.

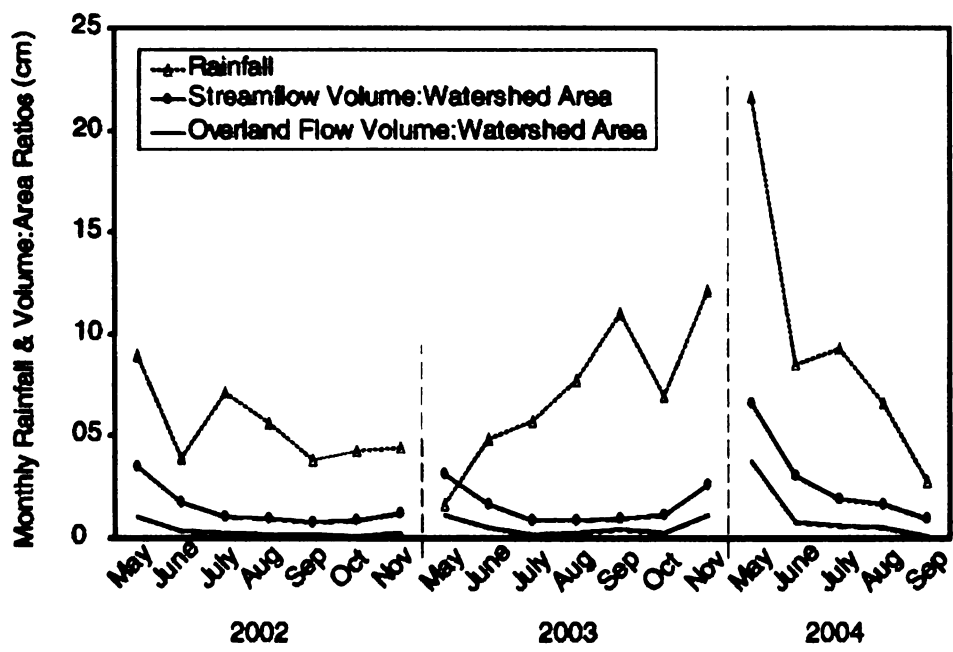


Figure 2-12. Total monthly streamflow, and overland flow volumes normalized by watershed area along with rainfall averaged across the 40 study watersheds.

We statistically analyzed ratios of streamflow, stream base flow and overland flow volumes to precipitation volume to examine factors that influence

the water mass balances for 40 watersheds across Michigan during the growing season. Observed differences are primarily attributed to land cover characteristics. Our analysis indicates that there is minimal growing season recharge in all of the studied watersheds, with high-intensity agricultural watersheds receiving essentially one third of the growing season recharge of moderate-intensity agricultural watersheds. Low runoff and base flow conditions and low streamflow:rainfall ratios in agricultural watersheds provide insight into the significant growing season water demands for intensive croplands. While this has significant implications for managing water resources, further analysis is required to interpret and quantify the detailed processes leading to these trends in terms of ET and other forms of water use related to agriculture.

Statistical evaluation of streamflow and its component volumes (base flow and overland flow) as a percentage of total precipitation can be correlated with land cover and other watershed attributes. This provides a fairly simple and efficient approach to characterize watershed behavior across a range of temporal and spatial scales. When accurate precipitation and flow data are available for watersheds, they can be used to evaluate seasonal or longer-term potential recharge, ET, and runoff volumes. These estimated fluxes provide critical inputs to transient hydrologic models. Relatively large uncertainties associated with base flow estimates as well as radar rainfall estimates at event and other short timescales (i.e., daily, weekly), however, makes it difficult to apply the ratio method to evaluate flux budgets in watersheds over short time windows.

The use of radar-derived precipitation estimates can simplify and potentially improve the quality of water resource analyses for some watersheds. This is especially true when large watersheds are involved because there are often significant spatial and temporal variations in precipitation at these scales. Spatial characteristics of precipitation are extremely difficult to capture solely from ground-based gauges; thus use of NEXRAD data is likely to improve the accuracy of regional water mass balances. While there are numerous merits to using NEXRAD precipitation data in hydrogeological studies, the temporal and spatial accuracy needs to be evaluated for any study region due to the known uncertainties currently associated with these data. The continued effort of the National Oceanic and Atmospheric Administration (NOAA) to improve the accuracy of the radar rainfall estimates is likely to make NEXRAD an indispensable resource for many hydrologic applications.

Acknowledgments

We greatly appreciate the funding provided by a grant from the National Science Foundation (EAR-0233648) and thank the Associate Editor and three anonymous reviewers for their constructive comments. Our sincere gratitude is extended to Dennis Gilliland of the Center for Statistical Consulting at Michigan State University for suggestions that greatly improved the quality of this manuscript. Special thanks are also extended to Jeffrey Andresen, James T. Brown, and Tracy Aichele of the Department of Geography, Michigan State

University for converting the NEXRAD data into arc grids and archiving these for extended time periods. We appreciate the suggestions and contributions of Bryan Pijanowski (Purdue), M.S. Phanikumar, and students in the hydrogeology research group at Michigan State University. Any opinions, findings, and conclusions or recommendations expressed in this material are those of the authors and do not necessarily reflect the views of the National Science Foundation.

References

- Anderson, J. R., E. H. Hardy, J. T. Roach, and R. E. Witmer (1976), A Land Use and Land Cover Classification System With Remote Sensor Data, U. S. Govt. Print. Off., Washington, D. C.
- Carpenter, T. M., K. P. Georgakakos, and J. A. Sperflage (2001), On the parametric and NEXRAD-radar sensitivities of a distributed hydrologic model suitable for operational use, *J. Hydrol.*, 253, 169–193.
- Cherkauer, D. S., and S. A. Ansari (2005), Estimating ground water recharge from topography, hydrogeology, and land cover, *Ground Water*, 43, 102–112.
- Costa, M. H., and J. A. Foley (2000), Combined effects of deforestation and doubled atmospheric CO₂ concentrations on the climate of Amazonia, *J. Clim.*, 13, 18–34.
- Di Luzio, M., and J. G. Arnold (2004), Formulation of a hybrid calibration approach for a physically based distributed model with NEXRAD data input, *J. Hydrol.*, 298, 136–154.
- Dow, C. L., and D. R. DeWalle (2000), Trends in evaporation and Bowen ratio on urbanizing watersheds in eastern United States, *Water Resour. Res.*, 36, 1835–1843.
- Economic Research Service (2004). State fact sheet for Michigan, U. S. Dep. of Agric., Washington, D.C (Available at <http://www.ers.usda.gov/StateFacts/MI.htm>).
- Farrand, W. R., and D. Bell (1982), Quaternary geology of Michigan, Michigan Geological Survey map, scale 1:500000, Mich. Dep. of Nat. Resour., Lansing.

- Finch, J. W. (1998), Estimating direct groundwater recharge using a simple water balance model-sensitivity to land surface parameters, *J. Hydrol.*, 211, 112–125.
- Fulton, R. A., J. P. Breidenbach, D. J. Seo, D. A. Miller, and T. O'Bannon (1998), The WSR-88D rainfall algorithm, *Weather Forecasting*, 13, 377– 395.
- Habib, E., W. F. Krajewski, and A. Kruger (2001), Sampling errors of tipping-bucket rain gauge measurements, *J. Hydrol. Eng.*, 6, 159– 166.
- Heinemann, A. B., G. Hoogenboom, and B. Chojnicki (2002), The impact of potential errors in rainfall observation on the simulation of crop growth, development and yield, *Ecol. Mod.*, 157, 1 –21.
- Holtschlag, D. J. (1997), A generalized estimate of groundwater recharge rates in the Lower Peninsula of Michigan, *U. S. Geol. Surv. Water Supply Pap.*, 2437.
- Isard, S. A., and R. J. Schaetzl (1998), Effects of winter weather conditions on soil freezing in southern Michigan, *Phys. Geogr.*, 19, 71– 94.
- Krajewski, W. F., and J. A. Smith (2002), Radar hydrology: Rainfall estimation, *Adv. Water Resour.*, 25, 1387– 1394.
- Mo, X., S. Liu, Z. Lin, and W. Zhao (2004), Simulating temporal and spatial variation of evapotranspiration over the Lushi basin, *J. Hydrol.*, 285, 125– 142.
- Neary, V. S., E. Habib, and M. Fleming (2004), Hydrologic modeling with NEXRAD precipitation in middle Tennessee, *J. Hydrol. Eng.*, 9, 339– 349.

- Pielke, R. A., R. Avissar, M. Raupach, A. J. Dolman, X. B. Zeng, and A. S. Denning (1998), Interactions between the atmosphere and terrestrial ecosystems: Influence on weather and climate, *Global Change Biol.*, 4, 461– 475.
- Rutledge, A. T. (1998), Computer programs for describing the recession of ground-water discharge and for estimating mean ground-water recharge and discharge from streamflow data-update, U. S. Geol. Surv. Water Resour. Invest. Rep., 98-4148.
- Scanlon, B., R. Healy, and P. Cook (2002), Choosing appropriate techniques for quantifying ground-water recharge, *Hydrogeol. J.*, 10, 18– 39.
- Seo, D. J., J. P. Breidenbach, and E. R. Johnson (1999), Real-time estimation of mean field bias in radar rainfall data, *J. Hydrol.*, 223, 131–147.
- Sevruk, B. (1996), Adjustment of tipping-bucket precipitation gauge measurements, *Atmos. Res.*, 42, 237–246.
- Sharif, H. O., F. L. Ogden, W. F. Krajewski, and M. Xue (2002), Numerical simulations of radar-rainfall error propagation, *Water Resour. Res.*, 38(8), 1140, doi:10.1029/2001WR000525.
- Smith, J. A., D. J. Seo, M. L. Baeck, and M. D. Hudlow (1996), An intercomparison study of NEXRAD precipitation estimates, *Water Resour. Res.*, 32, 035–2045.
- Szilagyi, J. S., F. E. Harvey, and J. F. Ayers (2004), Regional estimates of total recharge to groundwater in Nebraska, *Ground Water*, 43, 63– 69.
- U. S. Geological Survey (1999), Michigan land cover data set, Sioux Falls, S.D. (Available at <http://edcwww.cr.usgs.gov/programs/lccp/nationallandcover.html>)

U. S. Geological Survey (2004), MODIS Reprojection Tool user's manual, release 3.2a, USGS EROS Data Center, Sioux Falls, S.D.

Walker, G. R., L. Zhang, T. W. Ellis, T. J. Hatton, and C. Petheram (2002), Estimating impacts of changed land use on recharge: Review of modeling and other approaches appropriate for management of dryland salinity, Hydrogeol. J., 10, 68– 90.

Young, C. B., B. R. Nelson, A. A. Bradley, J. A. Smith, C. D. Peters- Lidard, A. Kruger, and M. L. Baeck (1999), An evaluation of NEXRAD precipitation estimates in complex terrain, J. Geophys. Res., 104, 19,691–19,703.

Chapter Three

Jayawickreme, D. H., R. L. Van Dam, and D. W. Hyndman (2008), Subsurface imaging of vegetation, climate, and root-zone moisture interactions, *Geophys. Res. Lett.*, 35, L18404, doi:10.1029/2008GL034690.

Abstract

Changes in global climate and land use affect important processes from evapotranspiration and groundwater recharge to carbon storage and biochemical cycling. Near surface soil moisture is pivotal to understand the consequences of these changes. However, the dynamic interactions between vegetation and soil moisture remain largely unresolved because it is difficult to monitor and quantify subsurface hydrologic fluxes at relevant scales. Here we use electrical resistivity to monitor the influence of climate and vegetation on root-zone moisture, bridging the gap between remotely-sensed and in-situ point measurements. Our research quantifies large seasonal differences in root-zone moisture dynamics for a forest–grassland ecotone. We found large differences in effective rooting depth and moisture distributions for the two vegetation types. Our results highlight the likely impacts of land transformations on groundwater recharge, streamflow, and land-atmosphere exchanges.

Introduction

Modification of temperatures and precipitation patterns due to global climate change will cause significant transformations of ecosystems and plant physiological functions (Betts et al. 2007). Climate changes will also affect water availability and plant productivity (Field et al. 1995; Nemani et al. 2003), and hence will impact soil moisture dynamics in many regions of the world. Compounding these effects are rapid changes in land cover, driven by factors including urbanization, energy demands, and food production (Evans and Kelley 2004; Jayawickreme and Hyndman 2007; Scanlon et al. 2007).

Vadose zone soil moisture is a key driver of climate, energy and carbon cycles (Niklaus et al. 2003; Koster et al. 2004; Seneviratne et al. 2006), as well as ecosystem dynamics (Rodriguez-Iturbe 2000). The amount and distribution of soil moisture also influences important processes from soil microbial activity to nutrient fluxes and groundwater recharge (Rushton et al. 2006; Hyndman et al. 2007). Characterizing the dynamic interactions between vegetation and soil moisture is critical to forecast global water resources and improve land-atmosphere feedback models. However, these interactions remain largely unresolved due to our inability to characterize transient subsurface water fluxes at high resolution under natural conditions.

There are significant gaps in resolution and sampling volume between common approaches to monitor root zone moisture. Remote sensing provides regional-scale estimates of water content, but has limited spatial and temporal

resolution and marginal depth penetration (Dubois et al. 1995; Jackson 2002; Entekhabi and Moghaddam 2007; Wagner et al. 2007); (Scott et al. 2003). In contrast, time domain reflectometry and other probes provide accurate point-scale estimates of soil moisture with high temporal resolution, but can not readily be up-scaled (Robock et al. 2000). In addition, remote sensing and point-based methods provide only limited information about moisture percolation below the root zone and thus groundwater recharge rates, which are essential for water resources management.

Electrical resistivity imaging (ERI) is an alternative approach to monitor subsurface hydrologic conditions and processes across a range of materials and spatial scales with high temporal resolution. In ERI, direct current is injected into the ground and potential differences are measured between a series of electrode pairs along an array to obtain 2D resistivity images; these can then be converted into soil moisture estimates based on petrophysical relationships between resistivity and pore-water content (Lesmes and Friedman 2005). Until now, hydrological applications of ERI have largely focused on solute transport and infiltration monitoring with little emphasis on vegetation effects (Daily et al. 1992; Slater et al. 2000; Berthold et al. 2004; LaBrecque et al. 2004; Singha and Gorelick 2005; Al Hagrey 2007).

Although ERI has been used to characterize temporal changes in moisture content (Binley et al. 2002; Amidu and Dunbar 2007), we explore for the first time natural interactions between seasonal soil moisture dynamics, climate variability, and vegetation differences using time-lapse ERI. For this analysis, we equipped

a forest-grassland ecotone with a suite of hydrogeophysical equipment. Our observations from this ecotone demonstrate that ERI can be used to accurately quantify the spatiotemporal distribution of root-zone moisture content, bridging critical gaps between remotely-sensed and in-situ point measurements. This information is essential to project the influence of changing climate and land covers on hydrologic fluxes and ecosystem sustainability.

Methods

At a field site near East Lansing, Michigan, USA, we instrumented an ecotone separating a mature Maple forest from a grassland. Data were collected at this site from October 2006 through September 2007. The ~4 m thick unsaturated zone has 40-60 cm of clay loam underlain by medium to fine sand across the site, with respective porosities of 0.47 and 0.39. Maximum expected rooting depths are ~7m for forest and ~2.5 m for grass (*Jackson et al.*, 1996). Along a 124.5 m transect centered on the forest-grassland boundary, 84 equally-spaced, 30 cm long graphite electrodes were installed. The permanent electrode array improves data reproducibility, maximizing the ability to identify changes in soil moisture. Capacitance-type soil moisture loggers (20 and 80 cm depth) and vertical temperature arrays (5, 10, 20, 40, 80, 117, and 147 cm depth) were installed under both land covers.

Climate data for the site were obtained from a weather station 1.5 km from the site; average daily air temperature ranged from -19°C to 28°C during the

study period. As expected, fluctuations in soil temperature were increasingly damped and phase-shifted with depth. The soils were insulated by continuous snow cover from mid January to mid March, and based on our soil temperature observations only the top 5-10 cm of the soils froze during the January to early February period. The trees lost their leaves in mid November and leafed out again in late April (See color bar in Figure 3-1). In contrast, the grass remained green for the entire study period except from mid January to mid March 2007.

Twenty-seven resistivity data sets were collected using a Wenner configuration during the study period, spanning a full cycle of seasons (Figure 3-1). Differential inversions were used to calculate changes in resistivity, minimizing the need to extensively characterize site stratigraphy. The differential inversion algorithm used in this study (LaBrecque and Yang 2001) first estimates the resistivity distribution for a base dataset and then calculates the resistivity change to a second data set. March 30, 2007 was selected for our base data set, because the site had relatively uniform soil moisture across the ecotone after spring snowmelt. To obtain the absolute resistivity distribution for each date, the estimated resistivity change is added to the inverted base dataset. Resistivity changes for each time interval were then obtained by subtracting the two absolute resistivity images.

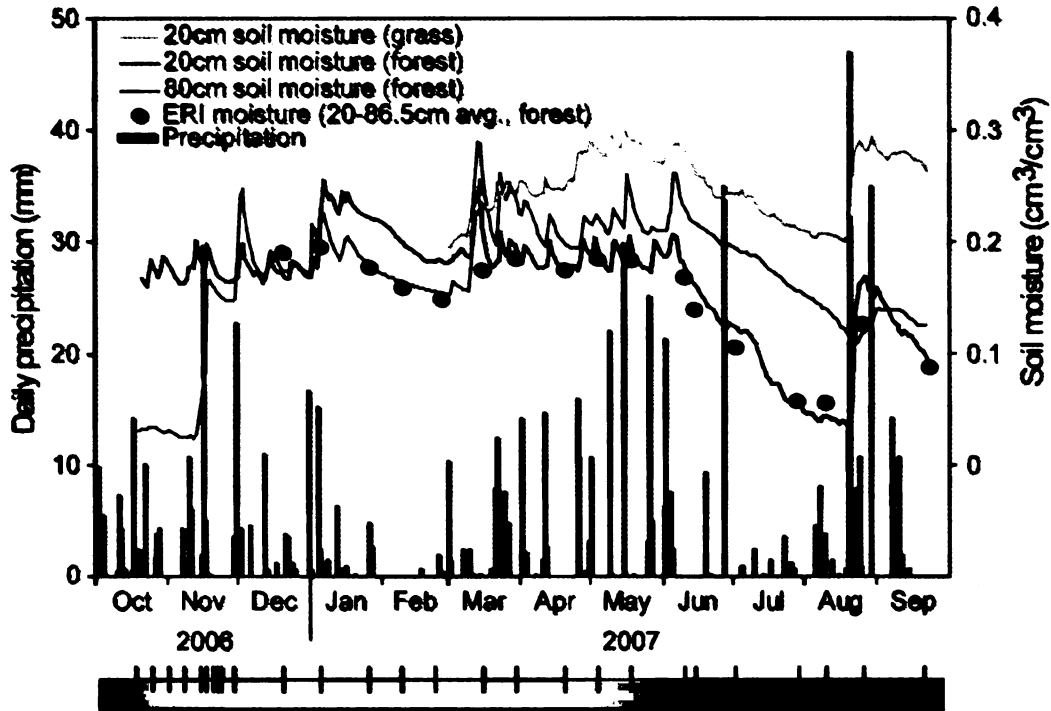


Figure 3-1. Soil moisture from probes at the site and the average of the 20 and 86.5 cm depth ERI moisture estimates for all datasets corrected with site temperatures. Precipitation data is shown for a nearby gage. The color bar shows the state of the forest canopy, vertical lines mark data collection dates, and shaded areas above the bar are differential inversion periods for Figure 3-2. Images in this dissertation are presented in color.

We corrected our inverted resistivity data for soil temperature differences using data from the vertical sensor arrays (Hayley et al. 2007). Average summer soil temperatures at 20 cm depth below the forest were $\sim 3^{\circ}\text{C}$ cooler than below the grassland, largely due to shading by the forest canopy. After leaf-off in November 2006, the near surface temperature difference became negligible. The temperatures were assumed to be laterally uniform below each land cover, except for the ~ 20 m wide portion of the grassland seasonally shaded by the adjoining forest, where we interpolated the temperatures. Seasonal fluctuations

were less significant at 147 cm, thus the temperature was linearly interpolated to a constant 10°C at 10 m depth based on observations below the water table.

Temperature distributions preceding the installation of temperature sensors were estimated with multi-depth soil temperatures from the nearby weather station.

To estimate moisture contents from the resistivity data, site- and material-specific relationships between resistivity (ρ) and volumetric water content (θ) were developed following ASTM standard G57-95. After oven drying at 105°C for 24 hours, ten soil samples from the field site were wetted in ~4% water content increments, homogenized, and placed in a test box for resistivity measurements. For these samples, as for most soil materials, the ρ - θ relationship is well approximated by a power function with coefficient m (sand = 1.16; clay loam = 0.67), which is used in (Archie 1942):

$$S = \left(\frac{\rho_s}{\rho} \right)^{\frac{1}{m}} \quad (3-1)$$

where S is saturation (volumetric water content / porosity), and ρ_s is bulk resistivity of the soil at 100% saturation, obtained from the field data (sand = 71.53 Ω m, clay loam = 68.15 Ω m). Since annual precipitation in Michigan greatly exceeds evapotranspiration (ET), we assume constant fluid conductivity. We calculated the soil moisture content for each resistivity value obtained from the differential inversions.

Results

Near the beginning of the study period, a significant growing-season soil moisture deficit existed below the shallow forest soils, which recovered after rain in November 2006. Beneath the snow, soil moisture declined until mid March, when snowmelt brought in a pulse of water. Both areas then experienced a steady moisture decline during the 2007 growing season, with a sharp increase following sustained rain in late August (Figure 3-1).

Important processes in the vadose zone are highlighted in Figure 3-2 using panels that show the profound seasonal influence of vegetation and climate on resistivity during the study period. The effects of different rooting depths between the forest and grassland on soil moisture are clear in early fall of 2006 (Figure 3-2a). A large rain four days prior to the end of the measurement interval initiated an infiltration pulse across the site (Figure 3-1). The shallow resistivity values below the forest then rapidly declined, yet values at similar depths below the grassland increased slightly. This implies that most of the infiltrated water below the grassland drained deeper within the profile because soils there were much closer to field capacity. Continued ET then caused a slight increase in shallow resistivity below the grassland. Increased resistivity at depth below the forest likely indicates that the trees were actively transpiring. In contrast, deep resistivity decreased below the grassland as water drained below the effective rooting depth.

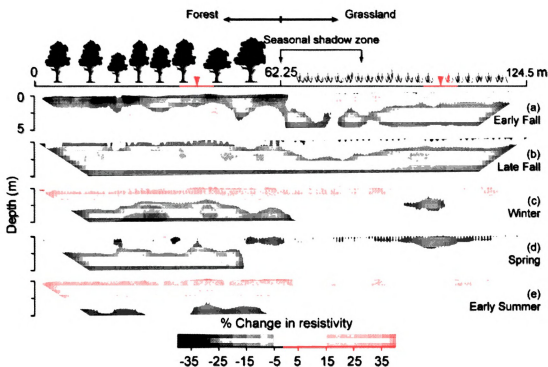


Figure 3-2. Differential resistivity panels for approximately one-month periods. a) Early fall (10/18 – 11/15), b) late fall (11/22 – 12/20), c) winter (1/5 – 2/9), d) spring (3/16 – 4/20), and e) summer (6/10 – 7/2). Trees are not to scale; 80 cm of relief along the array is included in the inversion. Red triangles locate moisture probes and temperature arrays. A decrease in resolution with depth and associated smoothing artifacts can cause resistivity differences below the water table. Images in this dissertation are presented in color.

Following the 2006 leaf senescence, resistivity below the forest decreased (Figure 3-2b), consistent with increases in soil moisture during a period of minimal transpiration and reduced evaporation under an insulating layer of leaf litter. In contrast, the shallow soils below much of the grassland, where the vegetation was still green, show no significant change in resistivity. However, the shallow soils below the grasses that were previously shaded by the trees show a small increase in resistivity during this period, suggesting a late period of active

ET in response to increased solar radiation. The resistivity of the deeper soils below the grass decreased, indicating that precipitation continued to percolate below the zone of root water uptake.

During the winter, consistent below-freezing air temperatures and snow cover reduced ET and surface infiltration, as indicated by the temperature-corrected resistivity increase (Figure 3-2c) and moisture probe data (Figure 3-1). Beneath the forest, the resistivity data show moisture redistribution deeper within the soil profile. The lack of significant resistivity changes below the grassland indicate that the moisture conditions there remained stable during this period.

The spring period is characterized by snowmelt infiltration, which resulted in a continued decrease in resistivity below the forest (Figure 3-2d). In contrast, moisture contents below most of the grassland remained largely stable as indicated by an absence of resistivity changes. This suggests that these soils were at or above field capacity during the spring months, and most snowmelt likely became recharge in the absence of significant runoff at the site.

Early in the summer, high ET reduced the root-zone soil moisture content, increasing the resistivity of the near surface soil layers (Figure 3-2e). Vegetation differences are prominently highlighted, with larger resistivity increases below the forest. The forest canopy intercepts more precipitation than the grasses, reducing infiltration. Greater transpiration in the forest is another likely contributor to the higher resistivity increases. Across the site, the resistivity increase was mostly limited to the upper 2 m, in contrast to the observations during early fall of 2006

(Figure 3-2a). This illustrates preferential uptake of near surface moisture, caused by the low suction potential of the relatively moist early-summer soils.

The soil moisture calculated from ERI data with Archie's equation (3-1) strongly correlates with the point-scale observations ($\theta_{\text{calculated}} = 1.04 \cdot \theta_{\text{observed}} - 0.04$; $R^2 = 0.92$, Spearman's ranked correlation = 0.88; $p\text{-value} < 0.0001$). The small underestimation of the calculated moisture contents is likely due to a preferred sensitivity of ERI to high resistivity layers as shown by the excellent match between ERI estimated values and the smallest of the two measured water contents in the forest (Figure 3-1). The small residual variation is partly due to differences in resolution and fluid conductivity, but this conductivity effect is minimal in the unsaturated zone where water saturation governs bulk resistivity.

The spatial and temporal evolution of moisture content through the study period shows a clear contrast across the ecotone (Figure 3-3). The largest contrast in moisture contents beneath the two vegetation types was observed in October 2006. The soil moisture deficit was much larger and extended deeper below the forest (Figure 3-3a), which implies that the forest has less recharge than the grassland. As expected, an increase in moisture contents is observed through early spring prior to significant transpiration by the trees. This resulted in the minimum observed contrast in moisture contents across the ecotone during the early growing season (Figure 3-3e). During the summer of 2007, the soil moisture deficit again began to build preferentially below the forest (Figure 3-3f). In contrast to the late growing season of 2006, most of the moisture is extracted

from the shallow zone during this period. The large increase in soil moisture below 4 m depth, from October 2006 to April 2007, is partly due to a rising water table.

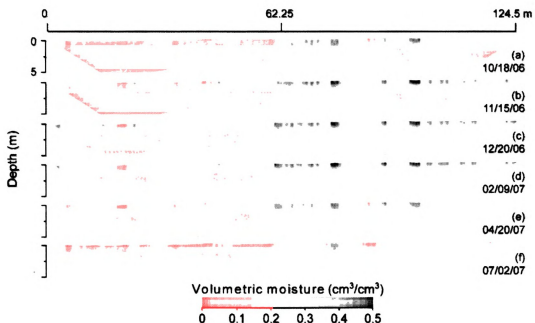


Figure 3-3. Spatial and temporal distribution of soil moisture estimated across the ecotone. Images in this dissertation are presented in color.

We computed spatially averaged subsurface soil moisture differences between peak-growing (July-August) and early-growing (April-May) periods for zones entirely within the forest and the grassland. These data clearly show both the effective rooting depth and contrasts in moisture abstraction characteristics of the two vegetation types (Figure 3-4). The total moisture change is much smaller below the grassland than the forest, and the zone of effective root water uptake is considerably shallower for the grass. The deep moisture depletion below the forest suggests that the tree roots tap into readily available water in the capillary

fringe, similar to phreatophytes in riparian areas. However, the largest moisture changes occur in the top 2 m of the subsurface in both vegetation types, consistent with field and modeling studies of root water abstraction (Jackson et al. 1996).

Conclusions

Our results quantify differences in root-zone moisture uptake below contrasting vegetation types and the evolution of vadose zone moisture in response to seasonal climate and vegetation processes using ERI. The results demonstrate the value of ERI for quantifying soil moisture distributions and understanding unsaturated zone processes. We believe that with such geophysical methods, significant insight can be gained about interactions between the atmosphere, hydrosphere, and biosphere. Understanding these interactions is essential for identifying the potential impacts of climate and land cover changes on the hydrologic cycle. Our findings show that land transformations would alter near surface soil moisture distribution patterns, impacting groundwater recharge rates, land-atmosphere energy exchange characteristics, and streamflow. For example, partial reforestation of the midwestern United States would likely reduce regional groundwater recharge rates. Until now, such tangible evidence at spatial and temporal scales considered in our study has been unavailable. Our analysis provides significant

new insights into the impacts that accompany ongoing and anticipated global changes in land use and climate due to anthropogenic and natural stressors.

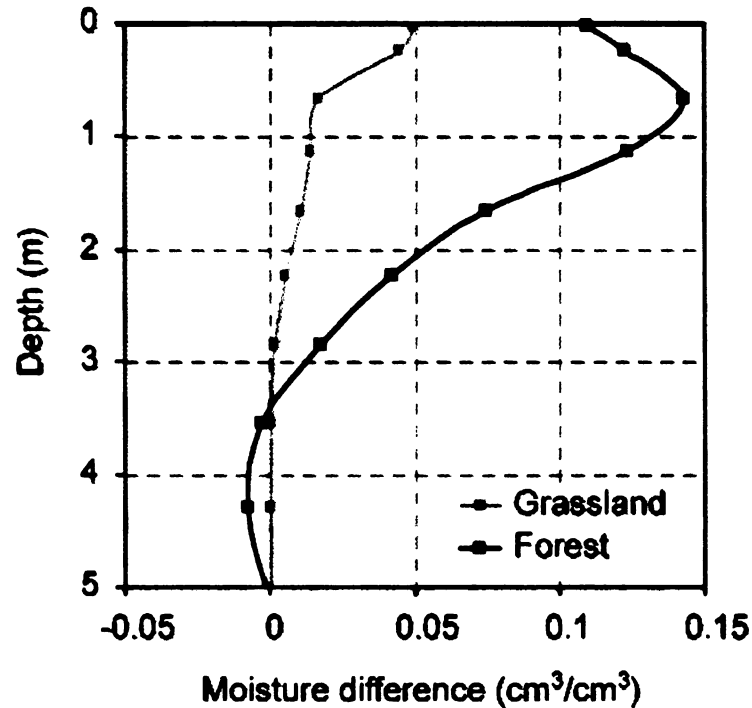


Figure 3-4. Laterally averaged changes in soil moisture below the forest (36-51 m) and the grassland (92-107 m) between early-growing (April to early May) and peak-growing periods (July to August). Images in this dissertation are presented in color.

Acknowledgements

This research was funded by NSF (EAR-0233648) and MSU Center for Water Sciences. We thank M. Malkowski, M. Morse, P. Bloese, and R. Klevickas for field support, and J. Butler, J. Hendrickx, and A. Kendall for discussions.

References

- Al Hagrey, S.A. (2007), Geophysical imaging of root-zone, trunk, and moisture heterogeneity, *J. Exp. Bot.*, 58(4), 839–854.
- Amidu, S.A., and J.A. Dunbar (2007), Geoelectric studies of seasonal wetting and drying of a Texas vertisol, *Vadose Zone J.*, 6(3), 511–523.
- Archie, G.E. (1942), The electrical resistivity log as an aid in determining some reservoir characteristics, *T. Am. Inst. Min. Metal. Eng.*, 146, 54–61.
- Berthold, S., L.R. Bentley, and M. Hayashi (2004), Integrated hydrogeological and geophysical study of depression-focused groundwater recharge in the Canadian prairies, *Water Resour. Res.*, 40(6), W06505.
- Betts, R.A., O. Boucher, M. Collins, P.M. Cox, P.D. Falloon, N. Gedney, D.L. Hemming, C. Huntingford, C.D. Jones, D.M.H. Sexton, and M.J. Webb (2007), Projected increase in continental runoff due to plant responses to increasing carbon dioxide, *Nature*, 448(7157), 1037–1041.
- Binley, A., P. Winship, L. J. West, M. Pokar, and R. Middleton (2002), Seasonal variation of moisture content in unsaturated sandstone inferred from borehole radar and resistivity profiles, *J. Hydrol.*, 267(3-4), 160–172.
- Daily, W., A. Ramirez, D. Labrecque, and J. Nitao (1992), Electrical-resistivity tomography of vadose water movement, *Water Resour. Res.*, 28(5), 1429–1442.
- Hayley, K., L.R. Bentley, M. Gharibi, and M. Nightingale (2007), Low temperature dependence of electrical resistivity: Implications for near surface geophysical monitoring, *Geophys. Res. Lett.*, 34(18), L18402.

- Jackson, R.B., J. Canadell, J.R. Ehleringer, H.A. Mooney, O.E. Sala, and E.D. Schulze (1996), A global analysis of root distributions for terrestrial biomes, *Oecologia*, 108(3), 389–411.
- Jackson, T.J. (2002), Remote sensing of soil moisture: implications for groundwater recharge, *Hydrogeol. J.*, 10(1), 40–51.
- Jayawickreme, D.H., and D.W. Hyndman (2007), Evaluating the influence of land cover on seasonal water budgets using Next Generation Radar (NEXRAD) rainfall and streamflow data, *Water Resour. Res.*, 43, W02408.
- LaBrecque, D.J., and X. Yang (2001), Difference inversion of ERT data: a fast inversion method for 3-D in situ monitoring, *J. Env. Eng. Geoph.*, 6(2), 83–89.
- Lesmes, D.P., and S.P. Friedman (2005), Relationships between the electrical and hydrogeological properties of rocks and soils, in *Hydrogeophysics*, edited by Y. Rubin and S.S. Hubbard, pp. 87-128, Springer, Dordrecht.
- Nemani, R.R., C.D. Keeling, H. Hashimoto, W.M. Jolly, S.C. Piper, C.J. Tucker, R.B. Myneni, and S.W. Running (2003), Climate-driven increases in global terrestrial net primary production from 1982 to 1999, *Science*, 300(5625), 1560–1563.
- Robock, A., K.Y. Vinnikov, G. Srinivasan, J.K. Entin, S.E. Hollinger, N.A. Speranskaya, S.X. Liu, and A. Namkhai (2000), The global soil moisture data bank, *Bull. Am. Met. Soc.*, 81(6), 1281–1299.
- Rodriguez-Iturbe, I. (2000), Ecohydrology: A hydrologic perspective of climate-soil-vegetation dynamics, *Water Resour. Res.*, 36(1), 3–9.
- Rushton, K.R., H.M. Eilers, and R.C. Carter (2006), Improved soil moisture balance methodology for recharge estimation, *J. Hydrol.*, 318(1-4), 379–399.

- Scanlon, B.R., I. Jolly, M. Sophocleous, and L. Zhang (2007), Global impacts of conversions from natural to agricultural ecosystems on water resources: Quantity versus quality, *Water Resour. Res.*, 43(3), W03437.
- Scott, C.A., W.G.M. Bastiaanssen, and M.U.D. Ahmad (2003), Mapping root zone soil moisture using remotely sensed optical imagery, *J. Irr. Drain. Eng.*, 129(5), 326–335.
- Seneviratne, S.I., D. Luthi, M. Litschi, and C. Schar (2006), Land-atmosphere coupling and climate change in Europe, *Nature*, 443(7108), 205–209.
- Singha, K., and S.M. Gorelick (2005), Saline tracer visualized with three-dimensional electrical resistivity tomography: Field-scale spatial moment analysis, *Water Resour. Res.*, 41(5), W05023.
- Slater, L., A. Binley, W. Daily, and R. Johnson (2000), Cross-hole electrical imaging of a controlled saline tracer injection, *J. Appl. Geoph.*, 44(2-3), 85–102.

Chapter Four

Integrating Geophysics and Hydrologic Models to Evaluate Land-use Impacts on Groundwater Resources

Introduction

Land-use and land cover (LULC) changes have important consequences on the hydrologic cycle. Transformation of vegetation that often results during LULC change can lead to hydrological shifts at local to regional scales (Oconnell et al. 1995; Pitman et al. 2004). The contrasts between plant species in their ability to intercept, access and transpire water affect the atmospheric and subsurface components of the hydrologic cycle (Nosetto et al. 2005; Pielke 2005; Beighley et al. 2008). A major concern related to LULC change is its potential effects on groundwater recharge, and hence the sustainability of a primary source of freshwater around the world (Scanlon et al. 2005). LULC and LULC change impacts not only the quantity (Farley et al. 2005; Scanlon et al. 2005), but it is also closely linked to quality of the groundwater (Blinn and Bailey 2001; Wayland et al. 2003; Jarvie et al. 2008). With changes in groundwater recharge patterns, the interlinked systems of streams, wetlands, and riparian environments along with their respective ecosystems are likely to be permanently altered (Rood et al. 2008).

The concern for potentially rapid land-use changes due to climate, population dynamics, social and economic development policy decisions both at

national and international arenas have increased in recent decades. The Clean Development Mechanism-Afforestation/Reforestation provisions of the KYOTO protocol for example could have unintended consequences on water resources of the local environments while only minimally supporting the intended objective (Trabucco et al. 2008).

Above ground vegetation changes lead to below ground alterations of plant root structures. While the above ground implications of vegetation change (e.g., precipitation interception, albedo, phenology, and leaf density) are readily identifiable, below ground consequences are often not. However it is necessary to accurately characterize and represent these changes in hydrologic, ecosystem, and biological models for reliable assessments of land-use impacts on our environment and natural resources. Globally, most land-use changes are associated with deforestation for agriculture, afforestation of open lands or natural conversion of grasslands to forests (Bryant et al. 1997). On average woody species such as trees are more deeply rooted than grasses (Canadell et al. 1996), but the bulk of the root mass (>~45%) is contained within the first 30 cm for both woody and grass species (Jackson et al. 1996). Significant differences in root biomass distributions within a species and differences driven by environmental aspects such as soil characteristics, nutrient availability, and climate are known (Vogt et al. 1996; Coomes and Grubb 2000). However, subsurface roots are generally described in models with limited parameters; i.e. maximum rooting depth and the vertical root distribution. The two parameters allow for the partitioning of water uptake based on the relative density of roots at

each depth (Jackson et al. 2000). It is clearly important to validate the parameters of root distribution models at appropriate scales. However, such validations have been rare because there haven't been many practical approaches to measure below ground impacts of vegetation over large spatial and temporal scales. These findings illustrate the need to understand variability in root distributions and dynamics in space and time based on geological, biological, and hydrological properties.

The utility of geophysics for characterizing the shallow subsurface is well recognized (Reynolds 1997). In recent years the value of certain methods for monitoring and quantifying moisture changes in the shallow subsurface has been reported by a number of researchers (Daily et al. 1992; Zhou et al. 2001; French et al. 2002; Hanafy and al Hagrey 2006). The sensitivity of electrical conductivity to changes in soil moisture contents allows the use of Direct Current Electrical Resistivity Imaging (ERI) method for hydrologic investigations. Employing the technique in a time-lapse mode, where the apparent resistivities are repeatedly measured with the electrodes at the same locations, provides valuable data for estimating transient characteristics of subsurface water fluxes (Looms et al. 2008). Such information provides an excellent platform to describe and understand recharge processes at large spatial scales, which has been difficult with traditional point observations. Moreover, the spatially explicit nature of subsurface geophysical measurements enables direct comparisons of these observations with above ground distributions of vegetation and their uptake processes. The depth sensitivity of the measurements, with either commonly

practiced surface electrode resistivity measurements or borehole techniques can help define the spatial distributions, and dynamics of root water abstraction processes at field scales. This approach avoids the practical difficulties and invasive nature of trenching and other methods that have been traditionally practiced for measuring root attributes to implement root water abstraction in hydrologic and ecosystem models.

Here we present evidence of significant differences in land-use driven subsurface fluxes that are important for groundwater resource sustainability. Soil temperature, moisture, water quality, and groundwater observations for different land-covers collected over multiple seasons are compared and contrasted. We evaluate a simplified approach to quantify the broader impacts of land-use differences on groundwater recharge by integrating spatially explicit soil moisture observations at field-scales with hydrologic modeling. Our field observations provide insight into below ground vegetation impacts at field scales. These observations along with the explored hydrologic and geophysical data integration are expected to help the community develop a scientific consensus on the effects and impacts of LULC on water resources (Petheram et al. 2002; Scanlon et al. 2005).

Study sites

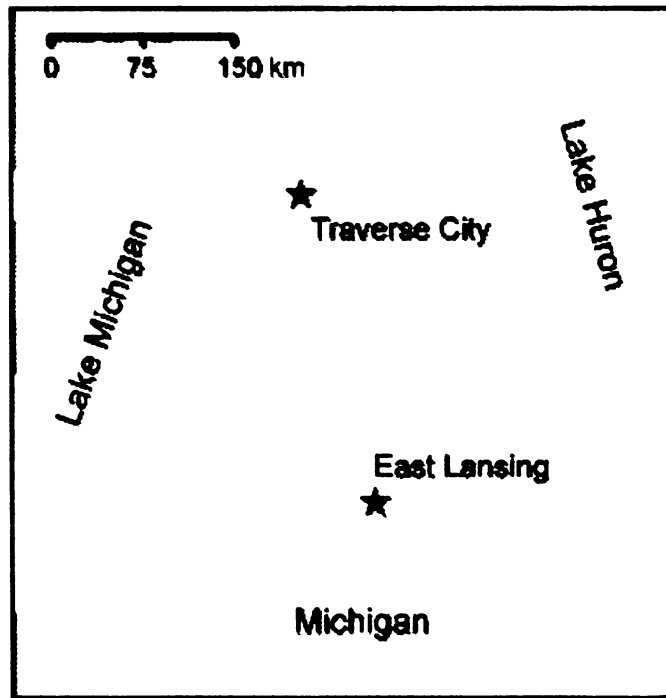


Figure 4-1. Locations of East Lansing and Traverse City, Michigan field sites where soil moisture dynamics were imaged with ERI.

Two field sites were established in Michigan to monitor the spatiotemporal interactions between climate, vegetation, and vadose zone soil moisture (Figure 4-1). The East Lansing study site is characterized by ~4m deep unsaturated zone composed of 40-60 cm of clay loam underlain by a layer of medium to fine sand extending to at least 5m depth. The soil distribution is laterally similar across the studied site transect. The vegetation at the site consists of a mature Maple forest (*Acer Saccharum*) and a grassland, which are separated by a sharp managed boundary. The grassland was established in 2004, prior to which it had been a Honeylocust (*Gleditsia Triacanthos*) plantation. The forest side of the ecotone

develops a dense canopy during the growing season (~May-October), which shades the ground during this time period. The trees are approximately 20-30 years old and are about 30m tall. The grassland is mowed once every year in late-summer or early-fall.

The site was initially equipped in September 2006 to monitor climate and vegetation impacts on near surface soil moisture distribution. Eighty four graphite electrodes (Φ 1.2 cm x 30 cm) were permanently installed at 1.5m separations along a 124.5m long transect, centered on the forest-grassland boundary for time-lapse electrical resistivity measurements (Figure 4-2). The permanent nature of the electrodes improves data quality, maximizing the potential to identify soil moisture changes. Capacitance-type soil moisture probes were installed at 20 cm and 80 cm depths in the forest in October 2006, and in the grassland in February 2007 (Figure 4-2). Soil temperature beneath the respective land-covers was monitored with two vertical temperature arrays with sensors at 5, 10, 20, 40, 80, 117, and 147 cm depths. The temperature sensors were installed in the forest in December 2006 and the grassland in February 2007. Additional temperature sensors were installed at 5 cm depth every 15m along the array at the beginning of the study period.

Groundwater elevations were monitored in ~ 5m deep observation wells installed below each land cover type in September 2007. Water table fluctuations and temperatures were logged every two hours with data logging pressure/temperature transducers. Climate data for the site were obtained from a

Michigan Automated Weather Network (MAWN) station approximately 1.5km from the site.

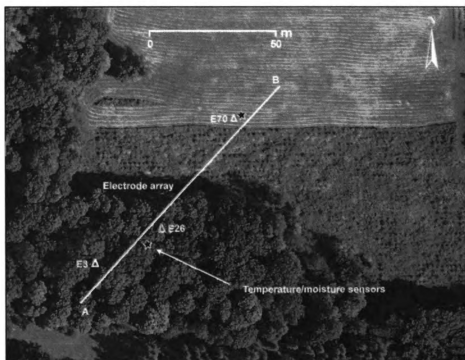


Figure 4-2. East Lansing field site. A-B: electrode array with 84 electrodes at 1.5m separation. E3, E26, E70 are groundwater observation wells. Temperature/soil moisture sensor locations have moisture probes at 20 & 80 cm depth. Temperature probes are at 5, 10, 20, 40, 80, 117, and 147cm depth at each location.

The Traverse City study site is located within a glacial outwash plain. The vadose zone consists of medium to fine clean sands in the first meter of the sub surface and based on available USGS well logs, the first 10 meters of the subsurface (the approximate unsaturated zone) consists of a system of sands and clays followed by sand and gravel to approximately 30 m depth. A sharp managed boundary separates an approximately 20 year old pine plantation from

a recreational grassland (Figure 4-3). The trees have a thin canopy, but 10 to 15 m tall trees are closely spaced (~3-4 m), resulting in significant shading. The needles that accumulate on the forest floor result in a thick litter layer that is significantly different from the one that develops at the East Lansing study site.

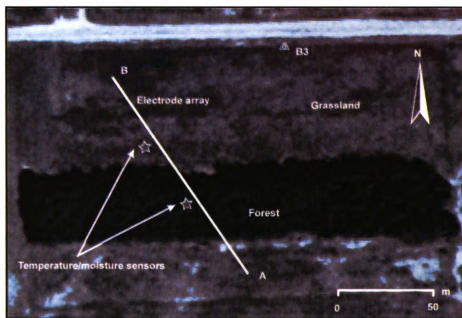


Figure 4-3. Traverse City study site. A-B: electrode array with 84 electrodes at 1.5m separation. B3 is the groundwater observation well. Moisture sensor locations shown have probes at 20 and 80 cm depths, and temperature sensors are at 5, 10, 20, 40, 80, 117, and 147 cm depths.

For long-term monitoring of soil moisture dynamics, the site was equipped similarly to the East Lansing study site with a permanent 84 electrode (1.2 cm diameter x 30 cm long) array for resistivity measurements. Capacitance-type soil moisture probes were installed in the forest at 20 and 80 cm depths, in addition to moisture probes under a canopy drip line and a tree line (close to tree stems) in July, 2006. The grassland soil moisture was monitored since October, 2006.

Data was logged at least every 30 minutes in both land-covers. Sensor arrays for monitoring soil temperature, constructed similar to those at East Lansing site, were installed below both land-covers in December 2006.

Field observations

At the East Lansing site, the deciduous Maple trees leaf out in late April and develop a dense canopy by mid to late June. The forest canopy insulates the forest floor resulting in only sparse undergrowth that is generally no more than a few centimeters tall. The trees shed their leaves in mid November, which deposits a litter layer on the forest floor each year. In contrast the adjacent grassland remains green until the first snowfall or the onset of below freezing temperatures which generally arrives in late December. Grasses again become active in late March after snowmelt with warm spring temperatures.

The evergreen trees at the Traverse City site are much smaller in diameter. The needle leaves are prominent only in the tree crowns, but a significantly thicker (5-15 cm) litter layer is present on the forest floor throughout the year. The adjacent grassland here is frequently mowed during summer months, resulting in \sim <5 cm tall grasses during the growing season. The Traverse City study site has a shorter growing season than East Lansing site because of its relatively northern latitude.

The two groundwater observation wells at the East Lansing site show a steady rise in water levels beginning in late fall (Figure 4-4). This corresponds to

the end of growing season and cessation of water use by the vegetation. The rising trend continues through March, where a significant rise in water table corresponds to the primary snowmelt of the year. The difference in water table elevations between the land covers disappear following snowmelt (Figure 4-4). While the overall long term water table behavior is similar within both land covers, the high frequency water table fluctuations observed in the grassland throughout the year are significantly damped in the forest. After May, a steady decline of water levels began, coinciding with the reemergence of leaves and active transpiration.

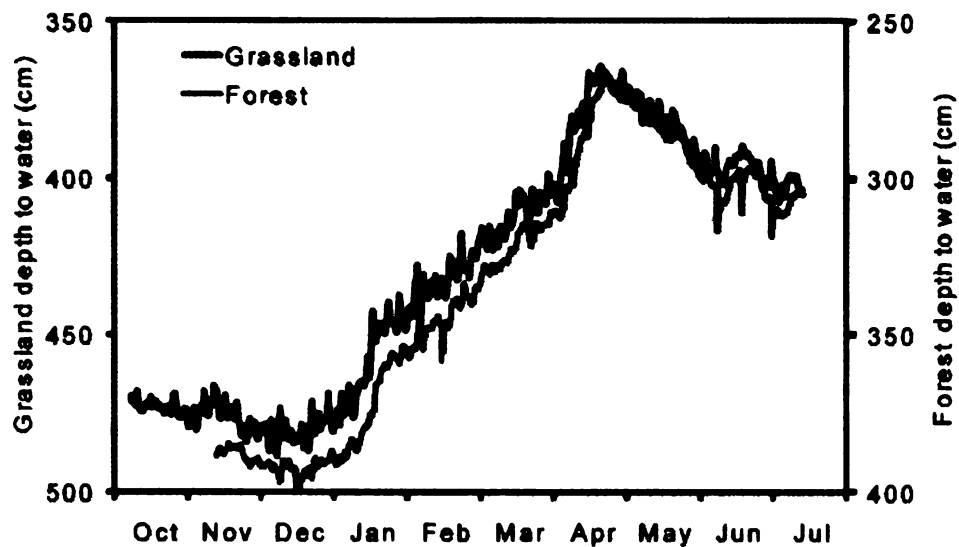


Figure 4-4. Groundwater observations since October 2007 at the East Lansing study site. Depth to water from the surface is shown for each well. Since the surface elevation at the forest well (E3, Figure 4-2) is 99 cm lower than the surface elevation at the grassland well the two vertical axis are offset by a similar amount. The wells are approximately 90 meters apart.

The Traverse City site has one USGS observation well located approximately 100 m northeast of the electrode array (Figure 4-5). Water levels

monitored there since June 2006 show the annual recharge-discharge cycles. Drops and rises in water table approximately coincide with the growing seasons and snowmelts respectively. Stable winter snowpack with no intermittent melting likely reduced recharge in 2007-2008 causing drainage and withdrawals to continuously lower the water table from November to early April.

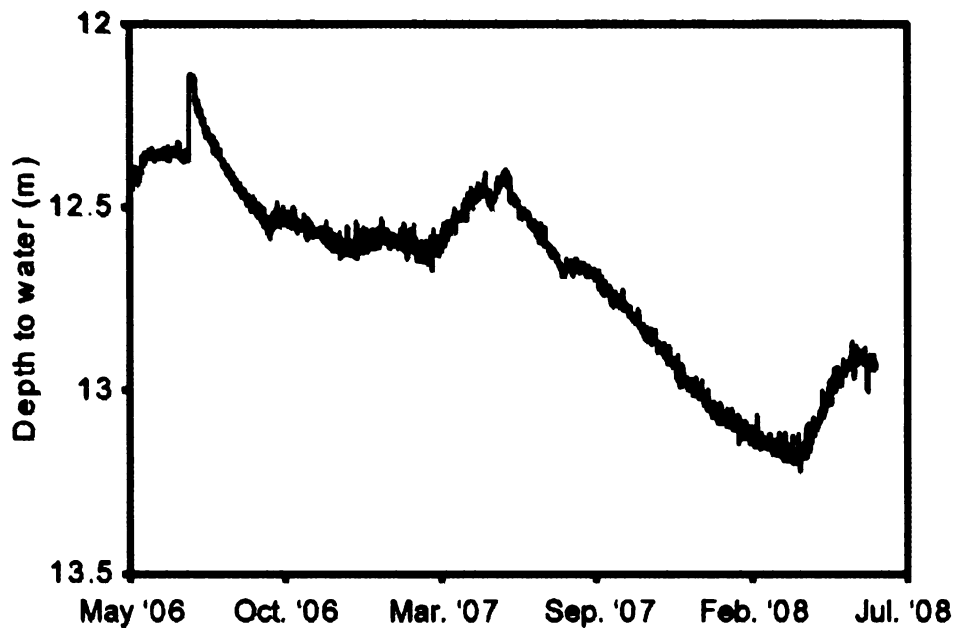


Figure 4-5. Groundwater observations at the Traverse City study site. Annual recharge-discharge cycles related to the growing season and spring snowmelt are evident in this well record.

Soil moisture measurements from the East Lansing site show substantial losses during the summer, marked by large declines in soil moisture below both land covers (Figure 4-6). Grassland moisture depletion however is significantly smaller than that below the forest.

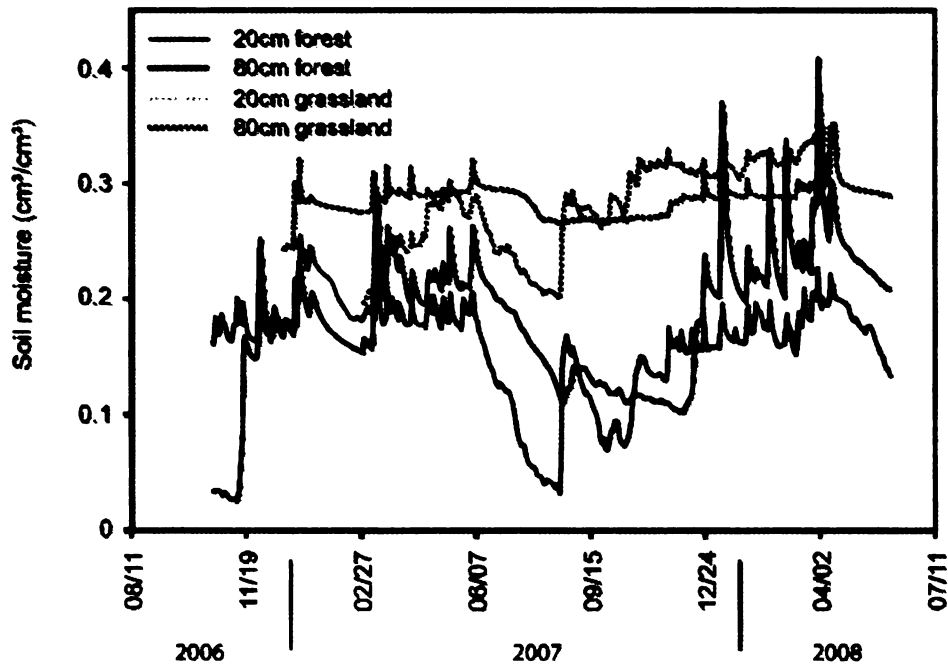


Figure 4-6. Soil moisture measurements below forest and the grassland at the East Lansing site.

Electrical Resistivity data acquisition and processing

Resistivity data were collected at both study sites using the Wenner and dipole-dipole electrode configurations. Data acquisition, on each visit, resulted in 1134 subsurface apparent resistivity measurements with the Wenner array, which was used for all the analysis and evaluations in this work. At the East Lansing study site, 53 datasets were collected from October 2006 to July 2008. Five datasets were collected at the Traverse City study site between July 2006 and June 2008, coinciding with important periods to capturing the impact of vegetation and climate processes on soil moisture fluctuations. Figure 4-7 and

Figure 4-8 illustrate two cross sectional views of the resistivity distributions in the subsurface and land cover characteristics at the two sites in summer.

The resistivity data acquired at the East Lansing site were inverted for resistivity changes using a difference inversion scheme (LaBrecque and Yang 2001), to focus on areas of the subsurface where soil moisture changes occur. All difference inversions were performed with respect to a single reference (background) dataset to preserve our ability to compare changes in soil moisture through time. A dataset collected on March 30, 2007 was selected as the base dataset, because the site had relatively uniform soil moisture across the ecotone after spring snowmelt. We first difference inverted all datasets relative to the base dataset, and then performed a pixel to pixel recalculation of each dataset using the percent difference and the base dataset. This approach minimizes uncertainties associated with inverting each dataset separately, especially when the goal is to identify differences in measured resistivity due to soil moisture changes (Daily et al. 2005).

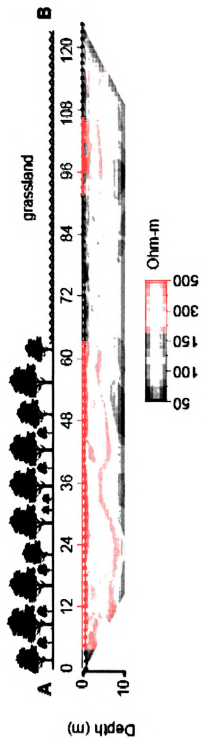


Figure 4-7. Cross-sectional view of the East Lansing study site with a representative late-summer subsurface resistivity distribution. Images in this dissertation are presented in color.

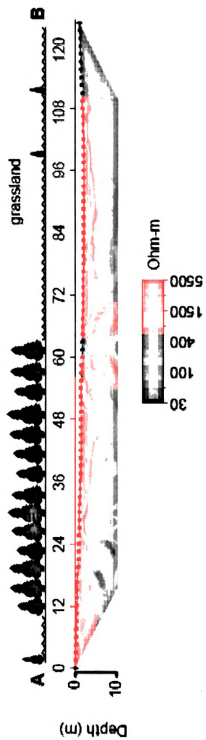


Figure 4-8. Cross-sectional view of the Traverse City study site with a representative late-summer subsurface resistivity distribution. Images in this dissertation are presented in color.

Interpreting resistivity data

Subsurface resistivity distribution below the two land covers at the East Lansing study site over time is shown in Figure 4-9. Distinct differences are evident below the two land-covers in both space and time. The groundwater data (Figure 4-4), which showed steady declines from June through November, and rises starting November are also evident in the vadose zone resistivity distributions. The within land-use resistivity variability is significantly higher in the forest compared to the grassland. A combination of potentially higher transpiration and canopy interception contribute to this higher resistivity variability observed in the forest. The grassland remained relatively homogeneous with respect to resistivity, reflecting apparently stable soil moisture characteristics. Slight increases in resistivity are evident during late summers in the grassland. Significantly lower interception here results in frequent soil wetting after precipitation events, making the grassland moisture behavior more dependent on precipitation frequency. Forest moisture dynamics in comparison are largely a function of vegetation dynamics during the growing season. A similar behavior was observed at the Traverse City study site between the grassland and the pine forest.

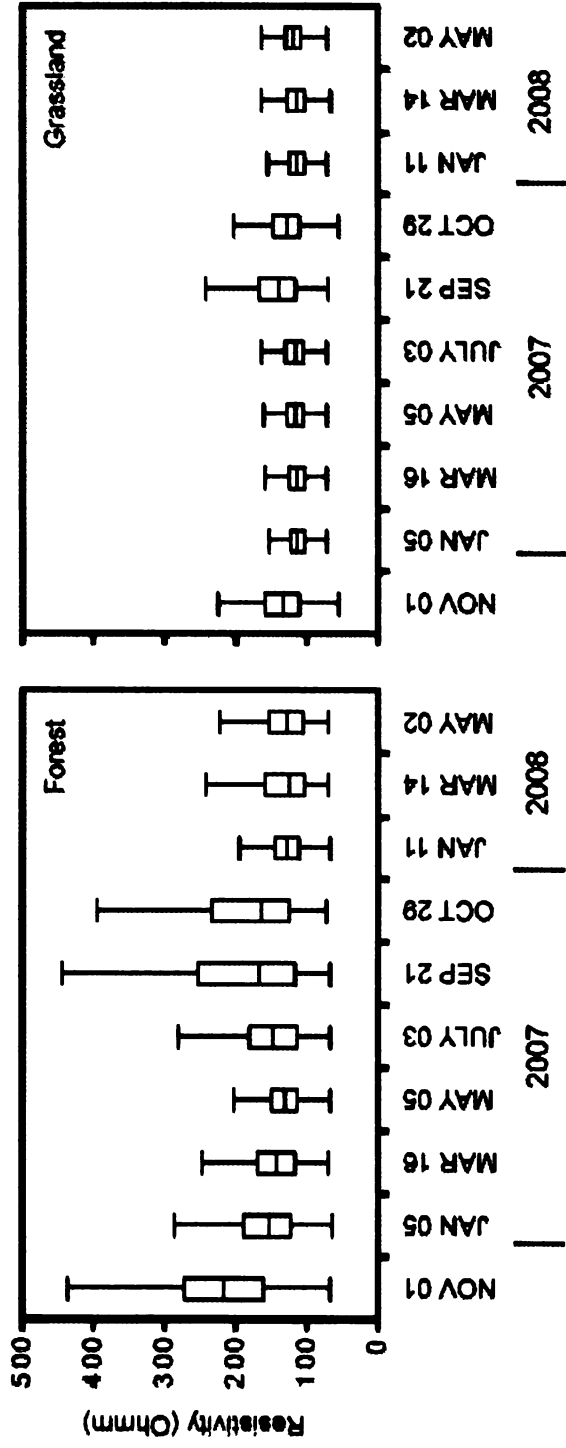


Figure 4-9. The temporal variability of subsurface (0-6m, surface to below seasonal water table) resistivity distribution below the forest and the grassland at the East Lansing site on selected dates. Mean, 25th & 75th percentiles, and the range for each date are shown.

The lowest resistivities observed below the grassland and the forest is approximately uniform across the land covers (Figure 4-9). A relatively higher pore water conductivity in the forest however results in minimum resistivities in the forest that are slightly lower than those below the grassland. Depth averaged (0-2m and 2-4m) resistivities shows the potential contrast in rooting zones between the two land covers and therefore the potential water withdrawal differences from the vadose zone (Figure 4-10). Resistivity changes occurred much deeper below the forest in 2006, potentially indicating the ability of trees to withdraw water from deeper parts of the subsurface (Figure 4-10). A similar increase in the 2-4m depth however did not occur in 2007.

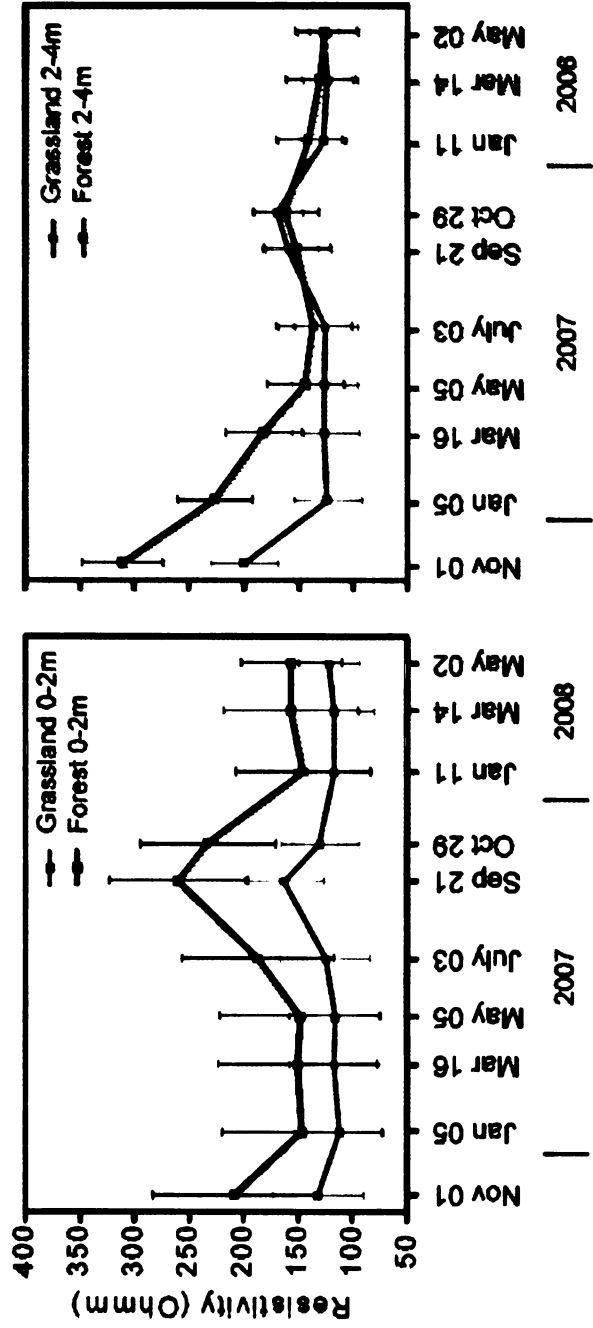


Figure 4-10. Mean resistivity values in the 0-2m and 2-4m depths through time. Similar resistivities in the 2-4m range during the latter part of the study period coincide with higher observed groundwater elevations at the research site.

Electrical resistivity and soil moisture

To estimate moisture contents from the resistivity data, site and material-specific relationships between resistivity (ρ) and volumetric water content (θ) were developed following ASTM standard G57-95. After oven drying at 105°C for 24 hours, ten soil samples from the field site were wetted in ~4% water content increments, homogenized, and placed in a test box for resistivity measurements. For these samples, as for most soil materials, the ρ - θ relationship is well approximated by a power function with coefficient m (sand = 1.16; clay loam = 0.67), which is used in (Archie 1942):

$$S = \left(\frac{\rho_s}{\rho} \right)^{\frac{1}{m}} \quad (4-1)$$

where, S is saturation (volumetric water content / porosity), and ρ_s is bulk resistivity of the soil at 100% saturation (sand = 71.53 Ω m, clay loam = 68.15 Ω m; based on field data). Since annual precipitation in Michigan greatly exceeds evapotranspiration (ET), we assume constant fluid conductivity values. We calculated the soil moisture content for each resistivity value obtained from the differential inversions. All resistivity data were corrected for temperature effects using an empirical relationship (Hayley et al. 2007). The soil moisture calculated with ERI is slightly underestimated compared to the point observations from the site (Figure 4-11).

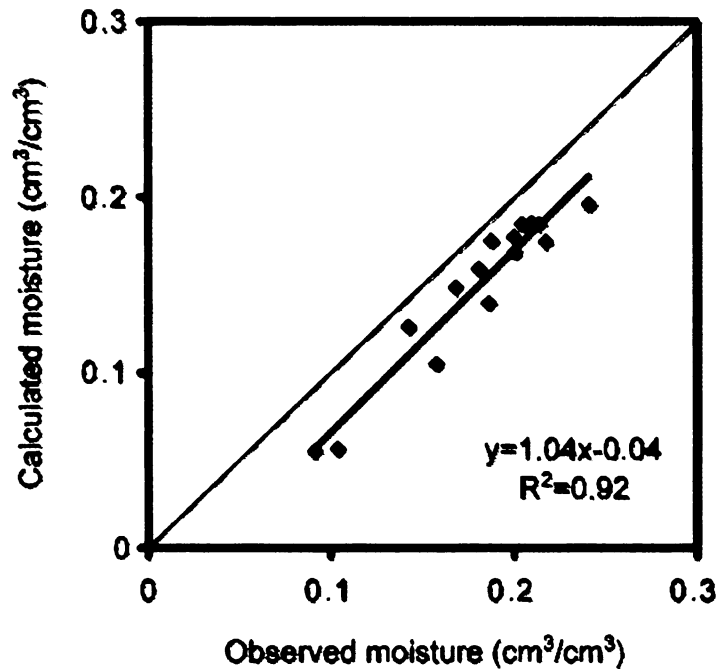


Figure 4-11. ERI estimated soil moisture and the observed moisture in the East Lansing study site (Forest). The arithmetic average of the 20 and 80cm cm moisture observations are shown.

Soil Moisture Dynamics and Relevance to Recharge

The calculated changes in soil moisture at the East Lansing site (Figure 4-12) show that the upper meter of the grassland subsurface has greater soil moisture retention than the forest. Field sampling of soils at the study site indicated that the soil texture characteristics within the two land-covers are generally similar. Therefore it is likely that this difference is due to water use differences between vegetation types, and potentially the relative compaction of the soils in the grassland. Resistivity data from the Traverse City study site also

showed a similar contrast in resistivity distribution between the forest and the grassland, with lower resistivities in the grassland.

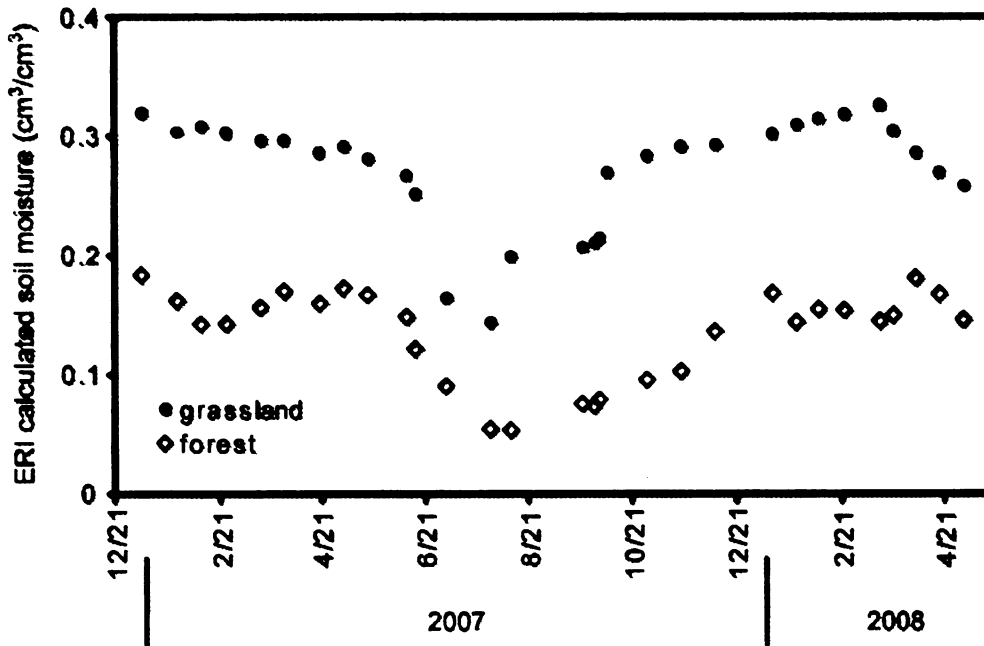


Figure 4-12. ERI calculated transient soil moisture (20-80cm cm arithmetic average) in the grassland and the forest. Higher moisture levels in the grassland are observed on each of the ERI data collection dates.

Knowledge of deep percolation is particularly important for groundwater recharge studies. Such information is often indirectly inferred from water table fluctuations and other localized observations. In contrast, broader spatial aspects of recharge characteristics can be better imaged with hydrogeophysical methods.

Figure 4-13 presents temporal soil moisture changes over the same time interval below the forest and the grassland at the East Lansing study site. These images show averages of an approximately 15m wide section of inverted data below each respective land cover for each collection date. The important times

when changes pertinent to groundwater recharge are identified using letters on the diagram. The early to mid growing seasons are represented by soil moisture losses in the shallow subsurface (A), followed by deeper moisture losses in the later part of the growing season (B), due to deeper drainage and surface infiltration during the growing season. Moisture depletion is higher in the forest. The main fall and spring recharge periods at the study site are represented by C and D when deep wetting is prominent. In the fall, deep wetting occurs after active transpiration. In spring, deep wetting is the result of snowmelt.

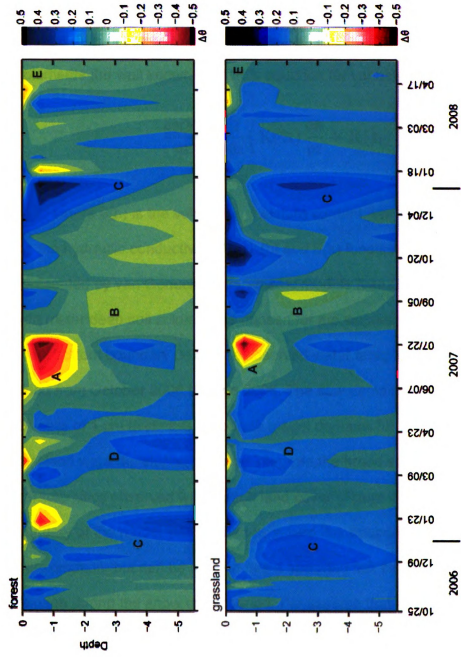


Figure 4-13. Temporal soil moisture changes in ~15 wide zones below the grassland and the forest. Cooler colors indicate moisture increases and warmer colors are moisture decreases. C is the main fall recharge period, followed by spring snowmelt (D). A, B, and E are growing season moisture deficits due to plant water use. Images in this dissertation are presented in color.

Hydrologic simulations

We integrated the ERI derived soil moisture with the one dimensional unsaturated zone flow model, HYDRUS-1D (Šimůnek et al. 1998) to quantify the recharge differences between the grassland and the forest. The modeling code implements the well known Richard's equation for variably saturated media;

$$\frac{\partial \theta(h)}{\partial t} = \frac{\partial}{\partial z} \left(K(h) \frac{\partial h}{\partial z} + K(h) \right) \quad (4-2)$$

where $\theta(h)$ is the volumetric moisture content, t is time, z is elevation, and K is the hydraulic conductivity. The $K(h)$ and $\theta(h)$ functions in Equation 4-2 are represented by van Genuchten parametric models (van Genuchten 1980). An eight meter deep soil column was chosen for the simulations, which keeps the model bottom boundary below the observed water table for the entire simulation period from October 2006 to June 2008. The flow domain was discretized into 801 cells of 1 cm thickness. Separate model domains for the forest and the grassland were developed to better integrate the broad soil and stratigraphic characteristics observed within each land cover (Figure 4-14). The bottom boundary of the model was defined as a zero flux boundary as a first approximation, but can be relaxed into a specified flux boundary based on the drainage during the snow cover period. We assume that lateral flows are insignificant in the system based on measured temporally consistent pore water conductivity differences ($\sim 100 \mu\text{S/cm}$) in the two wells at the site which are separated by $\sim 90\text{m}$.

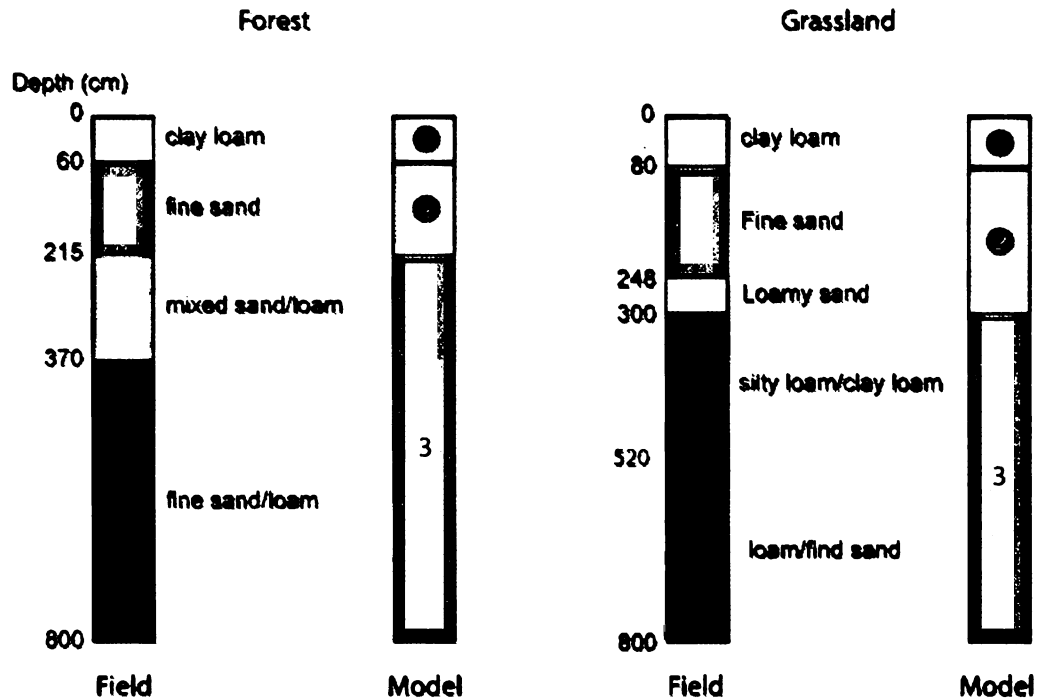


Figure 4-14. A simplified illustration of the soil texture and stratigraphy (from soil cores) in the forest and the grassland. Different soil texture units identified in field soil cores were combined to three representative layers in the vadose zone flow model (right). Images in this dissertation are presented in color.

The conceptual framework for integrating geophysical estimates of spatial soil moisture with HYDRUS-1D is illustrated in Figure 4-16. The subsurface soil moisture distributions obtained using the ERI data in step 1 were first used with an inverse flow model to obtain optimized soil parameters; θ_s , α , n , K_s (van Genuchten 1980) for each of the soil texture layers in the one dimensional models. Soil moisture estimates from late October to mid May of 2006/2007 and 2007/2008 were used in this step, because it should be possible to get better estimates of the soils alone during this period of low soil evaporation and vegetation water uses. Spatially averaged ERI derived soil moisture below the

two land-covers were used as calibration data for soil hydraulic parameter optimization in each model. The starting soil moisture for the modeled soil columns were obtained from a resistivity dataset collected on the same day the simulations were started (October 18, 2006).

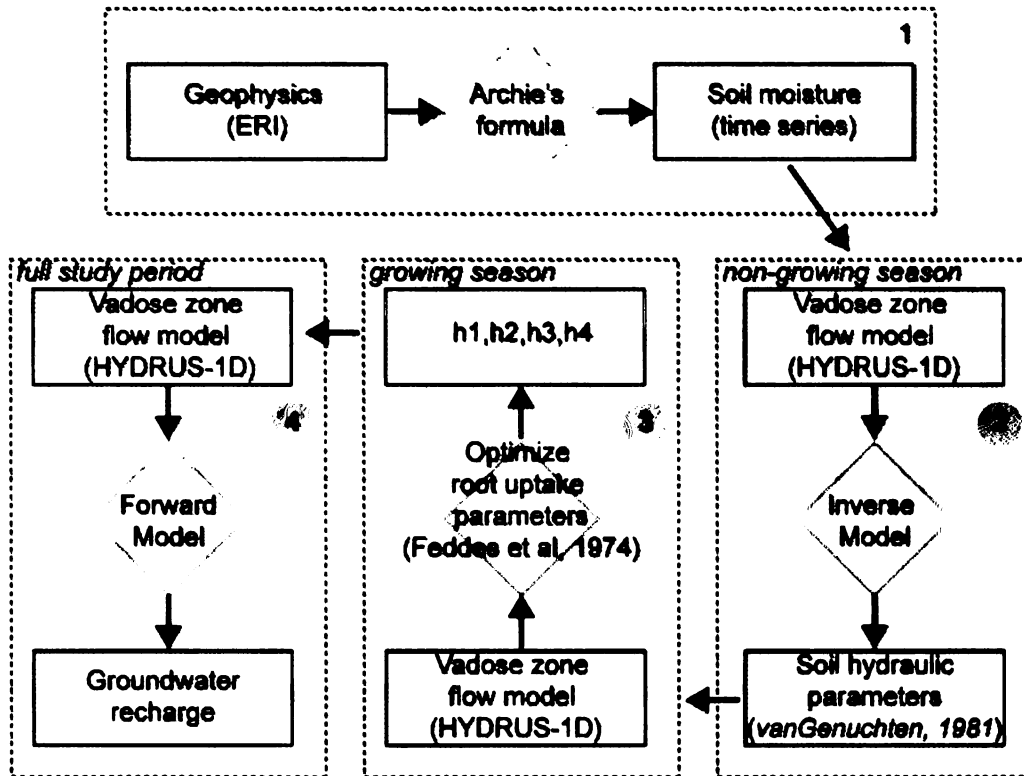


Figure 4-15. Conceptual framework for integrating geophysical soil moisture estimates with hydrologic modeling to estimate groundwater recharge. Soil parameters θ_s , α , n , K_s are optimized in stage 2, and plant water stress function parameters h_1 , h_2 , h_3 , h_4 , are calibrated in stage 3.

To define the root distribution within the model domains, we use information extracted from ERI data collected at the research site. The root zone distribution was interpreted based on the soil moisture changes computed between early-growing seasons and peak growing seasons with ERI data from

2007 (Figure 4-17). This is likely a better representation of the actual root distribution at the site. The sensitivity of the simulated hydrologic fluxes to root distribution was evaluated with a commonly used root distribution model;

$$\frac{L_r(z)}{L_{profile}} = e^{-cz} \quad (4-3)$$

where $L_r(z)/L_{profile}$ is the normalized root length density (0-1), z is depth, and c is a biome dependent empirical parameter, - 0.9 (forest) (de Rosnay and Polcher 1998). An initial set of root water abstraction parameters were selected from the HYDRUS-1D database (Šimůnek et al. 1998), and the same parameter set was used in both forest and grassland models.

Potential evapotranspiration rates at the site were calculated separately for the grassland and the forest (Figure 4-18) using the modified Penman-Monteith method (Monteith 1965), implemented in the Integrated Land Hydrology Model (ILHM) (Hyndman et al. 2007). Snowpack and snowmelt conditions under the two land-covers were assumed to be the same due to inadequate snowpack observations at the site.

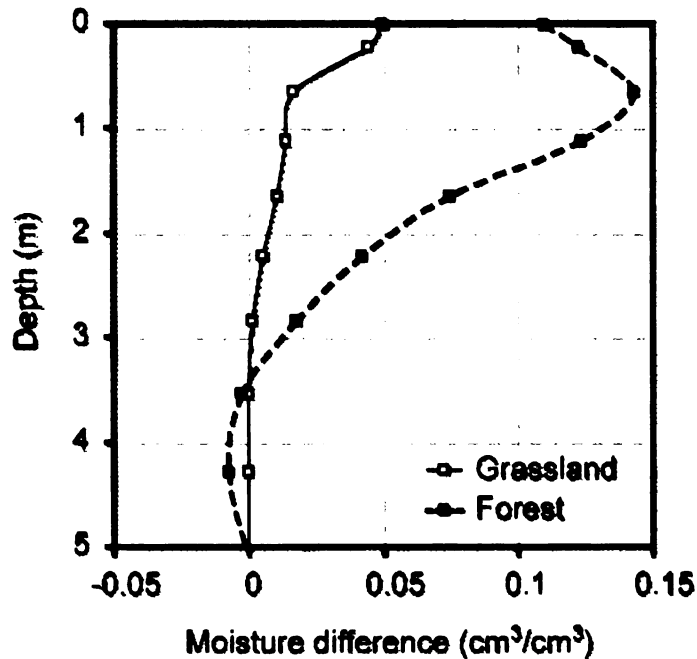


Figure 4-16. Laterally averaged changes in soil moisture below the forest and the grassland between early-growing (April to early May) and peak-growing periods (July to August) (from Jayawickreme et al., 2008).

With the soil parameters estimated with inverse modeling, only limited agreement between simulated and ERI estimated soil moisture was achieved (Figure 4-19 and Figure 4-20). However, the soil hydraulic parameters obtained are relatively representative of the soil texture types identified in field cores (Table 4-1 and Table 4-2). Simulations of hydrologic fluxes for the entire study period from October, 2006 to June, 2008 show that measured groundwater table elevations are fairly well estimated in the forest (Figure 4-20), but the simulated heads are relatively different in the grassland (Figure 4-21) due to among others an inadequate description of boundary conditions.

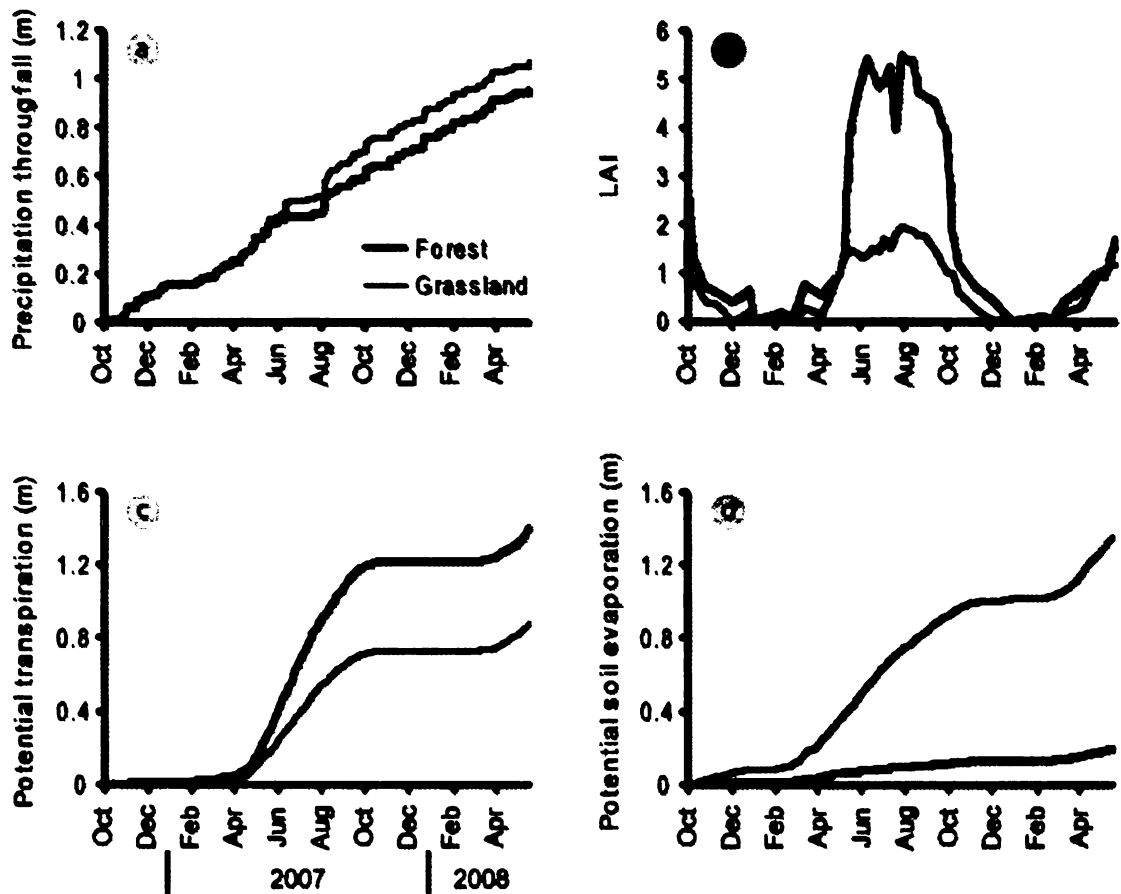


Figure 4-17. Cumulative precipitation throughfall (a), representative leaf area indexes (b) from MODIS, calculated cumulative potential transpiration (c) and soil evaporation (d) inputs for hydrologic simulations from ILHM.

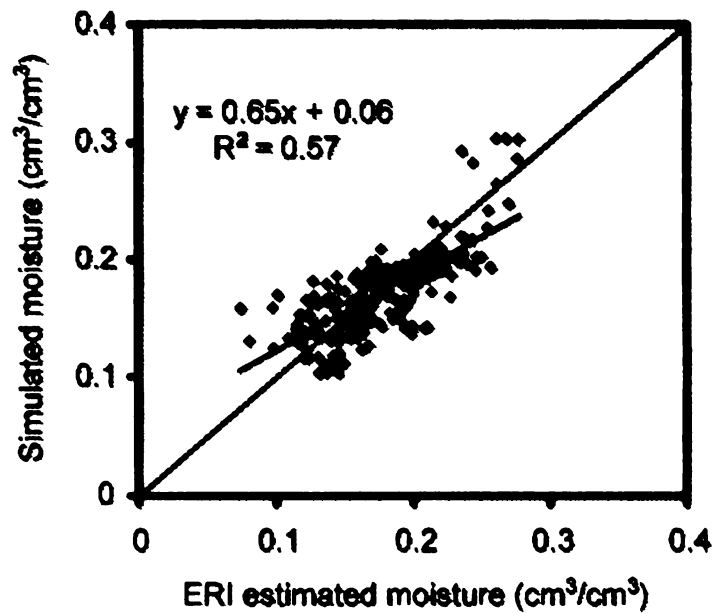


Figure 4-18. Simulated vs. ERI estimated soil moisture in the forest. Data is from 10 depths within the first 3m of the subsurface.

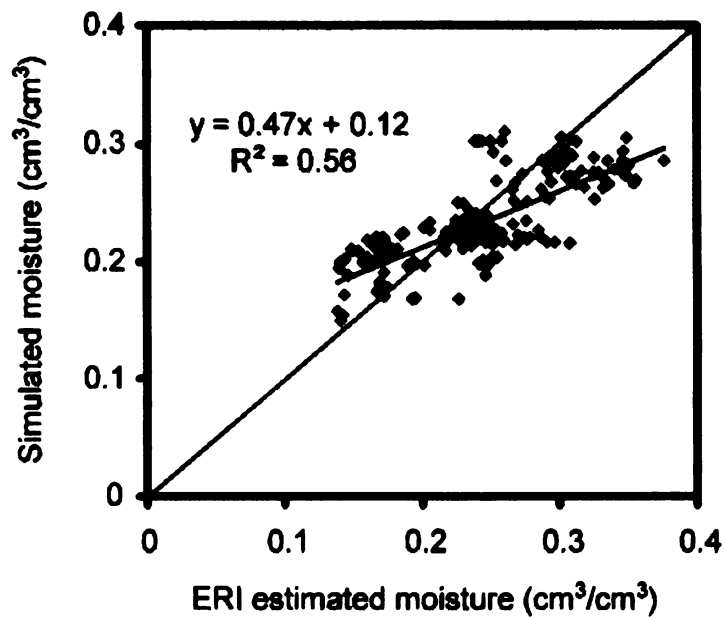


Figure 4-19. Simulated vs. ERI estimated soil moisture in the grassland with data from nine depths in the first 3m of the subsurface.

Layer	Parameter	Estimate	S.E. Coeff	95% CI	
				Lower	Upper
1	θ_s	0.30	0.06	0.19	0.42
	α	6.32	4.43	-2.40	15.03
	n	1.50	0.11	1.28	1.72
	Ks	1.46	2.16	-2.79	5.71
2	θ_s	0.29	0.03	0.23	0.35
	α	5.40	2.61	0.25	10.55
	n	1.36	0.08	1.19	1.53
	Ks	4.00	5.86	-7.55	15.55
3	θ_s	0.30	0.01	0.28	0.33
	α	2.80	0.66	1.50	4.10
	Ks	0.20	0.10	0.01	0.39

Table 4-1. Estimated soil hydraulic parameters for the three soil layers in the forest with standard errors of regression coefficients (S.E. Coeff) and confidence intervals.

Layer	Parameter	Estimate	S.E. Coeff	95% CI	
				Lower	Upper
1	θ_s	0.36	0.06	0.24	0.48
	α	7.84	9.21	-10.33	26.00
	n	1.20	0.08	1.04	1.36
	Ks	0.87	2.65	-4.35	6.09
2	θ_s	0.30	0.04	0.22	0.37
	α	4.40	4.77	-5.00	13.80
	n	1.20	0.07	1.07	1.33
	Ks	8.00	20.97	-33.35	49.35
3	θ_s	0.30	0.01	0.28	-0.33
	α	2.60	1.23	0.17	5.03
	Ks	0.20	0.18	-0.15	0.55

Table 4-2. Estimated soil hydraulic parameters for the three soil layers in the grassland.

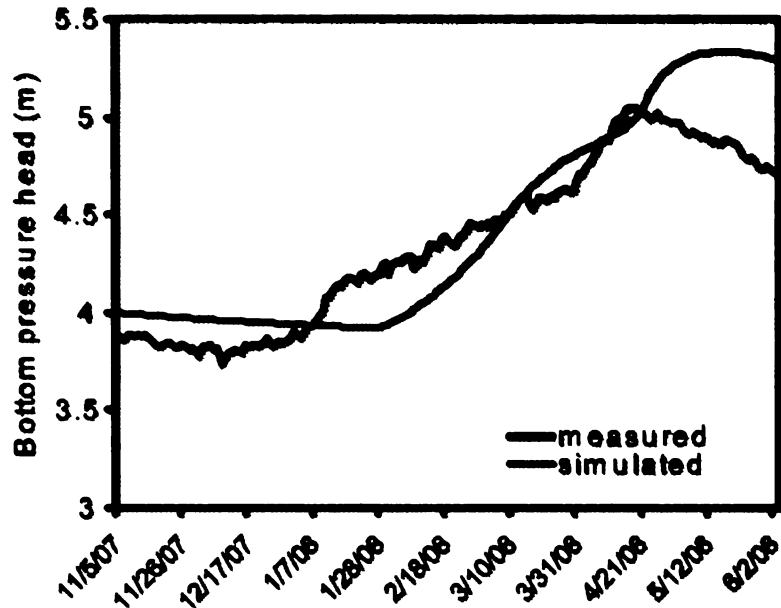


Figure 4-20. Measured and simulated groundwater table in the forest with optimized soil hydraulic parameter sets in the 1D-Hydrus model. These observation data were not used in the optimization for hydraulic parameters in the forest.

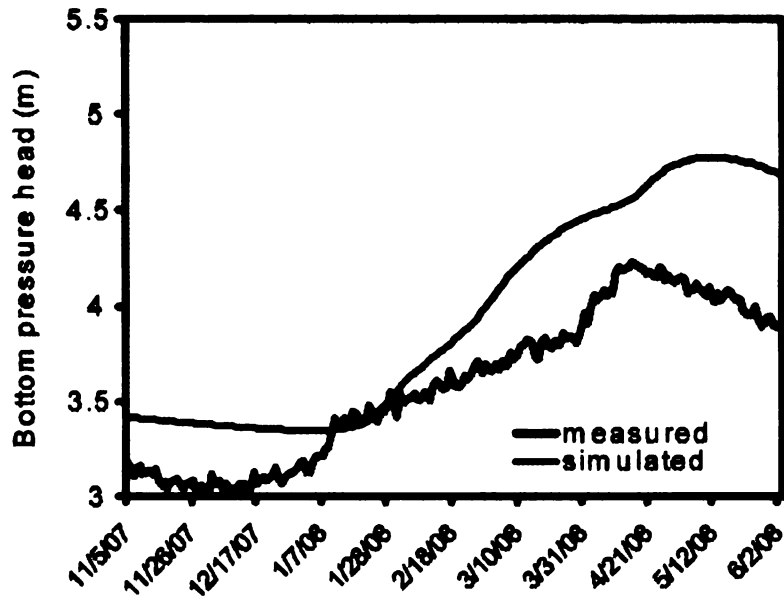


Figure 4-21. Measured and simulated groundwater table in the grassland with optimized soil hydraulic parameter.

The simulated summer growing season (June-October, 2007) soil moisture compares reasonably well in the forest (Figure 4-22), but the agreement is poor in the grassland where the simulated soil moisture content is lower than the ERI estimates (Figure 4-23). The cumulative transpiration in the forest and the grassland during the entire simulation period is 407 and 419mm respectively. Based on the discrepancy between ERI estimated and model simulated summer soil moisture in the grassland (Figure 4-23), it can be suggested that the simulated grassland transpiration is likely higher than the actual amount. The sensitivity of the simulated transpiration to root distribution (Table 4-3), root water abstraction parameters (Table 4-4), and soil hydraulic parameters (Table 5-1) indicate that simulated transpiration is likely to be most affected by the root water abstraction parameters h_1 and h_2 (Feddes et al. 1974). These parameters (h_1 , h_2 , h_3 , h_4) were initially assumed the same for both grassland and the forest. Based on the above analysis however, it is evident that this was an over simplification. But with the available ERI estimates of root zone soil moisture, root water uptake parameters for the grassland can be refined until a reasonable match between the simulated root zone soil moisture and ERI estimates is obtained. This process should also improve the simulated hydrologic fluxes in the grassland.

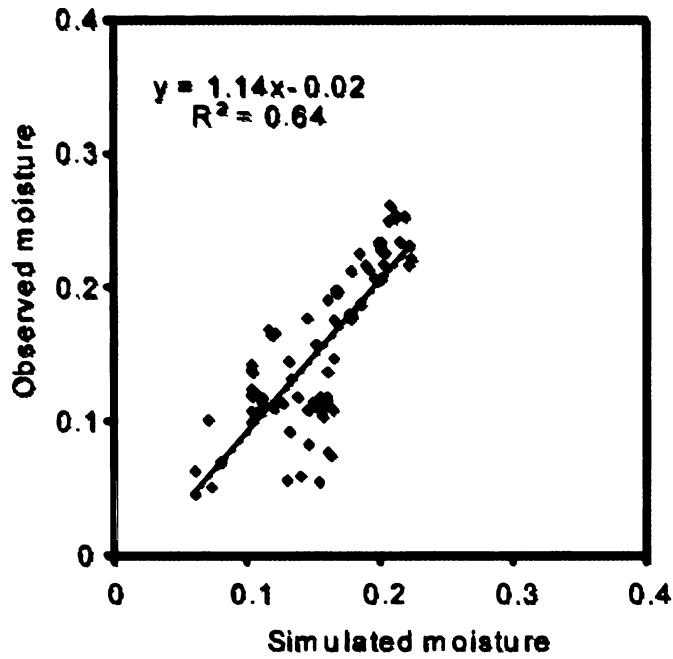


Figure 4-22. Observed (ERI calculated) vs. simulated moisture in the forest during summer (June-October, 2007).

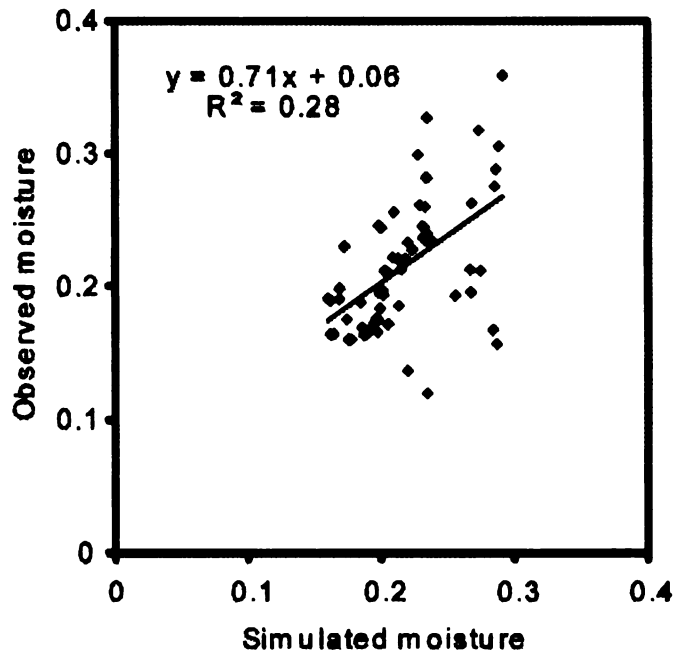


Figure 4-23. Observed vs. simulated soil moisture in the grassland from June to October, 2007.

Parameter	deRosany	ERI Root	$\Delta\%$
ΣT (mm)	394.17	407.69	-3.32
h	5.47	5.28	3.61

Table 4-3. Sensitivity of simulated cumulative transpiration ΣT and bottom pressure head (h) in the forest to different root distributions. ERI Root is root distribution estimated with resistivity data, deRosany model used with a distribution coefficient of -0.9 (de Rosnay and Polcher 1998).

Parameter	ΣE	ΣT	h	Base value (m)	$\pm 10\%$ base value
h1	0.43	-9.71	4.33	-0.8	-0.88
	-0.44	9.10	-3.88		-0.72
h2	0.44	-7.72	2.80	-2.5	-2.75
	-0.59	8.54	-3.16		-2.25
h3	0.00	0.00	0.00	-10	-11
	0.00	0.00	0.00		-9
h4	-0.01	0.36	-0.15	-80	-88
	0.01	-0.43	0.18		-72

Table 4-4. Sensitivity of simulated evaporation (ΣE), transpiration (ΣT), and model bottom pressure head (h) in the forest to a $\pm 10\%$ adjustment in root water abstraction parameters (Feddes et al. 1974). ΣE , and ΣT are given as percent changes relative the base model. h1-minimum pressure head for active transpiration, h2-pressure- head for maximum transpiration efficiency, h3-limiting pressure head where transpiration ceases to occur at maximum efficiency, and h4-wilting point.

Model layer	Parameter	Base value	± 10% base value	ΣI	ΣT	ΣE	h
Layer 1	θ _s	0.3	0.27	0.56	0.60	-2.44	1.21
			0.33	-0.50	-0.11	2.21	-1.26
	Alpha	6.32	5.688	-0.01	5.31	0.06	-2.23
			6.952	0.02	-4.24	-0.10	1.60
	n	1.5	1.35	-0.55	8.39	2.41	-5.80
1.65			0.61	-9.25	-2.68	5.57	
K _s	1.46	1.314	-0.06	-1.56	0.28	0.44	
		1.606	0.07	1.32	-0.32	-0.47	
Layer 2	θ _s	0.29	0.261	0.01	-8.20	-0.04	6.66
			0.319	0.00	4.84	0.01	-4.92
	Alpha	5.4	4.86	0.07	8.69	-0.33	-4.41
			5.94	-0.07	-9.28	0.31	5.04
	n	1.36	1.224	-0.03	2.31	0.15	-6.56
1.496			-0.05	-14.00	0.21	10.34	
K _s	4	3.6	-0.02	-3.10	0.10	1.35	
		4.4	0.04	2.28	-0.17	-1.17	
Layer 3	θ _s	0.3	0.27	-0.15	-9.35	0.67	19.18
			0.33	0.00	6.65	-0.01	-18.99
	Alpha	2.8	2.52	0.02	2.82	-0.07	-1.79
			3.08	-0.01	-2.72	0.02	1.50
	n	1.69	1.521	0.00	3.04	0.00	-1.87
1.859			0.00	-2.97	0.02	1.59	
K _s	0.2	0.18	0.00	-0.85	0.01	0.44	
		0.22	0.00	0.53	0.00	-0.20	

Table 4-5. Sensitivity of cumulative infiltration (ΣI), transpiration (ΣT), evaporation (ΣE), and bottom pressure head (h) in the forest to a $\pm 10\%$ adjustment in soil parameters. ΣI , ΣT , and ΣE shown are percent changes compared to the base model with optimized soil hydraulic parameters.

Discussion and Conclusion

In this chapter evidence for significant hydrologic differences driven by LULC characteristics at study sites in Michigan were presented. These differences are readily identified using geophysical methods that are both non-invasive and spatially explicit. Using time-lapse approaches, the spatial and temporal changes in soil moisture were identified and were related to vegetation and climate processes. Independent measurements of point soil moisture and groundwater table data substantiated the validity of geophysical measurements and subsequent interpretations.

Electrical resistivity measurements made at the study sites provided important information about subsurface consequences of above ground vegetation. Soil moisture and soil moisture change information derived from ERI data can be used to assess subsurface root distributions as well as to quantify spatial and temporal soil moisture use differences related to vegetation. Such spatially explicit information is generally difficult to obtain with point observations alone. By integrating this type of information with hydrologic models, better estimates of groundwater recharge and transpiration fluxes at any site can be obtained.

The approach devised in this study to directly integrate ERI estimated soil moisture is straight forward and simple. However the subsurface systems involved were inherently complex in terms of their properties and processes. Therefore the reasonable estimates of soil moisture and other hydrologic fluxes obtained with the forest model in particular are promising. Improvements to the

one dimensional models with better descriptions of boundary conditions could further improve their performance. Additionally, other approaches to integrate the geophysical estimates with the hydrologic models should be explored. The uncertainties of ERI estimated soil moisture in the grassland is particularly high, especially during the summer months as a result of greater variability of temperature and other environmental conditions compared to the forest. Evaluating these uncertainties prior to integrating ERI estimated grassland soil moisture with the hydrologic models could improve the relatively poor estimates of hydrologic quantities obtained.

References

- Archie, G.E. 1942. The electrical resistivity log as an aid in determining some reservoir characteristics. *T. Am. Inst. Min. Metal. Eng.* 146:54–61.
- Beighley, R.E., T. Dunne, et al. 2008. Impacts of climate variability and land use alterations on frequency distributions of terrestrial runoff loading to coastal waters in southern california. *Journal of the American Water Resources Association* 44:62-74.
- Blinn, D.W., and P.C.E. Bailey. 2001. Land-use influence on stream water quality and diatom communities in victoria, australia: A response to secondary salinization. *Hydrobiologia* 466:231-244.
- Bryant, D., D. Nielsen, et al. 1997. The last frontier forests: Ecosystems and economies on the edge. p. 16. World Resources Institute, Washington, DC.
- Canadell, J., R.B. Jackson, et al. 1996. Maximum rooting depth of vegetation types at the global scale. *Oecologia* 108:583-595.
- Coomes, D.A., and P.J. Grubb. 2000. Impacts of root competition in forests and woodlands: A theoretical framework and review of experiments. *Ecological Monographs* 70:171-207.
- Daily, W., A. Ramirez, et al. 2005. Electrical resistance tomography-theory and practice. p. 525. *In* D.K. Butler (ed.) *Investigations in geophysics*. Society of Exploration Geophysics.
- Daily, W., A. Ramirez, et al. 1992. Electrical resistivity tomography of vadose water movement. *Water Resources Research* 28:1429-1442.
- de Rosnay, P., and J. Polcher. 1998. Modelling root water uptake in a complex land surface scheme coupled to a gcm. *Hydrology and Earth System Sciences* 2:239-255.

- Farley, K.A., E.G. Jobbagy, et al. 2005. Effects of afforestation on water yield: A global synthesis with implications for policy. *Global Change Biology* 11:1565-1576.
- Feddes, R.A., E. Bresler, et al. 1974. Field-test of a modified numerical-model for water uptake by root systems. *Water Resources Research* 10:1199-1206.
- French, H.K., C. Hardbattle, et al. 2002. Monitoring snowmelt induced unsaturated flow and transport using electrical resistivity tomography. *Journal of Hydrology* 267:273-284.
- Hanafy, S., and S.A. al Hagrey. 2006. Ground-penetrating radar tomography for soil-moisture heterogeneity. *Geophysics* 71:K9-K18.
- Hayley, K., L.R. Bentley, et al. 2007. Low temperature dependence of electrical resistivity: Implications for near surface geophysical monitoring. *Geophysical Research Letters* 34:L18402.
- Hyndman, D.W., A.D. Kendall, et al. 2007. Evaluating temporal and spatial variations in recharge and streamflow using the integrated landscape hydrology model (ilhm). *In* D.W. Hyndman, F.D. Day-Lewis, and K. Singha (ed.) *Subsurface hydrology: Data integration for properties and processes*. American Geophysical Union.
- Jackson, R.B., J. Canadell, et al. 1996. A global analysis of root distributions for terrestrial biomes. *Oecologia* 108:389-411.
- Jackson, R.B., H.J. Schenk, et al. 2000. Belowground consequences of vegetation change and their treatment in models. *Ecological Applications* 10:470-483.
- Jarvie, H.P., P.J.A. Withers, et al. 2008. Influence of rural land use on streamwater nutrients and their ecological significance. *Journal of Hydrology* 350:166-186.

- LaBrecque, D.J., and X. Yang. 2001. Difference inversion of ert data: A fast inversion method for 3-d in situ monitoring. *Journal of Environmental & Engineering Geophysics* 6:83-89.
- Looms, M.C., K.H. Jensen, et al. 2008. Monitoring unsaturated flow and transport using cross-borehole geophysical methods. *Vadose Zone Journal* 7:227-237.
- Monteith, J.L. 1965. Evaporation and environment. *Symp. Soc. Exp. Biol.* 19:19.
- Nosetto, M.D., E.G. Jobbagy, et al. 2005. Land-use change and water losses: The case of grassland afforestation across a soil textural gradient in central argentina. *Global Change Biology* 11:1101-1117.
- Oconnell, M.G., G.J. Oleary, et al. 1995. Potential groundwater recharge from fallowing in north-west victoria, australia. *Agricultural Water Management* 29:37-52.
- Petheram, C., G. Walker, et al. 2002. Towards a framework for predicting impacts of land-use on recharge: 1. A review of recharge studies in australia. *Australian Journal of Soil Research* 40:397-417.
- Pielke, R.A. 2005. Land use and climate change. *Science* 310:1625-1626.
- Pitman, A.J., G.T. Narisma, et al. 2004. Impact of land cover change on the climate of southwest western australia. *Journal of Geophysical Research-Atmospheres* 109.
- Reynolds, J.M. 1997. *An introduction to applied and environmental geophysics.* John Wiley & Sons Ltd.
- Rood, S.B., J. Pan, et al. 2008. Declining summer flows of rocky mountain rivers: Changing seasonal hydrology and probable impacts on floodplain forests. *Journal of Hydrology* 349:397-410.
- Scanlon, B.R., R.C. Reedy, et al. 2005. Impact of land use and land cover change on groundwater recharge and quality in the southwestern us. *Global Change Biology* 11:1577-1593.

- Trabucco, A., R.J. Zomer, et al. 2008. Climate change mitigation through afforestation/reforestation: A global analysis of hydrologic impacts with four case studies. *Agriculture Ecosystems & Environment* 126:81-97.**
- van Genuchten, M.T. 1980. A closed-form equation for predicting the hydraulic conductivity of unsaturated soils. *Soil Sci. Soc. Amer. J.* 44:892-898.**
- Vogt, K.A., D.J. Vogt, et al. 1996. Review of root dynamics in forest ecosystems grouped by climate, climatic forest type and species. *Plant and Soil* 187:159-219.**
- Wayland, K.G., D.T. Long, et al. 2003. Identifying relationships between baseflow geochemistry and land use with synoptic sampling and r-mode factor analysis. *Journal of Environmental Quality* 32:180-190.**
- Zhou, Q.Y., J. Shimada, et al. 2001. Three-dimensional spatial and temporal monitoring of soil water content using electrical resistivity tomography. *Water Resources Research* 37:273-285.**
- Šimůnek, J., M. Šejna, et al. 1998. Code for simulating the one-dimensional movement of water, heat, and multiple solutes in variably saturated porous media.**

Chapter Five

Evaluating a range of approaches to derive hydrogeological information from electrical resistivity data

Introduction

Geophysical methods have often been used to develop spatially extensive estimates of subsurface hydrologic properties and characteristics (Daily et al. 1992; Hyndman and Gorelick 1996; Hyndman et al. 2000; Looms et al. 2008). In some cases, time-lapse geophysical approaches can help discern temporal changes that occur in the subsurface due to climate, vegetation, and other processes. Recent advances in instrument technology, as well as data acquisition and processing methods have resulted in many recent geophysical applications in environmental research (Slater et al. 2000; Pellerin 2002; al Hagrey 2007; Amidu and Dunbar 2007; Looms et al. 2008). Direct current electrical resistivity imaging (ERI) is a promising geophysical method that is commonly used for subsurface hydrologic characterizations (Binley et al. 2002; Israil et al. 2006; al Hagrey 2007; Nosetto et al. 2007). The sensitivity of electrical conductivity to changes in soil moisture and solute concentrations, and the potential ability of ERI to reasonably capture and quantify these changes in space and time with minimal disturbance are some of the major reasons for the popularity of ERI within the hydrologic science community (Kemna et al. 2002; French and Binley 2004; Israil et al. 2006).

Despite the significant use of ERI method for environmental investigations, its practical uses outside of experimental settings are complicated by a variety of factors. Survey techniques, measurement physics, inversions and other data processing methods are still being developed and improved. With time-lapse measurements necessary to image transient and dynamic subsurface processes, further uncertainties may emerge due to inconsistent data acquisition strategies and effects of natural environmental variability. These are inherently difficult to fully capture and describe in field settings. Soil temperature and moisture are two of the principal variables affecting changes in soil conductivity. Other biological, geochemical, and physical processes also have the potential to influence the measurements, allowing for potential misinterpretation of resistivity observations. Conversion of electrical resistivity estimates to other quantities of interest, such as soil moisture is generally done with two commonly accepted models (Archie 1942; Topp et al. 1980).

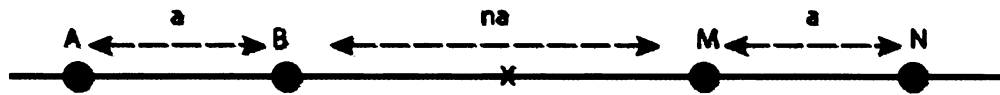
This chapter provides an overview of the ERI method based on our experience with imaging long-term subsurface soil moisture dynamics at a field site in East Lansing, Michigan. The literature does not provide extensive information on the opportunities provided by this non-invasive method for gaining insights into subsurface environments or the practical challenges to its effective long term use in natural settings. Resistivity data collected for two years at our East Lansing research site are used to examine the effects of data acquisition and processing strategies for quantifying the natural variability of subsurface electrical resistivity. We also evaluate the influence of these choices on our ability

to interpret and quantify soil moisture dynamics with the electrical resistivity data. Finally, we discuss approaches to further enhance the reliability of hydrologic quantities extracted from time-lapsed data.

Electrical Resistivity Imaging (ERI)

ERI is a method that estimates the subsurface distribution of electrical resistivity by introducing a known current into the ground using a pair of electrodes, and measuring the resulting potential difference between separate pairs of electrodes. The measured resistance is a function of electrical conductivity of the subsurface constituents (grain matrix, porosity, water content and conductance). By deploying arrays with multiple electrodes, many independent measurements of resistivity can be quickly collected in a repeatable manner. Several electrode configurations can be used for data acquisition with varying resolutions and sensitivities (Reynolds 1997; Dahlin and Loke 1998; Loke 2000; Dahlin and Zhou 2004). At our research site, we acquired data with the common Wenner and Dipole-Dipole electrode configurations (Figure 5-1) because of their robustness. The spatial data coverage for these array types at the research site are illustrated in Figure 5-2.

Dipole-dipole



Wenner

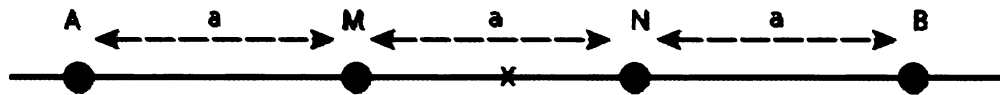


Figure 5-1 Electrode positions for Wenner (top) and Dipole-dipole (bottom) electrode configurations. A, B are current electrodes and M, N are potential electrodes. 'a' is the distance between electrodes used for measurements, and n is an integer.

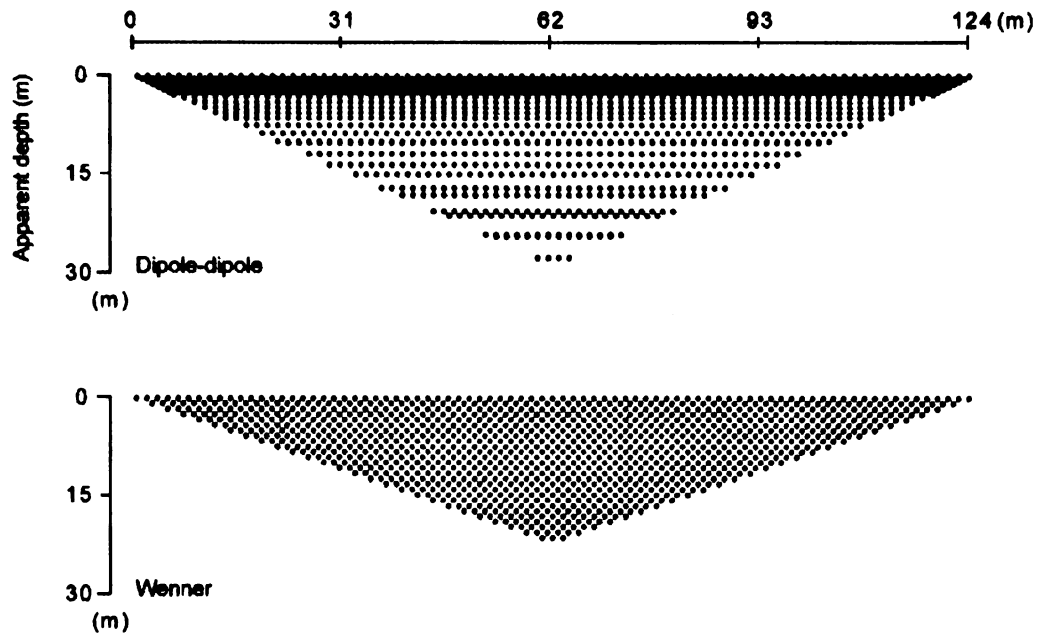


Figure 5-2. Data coverage for Wenner and dipole-dipole electrode configurations for an 84 electrode array with 1.5m electrode separations. Higher data density near the electrode positions is obtained with the dipole-dipole configuration compared to Wenner, where data coverage is evenly distributed. 1453 and 1134 measurements are obtained with these dipole-dipole and Wenner arrays respectively.

ERI and environmental variability

The solid constituents of shallow soils are generally good insulators. As a result, the electrical conductivity measured with ERI is primarily from ionic conduction through water in the pore spaces of soils, sediments, and rocks. This dependency between electrical conductivity and pore-water can thus be exploited to obtain quantitative estimates of soil moisture. While soil moisture variability is often the primary reason for temporal changes in subsurface resistivity, pore-water conductivity and soil temperature may also have significant effects on ERI measurements that may limit the ability to compare time-lapse measurements in some environments. These variables also vary spatially, and thus their effects tend to be different along the electrode array where the data is collected. Soil structure, porosity, and other physical characteristics can also affect conductivity over time, but these are relatively less important, particularly for seasonal or annual estimates.

Electrical conductivity and volumetric soil moisture

A general approach to estimate soil moisture from ERI data is to relate the measured electrical conductivity to water saturation through petrophysical models. The most general is Archie's law (Archie 1942); which describes the electrical conduction of a material, related to the conductivity and water saturation in the pore spaces. The relationship, derived through experimental results, can be written in terms of electrical resistivity as;

$$\rho_i = a\rho_w\phi^{-m}S_w^{-n} \quad (5-1)$$

where ρ_w is the resistivity of the pore fluid, ϕ is porosity, and S is fractional water saturation; $S=\theta/\phi$ where θ is the water content. The exponential constant m , known as the cementation factor, depends on the interconnectedness of pore spaces; 1.3 is commonly used for unconsolidated clean sand formations (Knight and Endres 2005). The constant a is a fitting parameter with values ranging between 0.62 and 2.45, however it is often considered unity in practice. The exponent n , called the saturation exponent, accounts for the connectedness of water in the partially saturated soils (Knight and Endres 2005). Archie's model assumes the primary conduction occurs through the pore fluid. Therefore in places where clay and other conductive materials are present, the effective contributions of these materials to the bulk conductivity should be assessed by integrating other empirical components with Archie's equation (Waxman and Smits 1968). Alternatively, the contribution of clay and other conductive components can be accounted for by measuring the resistivity-soil moisture relationship for site specific soils in a laboratory setting.

A common approach to estimating Archie's parameters for a particular soil is to perform laboratory measurements using standard procedures (ASTM standard G57-95). Such methods however suffer from a number of practical difficulties such as the need to extensively disturb the soil samples to facilitate even wetting and packing in a test box. However, a general relationship obtained with multiple sample tests in combination with other independent estimates of

saturated soil resistivities and porosities from undisturbed field samples are often sufficient to describe the resistivity-soil moisture relationship for a particular soil. In this study, a relationship was constructed between laboratory measurements of soil saturation and resistivity to estimate m for the simplified form of the Archie's equation.

$$S = \left(\frac{\rho_s}{\rho} \right)^{\frac{1}{m}} \quad (5-2)$$

This equation was used to convert field resistivity images into soil moisture based on estimates of porosity from soil cores collected at the site and saturated resistivity values from field datasets. ρ_s here is saturated bulk resistivity.

Parameter	Mean	Stdev	Max	Min	Soil
Φ	0.47	0.03	0.51	0.43	Clay (n=6)
m	0.67	0.09	0.84	0.6	
ρ_s	68.15	-	-	-	
Φ	0.39	0.03	0.43	0.36	Sand (n=6)
m	1.16	0.11	1.29	0.99	
ρ_s	71.53	-	98	65	

Table 5-1. Parameters for Archie's equation from laboratory measurements of soils at the study site. ρ_s is obtained from field resistivity data (for sand estimated with resistivity data from below the water table, and for clay estimated from datasets collected when the site was extremely wet).

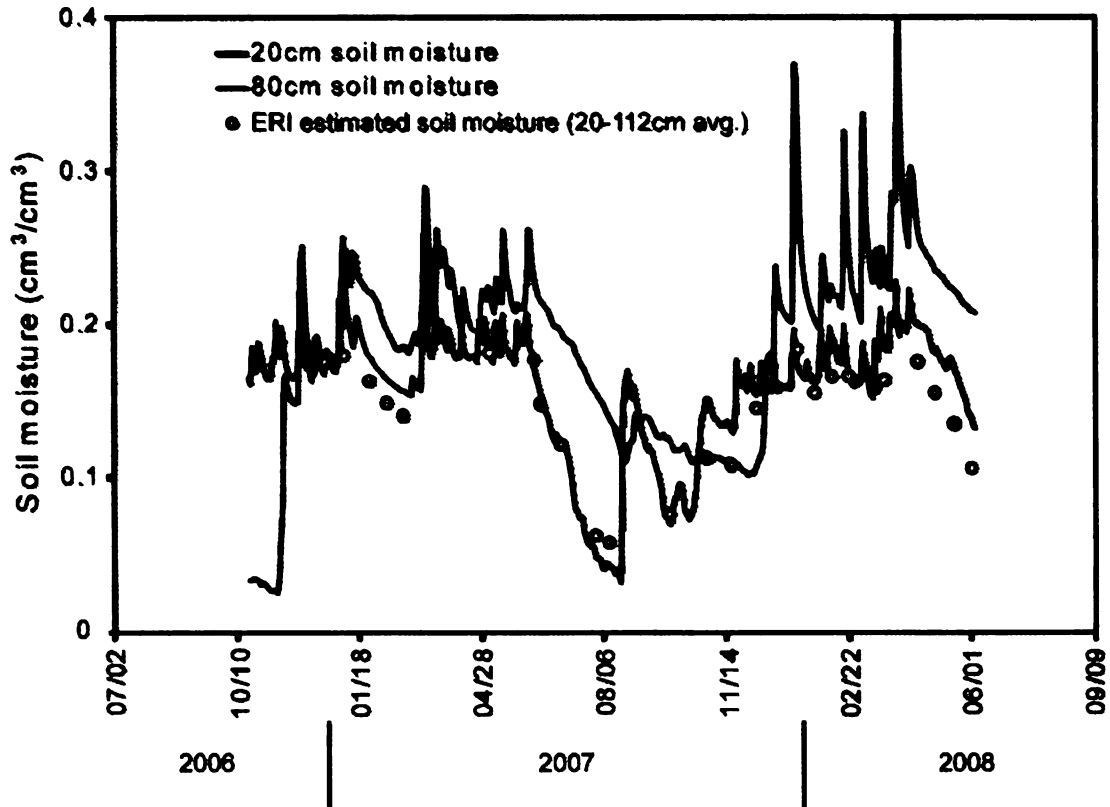


Figure 5-3. Soil moisture estimates from ERI (dipole-dipole) data compared to other independent measurements of soil moisture at the study site.

The ERI estimated soil moisture, based on laboratory derived parameters (Table 5-1) and equation 5-1, correlates well with point soil moisture measurements made at the site with automated data loggers (Figure 5-3). Figure 5-4 illustrates the potential uncertainty in ERI estimated soil moisture due to uncertainty in Archie's parameters. The fitting parameter m has a stronger influence on soil moisture estimates for higher resistivities or lower soil moisture contents. Estimation error of saturated resistivity has more impact on the computed soil moisture at lower resistivity ranges, which may complicate attempts to identify the elevation of the capillary fringe from ERI (Figure 5-5).

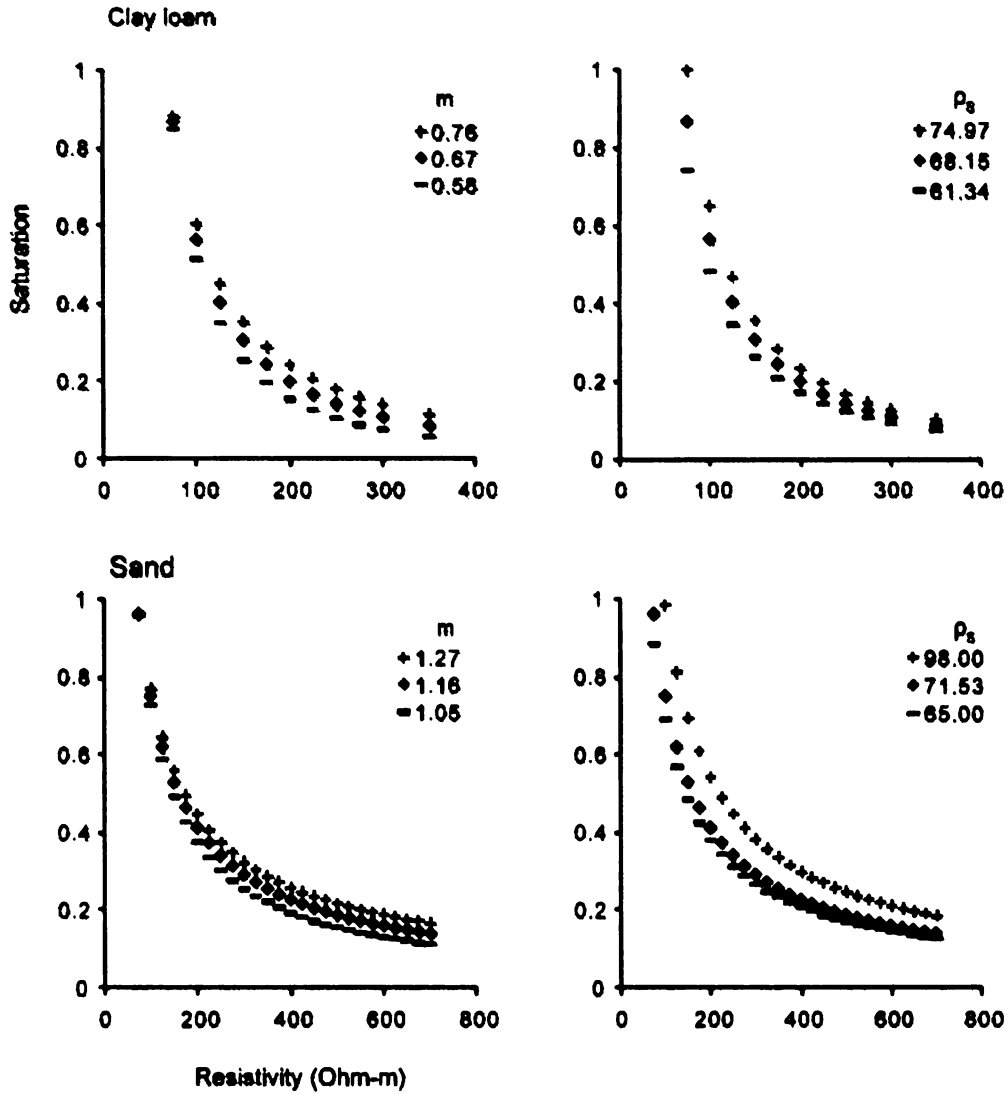


Figure 5-4. The sensitivity of ERI derived saturation to m , and ρ_s estimates. The high (grassland-98 Ohm-m) and low (forest-65 Ohm-m) values for saturated resistivity were derived from field resistivity data. Some of the differences in saturated resistivity between the grassland and forest are due to observed groundwater conductivity differences.

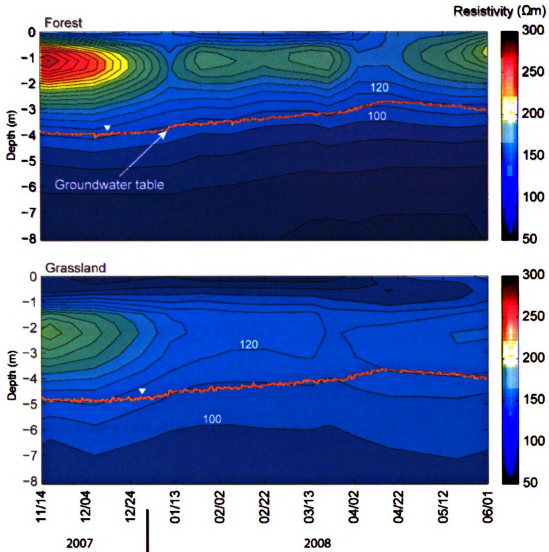


Figure 5-5. Water table elevation observations and resistivity measurements in the forest (a), grassland (b) from November 2007 to June 2008. The correlation between water table elevation and contours of the resistivity estimates is much clearer in the forest relative to the grassland. Images in this dissertation are presented in color.

Figure 5-5 illustrate the temporal changes in resistivity measured near the grassland (spatially averaged data within a ~3 zone near the well) and forest (spatially averaged data within ~3m zone, ~10m away from the well) groundwater

observation wells at the study site. The changes in water table elevation are similar to the pattern of resistivity changes in the forest, but this relationship is relatively less clear in the grassland. The inability of ERI to image the water table in the grassland could result from a number of different factors. The presence of the shallow high conductivity zone (low resistivity) in the grassland is one contributing factor that likely affects the resolution of ERI measurement below it resulting in a lower vertical resistivity contrast. Alternatively, it is also possible that the vertical soil moisture contrast is low in the grassland due to the lower soil moisture deficit there at the end of the growing season, which recovers relatively quickly with fall precipitation.

Soil temperature and electrical conductivity

The electrical conductivity of pore fluids is influenced by soil temperatures. Temperature variations are largest in the shallow subsurface (0-1m), especially over relatively short time frames. However, over seasonal time scales, temperature also vary down to the water table at this site. Additionally, soil temperatures can differ spatially, particularly during warm summer months depending on land-cover characteristics and associated shading (Figure 5-6).

Observations made at our study site show that summer diurnal soil temperatures in the top 10 centimeters change by $\sim 20^{\circ}\text{C}$ in the grassland but only $\sim 10^{\circ}\text{C}$ in the forest (Figure 5-6, inset). At the same site, consistent long-term groundwater temperature differences of $\sim 2^{\circ}\text{C}$ were also recorded between

the land-covers. Our temperature observations show that overall, the subsurface in the grassland is ~2~3°C warmer than the forest throughout the year due to differences in solar insolation.

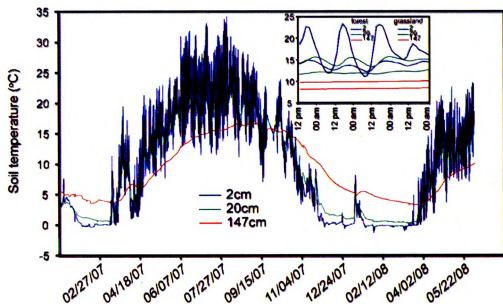


Figure 5-6. Seasonal grassland soil temperature fluctuations at the study site. Inset shows diurnal soil temperature differences between the grassland and the forest stand over a span of three days in June.

There are several models to describe the effect of temperature on electrical conductivity of soils. In the 0-25°C range, the relationship can be approximated using

$$\sigma_{\text{std}} = \left(\frac{m(T_{\text{std}} - 25) + 1}{m(T_i - 25) + 1} \right) \sigma_i \quad (5-3)$$

(Hayley et al. 2007); where T_{std} is a reference temperature, σ_{std} is conductivity at the reference temperature T_{std} . T_i and σ_i are measured temperature and

electrical conductivity values, and m is a material dependent temperature coefficient (Hayley et al. 2007). Figure 5-7 illustrates the effect of different soil temperatures on the resistivities typically measured at the research site. Over seasonal scales and at higher soil resistivity ranges the temperature induced resistivity variations could be relatively high (~25%). The effect of temperature however is more important in lower resistivity ranges near soil water saturation. The resistivity-soil moisture relationship computed with Archie's equation shows that a ~12°C temperature change leads to a ~20% difference in the calculated soil moisture at lower resistivities (a saturated resistivity of 73Ωm, m coefficient of 1.16 used in the calculation). The effect of m in the temperature-resistivity relationship is less important at lower measured resistivities. However, at the 400Ωm and 28°C illustrated, m (0.018-0.022) range results in a ~13% resistivity difference in the correction (Figure 5-8).

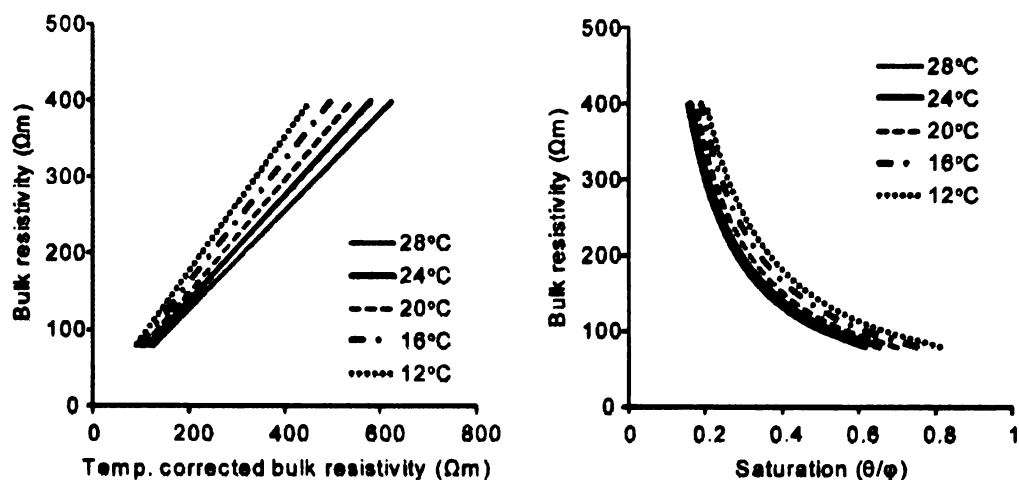


Figure 5-7. The influence of temperature on resistivity and the resulting difference in calculated soil moisture with Archie's equation.

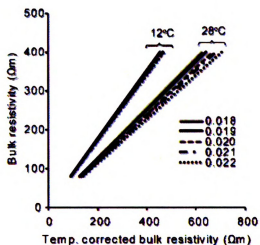


Figure 5-8. The influence of m on soil resistivity-temperature dependence at two different soil temperatures (28°C and 12°C). The sensitivity to m is important at higher temperature ranges.

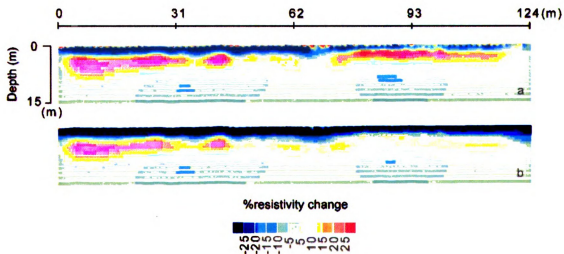


Figure 5-9. Percent change in resistivity from August 10, 2007 to January 11, 2008 without (a) and with (b) temperature correction. Prominent changes in the grassland (a) do not appear once the temperature correction is added (b). Images in this dissertation are presented in color.

The differences computed between two resistivity datasets from the East Lansing field study site are compared in Figure 5-9. The noticeable change in grassland resistivity (Figure 5-9a), prior to temperature correction do not appear in the difference computed with the temperature corrected data (Figure 5-9b). In general the temperature variability is larger in the grassland. With limited spatial measurements of temperature the uncertainty due to this variation is likely to be higher in the grassland.

The effect of pore-water conductivity

Dissolved ion concentrations in the subsurface depend on a number of factors. Biological degradation and ion leaching processes along with concentration of solutes due to evaporation and transpiration are important factors that may introduce land-use driven pore water conductivity differences in the vadose zone. Anthropogenic inputs such as road salt and agricultural fertilizers are other potential considerations. Seasonal differences in biological processes and variations in ion concentrations in the precipitation (Rein et al. 2004) can also introduce temporal variations in water conductivity.

Groundwater conductivity measured in two observation wells at the research site show that the groundwater conductivity differs between the land covers (Figure 5-10a). The difference is fairly consistent over the course of the measured period. The relative influence of this difference on measured resistivity in the grassland and the forest can be evaluated with the Archie's equation (5-1).

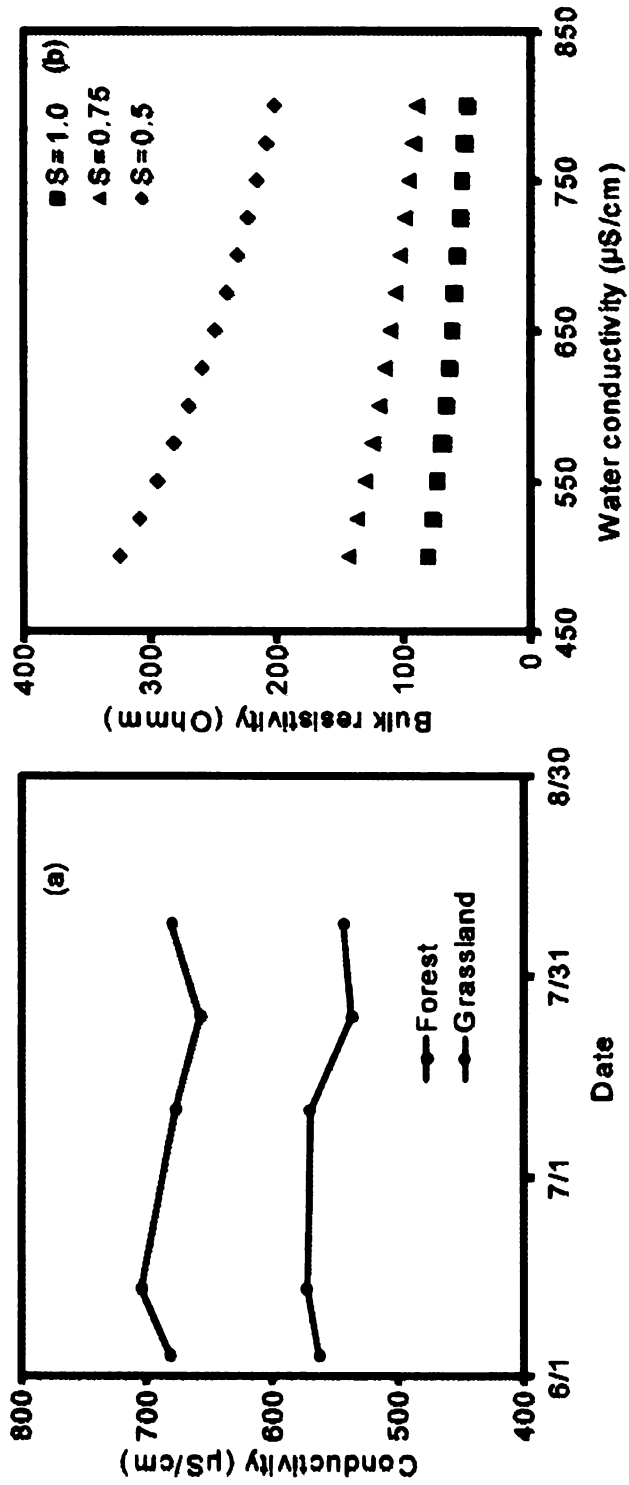


Figure 5-10. Groundwater conductivity measured at the research site in the grassland and forest observation wells (a). Pore-water and bulk electrical resistivity relationship calculations based on Archie's equation for various degrees of saturation (b). A soil with 30% porosity, fitting constant, $m=1.16$ and an n value of 2, characteristic of sandy soils, was used in the calculation.

The effect of pore water conductivity on bulk electrical conductivity is largest at lower water saturations and much smaller in the saturated zone. When pore-water conductivities are similar along with similar subsurface soil and sediment characteristics, the measured resistivities below the water table are expected to be similar. However, at the study site, with comparable soil conditions, a consistent discrepancy in resistivities between the grassland and the forest is observed below the water table (Figure 5-11).

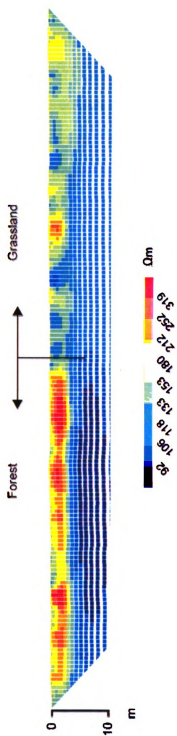


Figure 5-11. Potential influence of groundwater conductivity differences below the grassland and forest. Higher resistivity values below water table (~4 m from surface) in the grassland is likely due to the lower measured groundwater conductivities in the grassia grassland. Data shown is temperature corrected and the soils are similar on either side of the ecotone (the forest-grassland boundary). Images in this dissertation are presented in color.

The measured bulk electrical resistivities are approximately 30-50 Ω m higher in the grassland (Figure 5-12), which is consistent with the measured lower groundwater conductivity. An adjustment for the conductivity difference ($\sim 137\mu\text{S}/\text{cm}$) would result in a resistivity adjustment of $\sim 26\%$, which lowers the measured saturated zone grassland resistivity ($\sim 98\Omega\text{m}$) to $\sim 72\Omega\text{m}$, approximately equivalent to that measured in the saturated zone of the forest ($\sim 70\text{-}75\Omega\text{m}$). In the unsaturated zone a similar adjustment would further reduce the measured resistivity in the grassland. However, no measurements of pore water conductivity in the vadose zone are available for this purpose.

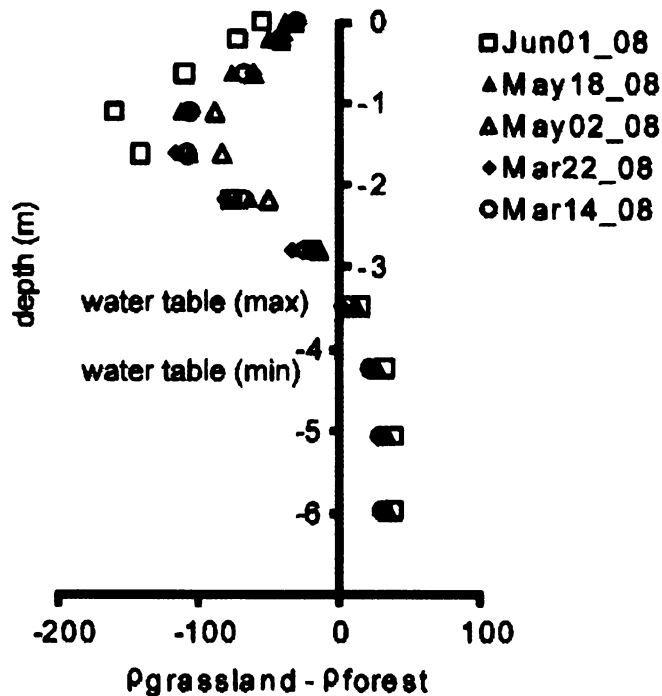


Figure 5-12. Measured bulk electrical resistivity difference between the grassland and the forest ($\rho_{\text{grassland}} - \rho_{\text{forest}}$). Higher resistivities below the water table in the grassland are consistent with the lower measured groundwater conductivities there. The shaded area indicates the approximate range of water table change in the grassland between March and June 2008.

ERI and time-lapse differencing

The primary objective of time-lapse ERI is to obtain temporal variations of subsurface hydraulic quantities of interest. Two approaches are often adopted for computing the differences between time-lapse ERI datasets. The simplest is to invert each ERI dataset independently and then compute the difference with respect to a reference background dataset. This approach however is often considered unreliable because data related errors tend to mask small variations in the amount of moisture or solute (Daily et al. 2005).

An alternative is to use a difference inversion algorithm (LaBrecque and Yang 2001), where the ratios of two data sets or the differences in the data itself are associated with the inversion. The ratio approach can be expressed as;

$$d_n = \frac{d_t}{d_0} d_h \quad (5-4)$$

where d_n the new data vector with normalized data, d_t is monitoring or time lapse data, d_0 is data for the reference state or base data, and d_h is an arbitrary homogenous conductivity representative of data that would be observed in a homogeneous subsurface. The d_n data set is then inverted to obtain changes relative to the reference d_h (Daily and Owen 1991).

All data processing in this study were based on the difference inversion approach above. One contentious issue related to this method is the selection of an appropriate base dataset t for the difference computations. The choice of

base dataset was complicated by the fact that the resistivity distributions were highly variable at the research site both in space and time, driven by the sharp vegetation difference. How these contrasts embedded in a base dataset would affect and propagate through subsequent datasets processed relative to it were initially difficult to evaluate. A simple analysis of the potential errors and uncertainties related to base dataset selection is therefore presented in this section as a foundation for further work.

The following analysis evaluates three resistivity datasets, B1 (collected on October, 2006, B2 (July 2007), and B3 (January 2008) from the study site, and difference inversion related computations made with them as base datasets. The characteristics of the three datasets as acquired from the field site are illustrated in Figure 5-13. Dataset B1 has a significant spatial coverage of higher resistivities and a larger contrast with the forest. B2 in comparison has a sharper contrast between the shallow and deep soils below the forest, and B3 has a relatively uniform resistivity distribution across the ecotone, which is most uniformly wet compare to B1 and B2 (Figure 5-13).

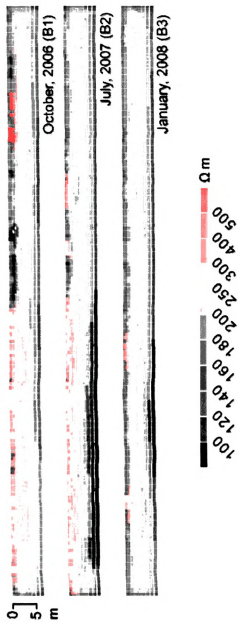


Figure 5-13. Data characteristics of three resistivity data sets from the study site, which were used for difference inversion method analysis. Images in this dissertation are presented in color.

The comparisons between independent inversions of the three datasets with the same datasets derived using difference inversions and the other two datasets as base data is illustrated in Figure 5-14. The two approaches clearly lead to relatively different outcomes. Overall the direct inversions appear to result in lower inverted resistivities compared to difference inversions. Figure 5-14 b & c shows that difference inversion of B1 with B3 as the base result in a better comparison with independently inverted B1. Using B3 however for computing B2 results in a poor correlation between the two inversions. B3 which has the lowest resistivity range among the three datasets is relatively poorly computed with the difference inversion when datasets with larger resistivity ranges (B1, B2) are used as base datasets (Figure 5-14, g & h). Overall, all selected datasets lead to different inverted resistivities with no particular dataset performing better or worse as a suitable base dataset.

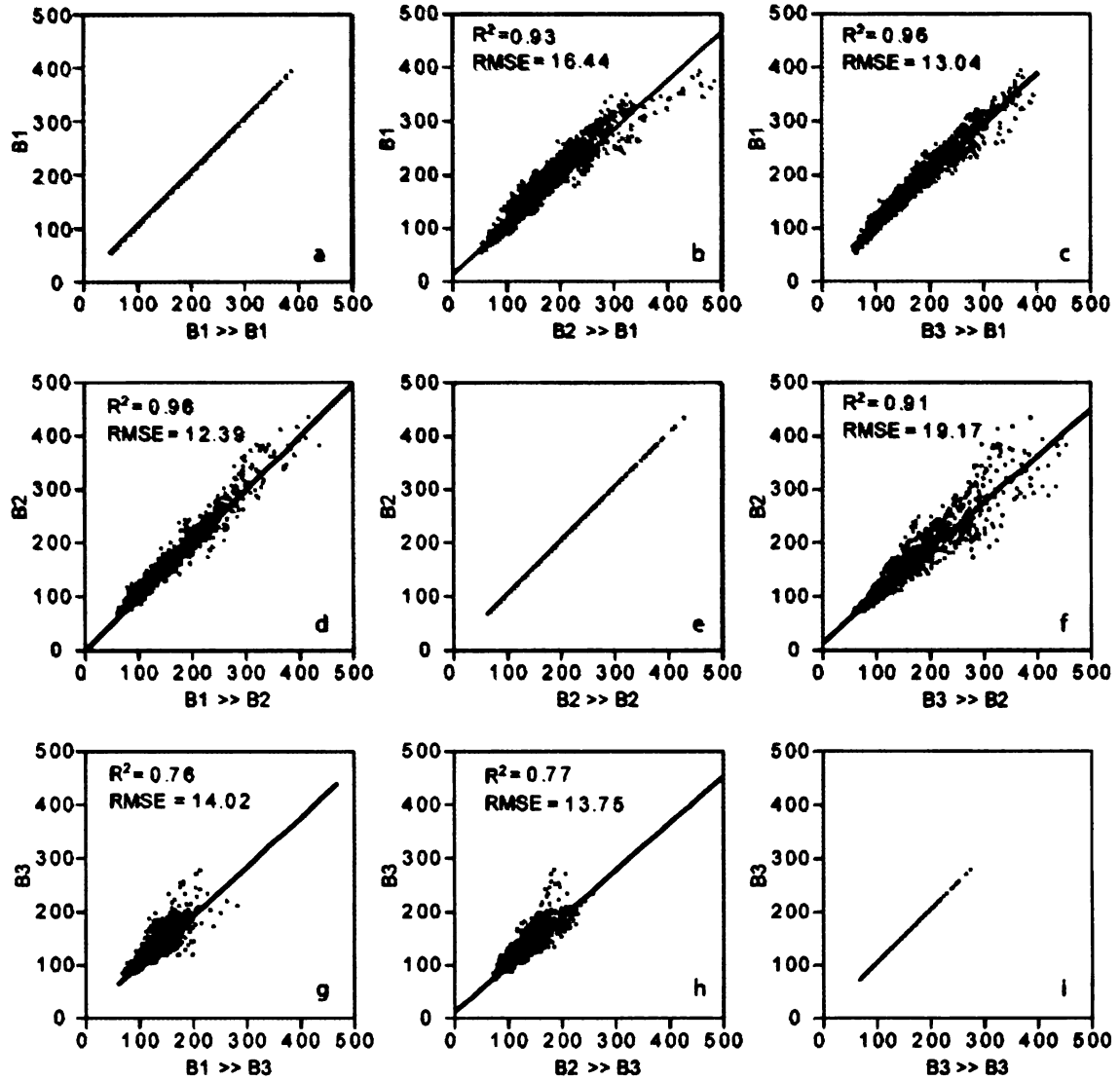


Figure 5-14. Comparisons of base dataset effects. B1, B2, and B3 are three separate inverted field datasets. The notation B1>>B3 refers B3 calculation with B1 as the base dataset in the difference inversion. Only the data from the top 5m were selected for the analysis.

A similar comparison where one particular dataset was derived using the other two as the base dataset also was performed for this analysis (Figure 5-15). Most differences among the three are associated with computing the dataset B2, which has a significant high-low resistivity contrast in the forest (Figure 5-13).

The spatial distribution of these differences illustrate that the choice of base dataset may be an important consideration in the forest, where large resistivity heterogeneities is common throughout the year (Figure 5-16)

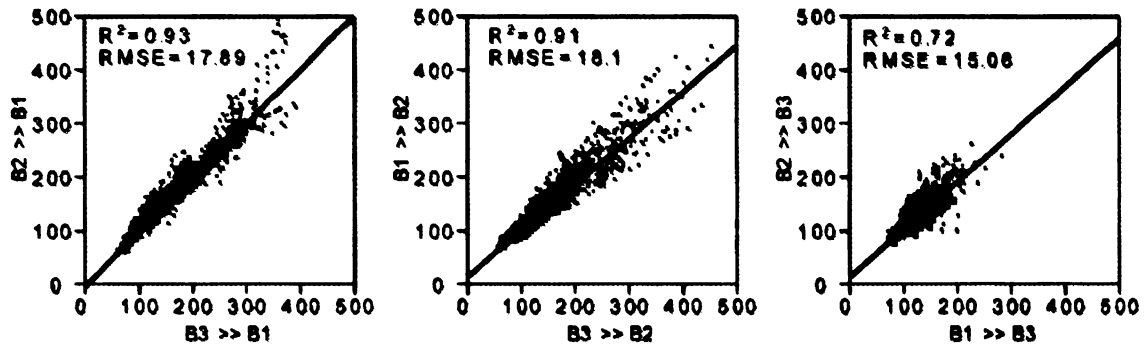


Figure 5-15. Comparison of computed B1, B2, B3 with different with respect to others in the difference inversion.

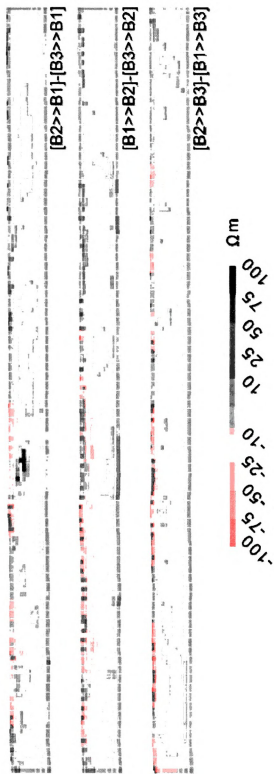


Figure 5-16. Spatial distribution of differences from difference inversions with B1, B2, and B3 datasets. Correlations between each dataset are shown in Figure 5-15. The choice of base dataset has a larger impact on the resistivity based interpretations in the forest. Images in this dissertation are presented in color.

Soil moisture estimates with resistivity ratios

An alternative approach to derive soil moisture change information from ERI is to use resistivity ratios in combination with laboratory derived petrophysical relationships. By focusing only on resistivity changes at a location, the uncertainties related to spatial variability of soil texture characteristics could be largely avoided. It also is a potentially useful method to make comparisons between for example the grassland and the forest at our study site where conductivity differences result in biased estimates of absolute soil moisture between the two land covers. The ratio method is also affected by temporal variability of soil water conductivity and temperature.

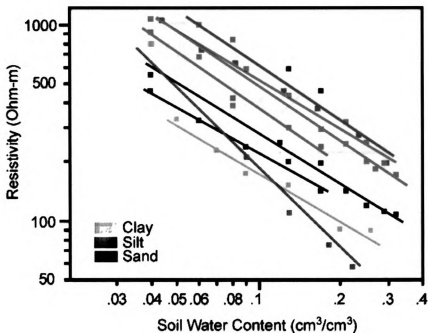


Figure 5-17. Laboratory measure resistivity and soil water contents for soil samples collected from multiple locations at the study site. Images in this dissertation are presented in color.

Based on the similar behavior of the resistivity-soil water content relationship (Figure 5-17) for a number of soil samples from the study site, the resistivity and water content change can be derived as;

$$\frac{\theta_1}{\theta_2} e^{\left\{ \frac{\ln\left(\frac{\rho_1}{\rho_2}\right)}{m} \right\}} \quad (5-5)$$

where θ_1 and θ_2 are volumetric water contents at two different data collection dates, ρ_1 , ρ_2 calculated resistivities from differential inversions for the respective dates, and m is the average slope of the log-log relationship between temperature corrected resistivity and water content for soil samples from the site.

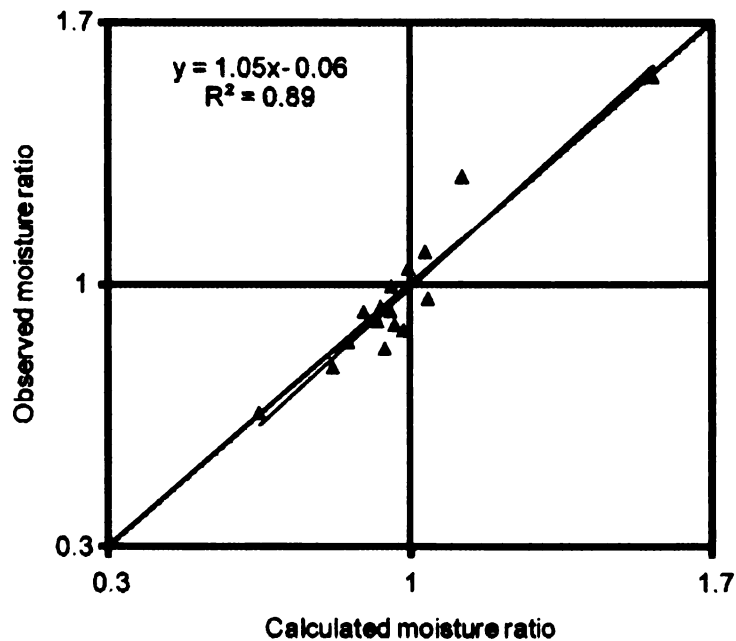


Figure 5-18. Soil moisture ratios observed with point gauges and soil moisture ratios calculated with ERI near the location where point gauges are located.

The calculated moisture changes (θ_1 / θ_2) were compared with soil moisture changes observed in automated soil moisture loggers installed in the forest. The comparisons yield a reasonable correlation indicating the potential viability of the approach for understanding and quantifying soil moisture change with ERI data (Figure 5-18).

Conclusions

Many practical challenges still remain in the use of ERI for environmental monitoring and hydrologic characterizations. Natural environmental variability related to temperature and pore-fluid conductivity is a major concern for obtaining accurate temporal soil moisture estimates from ERI. As highlighted in this study, such variability is to be anticipated in any natural setting. If the effects of these variables are not well constrained, significant uncertainty may exist in the estimated hydrologic quantities. Applying petrophysical relationships to obtain soil moisture information from resistivity data is another potential source of uncertainty. The best approach to minimize the uncertainties related to these is to develop site specific relationships with laboratory experiments, regardless the various practical limitations associated with the existing laboratory methods. Alternatively, when only information on subsurface moisture change is required, the potential of the resistivity ratio approach discussed can be explored. Soil moisture computed with both types of ERI datasets (Wenner and dipole-dipole) compared relatively well with the point soil moisture measurements made with

other probes at the site. However, data errors were more significant with the dipole-dipole measurements. As shown in this research, resistivity estimated soil moisture often tend to under predict or closely relate to the lowest measured (with other instruments) moisture in a given soil volume. While ERI is inherently an estimate of a larger volume than point measurements, the general tendency to be biased towards the lowest estimates need to be further explored.

The simple analysis of uncertainty resulting from difference inversion of ERI data suggests that the choice of base dataset influences the resistivity data interpretations and parameter derivations. All difference inversions with the selected base datasets resulted in different outcomes, with largest differences in areas with significant heterogeneity such as in the forest portion of the study site.

References

- al Hagrey, S.A. 2007. Geophysical imaging of root-zone, trunk, and moisture heterogeneity. *Journal of Experimental Botany* 58:839-854.
- Amidu, S.A., and J.A. Dunbar. 2007. Geoelectric studies of seasonal wetting and drying of a texas vertisol. *Vadose Zone Journal* 6:511-523.
- Archie, G.E. 1942. The electrical resistivity log as an aid in determining some reservoir characteristics. *Transactions of the American Institute of Mining and Metallurgical Engineers* 146:54-61.
- Binley, A., P. Winship, et al. 2002. Seasonal variation of moisture content in unsaturated sandstone inferred from borehole radar and resistivity profiles. *Journal of Hydrology* 267:160-172.
- Dahlin, T., and M.H. Loke. 1998. Resolution of 2d wenner resistivity imaging as assessed by numerical modelling. *Journal of Applied Geophysics* 38:237-249.
- Dahlin, T., and B. Zhou. 2004. A numerical comparison of 2d resistivity imaging with 10 electrode arrays. *Geophysical Prospecting* 52:379-398.
- Daily, W., and E. Owen. 1991. Cross-borehole resistivity tomography. *Geophysics* 56:1228-1235.
- Daily, W., A. Ramirez, et al. 2005. Electrical resistance tomography-theory and practice. p. 525. *In* D.K. Butler (ed.) *Investigations in geophysics*. Society of Exploration Geophysics.
- Daily, W., A. Ramirez, et al. 1992. Electrical resistivity tomography of vadose water movement. *Water Resources Research* 28:1429-1442.

- Day-Lewis, F.D., K. Singha, et al. 2005. Applying petrophysical models to radar travel time and electrical resistivity tomograms: Resolution-dependent limitations. *Journal of Geophysical Research-Solid Earth* 110.
- French, H., and A. Binley. 2004. Snowmelt infiltration: Monitoring temporal and spatial variability using time-lapse electrical resistivity. *Journal of Hydrology* 297:174-186.
- Hayley, K., L.R. Bentley, et al. 2007. Low temperature dependence of electrical resistivity: Implications for near surface geophysical monitoring. *Geophysical Research Letters* 34:L18402.
- Hyndman, D.W., M.J. Dybas, et al. 2000. Hydraulic characterization and design of a full-scale biocurtain. *Ground Water* 38:462-474.
- Hyndman, D.W., and S.M. Gorelick. 1996. Estimating lithologic and transport properties in three dimensions using seismic and tracer data: The kesterson aquifer. *Water Resources Research* 32:2659-2670.
- Israil, M., M. al-hadithi, et al. 2006. Groundwater-recharge estimation using a surface electrical resistivity method in the himalayan foothill region, india. *Hydrogeology Journal* 14:44-50.
- Kemna, A., J. Vanderborght, et al. 2002. Imaging and characterisation of subsurface solute transport using electrical resistivity tomography (ert) and equivalent transport models. *Journal of Hydrology* 267:125-146.
- Knight, R.J., and A.L. Endres. 2005. An introduction to rock physics principles for near-surface geophysics. *Investigations in geophysics. Society of Exploration Geophysics.*
- LaBrecque, D.J., and X. Yang. 2001. Difference inversion of ERT data: A fast inversion method for 3-d in situ monitoring. *Journal of Environmental & Engineering Geophysics* 6:83-89.
- Loke, M.H. 2000. Electrical imaging surveys for environmental and engineering studies: A practical guide to 2-d and 3d surveys.

Looms, M.C., A. Binley, et al. 2008. Identifying unsaturated hydraulic parameters using an integrated data fusion approach on cross-borehole geophysical data. *Vadose Zone Journal* 7:238-248.

Nosetto, M.D., E.G. Jobbagy, et al. 2007. The effects of tree establishment on water and salt dynamics in naturally salt-affected grasslands. *Oecologia* 152:695-705.

Pellerin, L. 2002. Applications of electrical and electromagnetic methods for environmental and geotechnical investigations. *Surveys in Geophysics* 23:101-132.

Rein, A., R. Hoffmann, et al. 2004. Influence of natural time-dependent variations of electrical conductivity on dc resistivity measurements. *Journal of Hydrology* 285:215-232.

Reynolds, J.M. 1997. An introduction to applied and environmental geophysics. John Wiley & Sons Ltd.

Slater, L., A.M. Binley, et al. 2000. Cross-hole electrical imaging of a controlled saline tracer injection. *Journal of Applied Geophysics* 44:85-102.

Topp, G.C., J.L. Davis, et al. 1980. Electromagnetic determination of soil-water content - measurements in coaxial transmission-lines. *Water Resources Research* 16:574-582.

Waxman, M.H., and L.J.M. Smits. 1968. Electrical conductivities in oil-bearing shaly sands. *Society of Petroleum Engineers Journal* 8:107-122.



MICHIGAN STATE UNIVERSITY LIBRARIES



3 1293 02956 9443